Concept of Local Polaritons and Optical Properties of Mixed Crystals and Quantum Heterostructures

D i s s e r t a t i o n

Department of Physics, Queens College
The City University of New York

by
Alexey G. Yamilov

November 13, 2004

Thesis advisor
Prof. Alexander A. Lisyansky

A dissertation is submitted to the Graduate Faculty in Physics
in partial fulfillment of the requirements for the degree of
Doctor of Philosophy (PhD)

Acknowledgment

This thesis could not have been were it not for the generosity of spirit, talent and care of many people.

There are no words ample or deep enough to express my gratitude to Prof. Alexander Lisyansky, who has been my mentor during these four years. His profound commitment to science and people instilled in me self confidence and persuit of autonomy.

I am grateful to Prof. Lev Deych, whose dedication, mastery of the subject and intuition have sustained me and the project every step along the way.

A heart felt thank you to Prof. Michael Foygel for hours of conversations and insights during my long journey.

Thanks to Profs Joseph Birman, Azriel Genack, and Steven Schwarz for giving me valuable time and invaluable feedback on several manuscripts.

I would like to thank the Physics Department of Queens College for providing resources and funding for my research assistantship throughout this PhD. Creating a productive scientific environment in such small department and in Queens College is not an easy task. I am thankful to Profs. Azriel Genack, Alexander Lisyansky, and Steven Schwarz for running regular seminars with outstanding speakers.

There are two people who planted the seeds of my love for physics. My initial interest in physics was inspired by Prof. Anatoli Yu. Zakharov, whose eyeopenning physics classes, conversations and personal advice led to my choice of career in physics. I want also to thank Prof. Alexander E. Filippov for always having my best interest at heart. His support, enormous investment of time and effort during my last three years in university allowed me to go on with my physics career and to enter the PhD program.

I am also indebted to all colleagues and friends at the school who pitched in and made working on this an even greater delight, in particular to Alexander Yelnikov, Andrey Chabanov, who spent countless hours, late in to the night, assisting me in the process. I could not have made it without you!

Last but not least I would like to extend my deepest appreciation to my parents and dear sister. They are an ever present source of support, inspiration and love.

Contents

List of Figures

Chapter 1

Introduction

Optical properties of materials with band gaps in their electromagnetic spectrum has recently attracted a great deal of attention. It was suggested that fundamental electromagnetic processes such as spontaneous emission [1, 2], photon-atom interaction [2, 3], optical energy transfer [4], and others are strongly modified at band gap frequencies comparing to the similar processes occurring in vacuum. Photonic crystals, which are periodic structures with a macroscopic period [5], present one of the examples of systems with electromagnetic band gaps. The periodicity in photonic crystals gives rise to allowed and forbidden bands for electromagnetic waves in the same manner as the periodicity in arrangement of atoms causes the band structure for electrons in solids.

An important property of photonic crystals is occurrence of local photon states with frequencies inside band gaps, when the periodic structure is locally distorted [1]. The fact that an isolated defect in an otherwise perfect periodic crystal can give rise to local modes with frequencies in forbidden gaps of a host structure is well known in solid state physics. One could mention local states of electrons in semiconductors [6], lattice vibrations [7, 8, 9, 10], excitons [11, 12, 13], and other elementary excitations. Local photons in a photonic crystal are similar in many aspects to other types of local states. Their frequencies belong to forbidden gaps, in 3D systems they split off the continuous spectrum only if the "strength" of a defect exceeds a certain threshold [14, 15, 16]. At the same time, while all other local states appear due to microscopic (of atomic dimensions) defects, local photons require both an artificial macroscopical host structure and its *macroscopic* distortion. This fact is obviously due to large wavelengths of electromagnetic waves in frequency regions of interest.

It may seem apparent that *microscopic* defects cannot give rise to local photon states. However, if one considers an electromagnetic wave inside a crystal, where it interacts with crystal elementary excitations (phonons, excitons, etc.), one has to deal with a different type of elementary excitation - polariton. When a spectrum of corresponding excitation has a negative dispersion, a polariton spectrum has a forbidden gap in all crystallographic directions. Then a microscopic polar impurity may cause a reconstruction of the spectrum in the way that both polariton components including the electromagnetic one are localized around the impurity [17]. The properties of these impurity induced states, local polariton modes (LPM's), are the subject of this thesis.

Different type of local photonic states was recently suggested in Ref. [18]. These states are formed by an optically active impurity atom, which possesses some natural frequency

(for instance, in a 2-level atom the natural frequency corresponds to the transition between the levels) inside the forbidden range of the host crystal, it gives rise to the EM local state. These states are analogous to "photon-atom bound" states [3] in photonic crystals, therefore it is natural to call them polariton-atom bound states.

Contrary to defect modes in photonic crystals where the defect has the size comparable to the wavelength of light [14, 15], LPM's appear due to a *microscopic* defects in regular crystal lattices. LPM's can be considered as local excitations of a crystal coupled to the electromagnetic field. Regular local phonons (excitons) also interact with the electromagnetic field, but this interaction results mainly in absorption of light and radiative decay of the states [8]. LPM's arise in the region where electromagnetic waves cannot propagate and, therefore, there are neither defect induced absorption of light nor radiative damping of the local states. The electromagnetic interaction leads in this case to new optical effects, and strongly affects the properties of the local states. It is well known, for instance, that local phonons or excitons in a 3D system (as well as local photons in photonic crystals) arise only if the "strength" of a defect exceeds a certain threshold. Local polaritons in systems with an isotropic dispersion split off the allowed band without a threshold even in three dimensions [17]. This effect is caused by the interaction with electromagnetic field, which results in the Van-Hove singularity in the polariton density of states (DOS).

One of the optical effects caused by LPM's that we study in Chapter 2 is resonant tunneling of electromagnetic wave with gap frequencies (see also Ref. [19]). We find that the transmission coefficient at the frequency of the local polariton state increases dramatically and can be as high as unity. In spite of the general understanding that local states should produce local tunneling, this result still seems surprising because transmission of light is affected by a defect with microscopic dimensions, much smaller than the light's wavelength. In addition, the energy of the electromagnetic component of local polaritons is much smaller than that of the phonon component. Traditional wisdom based upon properties of conventional propagating polaritons tells that, in such a situation, most of the incident radiation must be simply reflected. As we will see here, this logic does not apply to LPM's. The physical explanation of the result can be given on the basis of consideration of local polaritons as the result of interaction between the electromagnetic field and local phonons. The latter have macroscopic dimensions comparable with light's wavelength, making the interaction effective. An electromagnetic wave is carried through a sample by phonons, which tunnels resonantly due LPM with mostly phonon contribution. We perform an analytical calculation of the transmission coefficient through a linear chain with a single defect and find that the impurity indeed gives rise to the resonance transmission through the forbidden gap of the polariton spectrum. The resonance occurs when the defect is placed at the center of the chain. The transmission at the resonance becomes independent of the system size and reaches the value of unity although its width decreases exponentially with the size.

When number of the defects increases, one can expect a crossover from a set of noninteracting LPM's to an impurity band. We show first in numerical simulations that for a finite concentration of impurities an impurity polariton band (IPB) develops inside the original polariton gap.

Neglecting spatial dispersion of phonons, in Chapter 3 we obtain analytical expressions with concentration of defects varying in the range $0 < p < 1$, for DOS and the localization length in the band. When the localization length of the single local polariton state exceeds average distance between impurities, the method of microcanonical ensemble [20] gives DOS of an effective system with a uniform distribution of impurities, and describes its renormalization caused by local fluctuations of impurity positions. It also reveals localization of the

states of IPB, which are all localized due to the one-dimensional nature of the model. We found that the impurity-induced band has a number of interesting properties. The group velocity of electromagnetic excitations propagating in this band is found to be proportional to the concentration of the impurities, and can be significantly smaller than the speed of light in vacuum. The analytical results show excellent agreement with numerical calculations in the presence of spatial dispersion.

The knowledge obtained from analytical dependencies of DOS in the one-dimensional model of Chapter 3 gives us an insight to a treatment of three dimensional mixed polar crystals. The spatial size of local polariton states may be as large as the EM wavelength, meaning that even at a very low impurity concentration, $\sim 10^{12}\ cm^{-3}$, the local polaritons significantly overlap. This fact allows us to develop a continuous approximation for calculating properties of the polariton-induced band. Applying this approximation to the one-dimensional case, we recover the results of exact analytical solution obtained in Chapter 3. In Chapter 4 we use this approximation to study the properties of the impurity-induced polariton band in 3D such as dispersion laws and density of states of the respective excitations. We derive the dielectric function of mixed polar crystal for an arbitrary concentration of the defects. Studying the concentration dependence of poles and zeroes of the dielectric function, we put forward a simple explanation of far infrared optical properties of mixed polar crystals.

In Chapter 5 we propose a mechanism to make LPM's tunable. We show that electron transitions involving deep centers in semiconductors may lead to a reversible changes of the frequency of the existing LPM's. We also discuss an even more interesting possibility of creating/eliminating LPM's by changing the charge-state of a deep center. The ability to create/eliminate LPM's also leads to interesting possibility to dynamically control the concentration of the polariton states. When the concentration of the deep centers is sufficiently high LPM's develop into an impurity polariton band. We show that in this case the alteration of the local elastic constants can lead to the creation of the polariton band or to the shift of the existing band (and/or to alteration of its shape). We also review materials where these effects may be observed experimentally.

The formalism developed for 1D chain model of discrete non-interacting point-like dipoles coupled with the retarded electromagnetic field can also be considered in an absolutely different context. It can be shown that this model describes normal propagation of light through a system of multiple quantum wells (MQW's), which were studied in a number of theoretical and experimental papers [21, 22, 23, 24, 25, 26, 27]. LPM in this context corresponds to an interface mode, which is localized only in the growth direction of MQW structure, but is extended in the in-plane directions. The presence of interface modes in various multilayered systems is not new. These modes arise and are well studied in ideal periodic structures, see for instance, Refs. [28, 29] and references therein. What distinguishes the interface mode, which arises in our model due to presence of a defect layer, is that its in-plane wave vector $k_{\|}$ is equal to zero, while localized interface modes in ideal periodic multilayers exist only for $k_{\|} > \omega/c$, where ω is the frequency, and c the speed of light in the respective background medium. This LPM, therefore, can be excited by an evanescent electromagnetic mode at normal incidence, and may cause its resonant transmission. An application of the results obtained in earlier chapters, to MQW's structures is of significant experimental interest, it is discussed in Chapter 6.

In what follows we represent the results published in Refs. [30, 31, 32, 33, 34, 35, 36, 37] without further reference to these papers.

Chapter 2

Local polariton modes in one dimension

2.1 Model

The system under consideration is a chain of atoms interacting with each other and with a scalar "electromagnetic" field. Atoms are represented by their dipole moments P_n, where the subscript n represents a position of an atom in the chain. Dynamics of the atoms is described within the tight-binding approximation with an interaction between nearest neighbors only,

$$(\Omega_n^2 - \omega^2)P_n + \Phi(P_{n+1} + P_{n-1}) = \alpha E(x_n), \tag{2.1}$$

where Φ is a parameter of the interaction, and Ω_n^2 represents a site energy. Impurities in our model differ from host atoms in this parameter only, so

$$\Omega_n^2 = \Omega_0^2 c_n + \Omega_1^2(1 - c_n), \tag{2.2}$$

where Ω_0^2 is the site energy of a host atom, Ω_1^2 describes an impurity, c_n is a random variable taking values 1 and 0 with probabilities $1 - p$ and p, respectively. Parameter p, therefore, sets a concentration of the impurities in our system. This choice of the dynamical equation corresponds to exciton-like polarization waves, phonon-like situation can be presented in the form similar to Eq. (2.1) with $\Omega_n^2 = \Omega_0^2 + (1 - c_n)(1 - M_{def}/M_{host})\omega^2$, where M_{def} and M_{host} are masses of defects and host atoms, respectively.

Polaritons in the system arise as collective excitations of dipoles (polarization waves) coupled to the scalar "scalar" electromagnetic wave, $E(x_n)$, by means of a coupling parameter α. The electromagnetic subsystem is described by the following equation of motion

$$\frac{\omega^2}{c^2}E(x) + \frac{d^2E}{dx^2} = -4\pi\frac{\omega^2}{c^2}\sum_n P_n\delta(na - x), \tag{2.3}$$

where the right hand side is a the polarization density caused by atomic dipole moments, c is speed of the wave in vacuum. The coordinate x in Eq. (2.3) goes along the chain with the interatomic distance a. Eqs. (2.1) and (2.3) present *microscopic* description of the transverse electromagnetic waves propagating along the chain in a sense that it does not

make use of the concept of the dielectric permeability, and takes into account all modes of the field including those with wave numbers outside of the first Brillouin band.

This approach enables us to address several mathematical questions. A local state is usually composed of states with all possible values of wave numbers k. States with large k cannot actually be considered within macroscopic dielectric function theory, and attempts of doing so lead to diverging integrals that have to be renormalized. The renormalization procedure is rather arbitrary [18]. In our approach all expressions are well defined, so we can check if a contribution from large k is important, and if long wave approximation gives reliable results. Calculation of the integrals appearing in the theory in the 3D situation requires knowledge of detailed information about the spectrum of excitations of a crystal in the entire Brillouin band. This makes analytical consideration practically infeasible. In our 1D model we can carry out the calculations analytically (in a single-impurity case) and examine the influence of different factors (and approximations) upon the frequency of a local state and the transmission coefficient. Using a certain caution, the obtained results can be used to assess approximations in 3D situations.

2.2 Local polariton modes

Let us first derive an equation for the frequency of the local polariton state in the case when only one impurity is present. In this case Eq. (2.1) can be presented in the form

$$(\Omega_0^2 - \omega^2)P_n + \Phi(P_{n+1} + P_{n-1}) + \Delta\Omega^2\delta_{n,n_0}P_n = \alpha E(x_n), \tag{2.4}$$

where $\Delta\Omega^2 = \Omega_1^2 - \Omega_0^2$ in the exciton-like case and $\Delta\Omega^2 = (1 - M_{def}/M_{host})\omega^2$ in the phonon-like situation; the respective term describes an impurity at n_0-th site. Let us introduce Fourier transforms for site dipole moments

$$P_n = \frac{1}{N}\sum_k \exp(ikna)\, P_k \tag{2.5}$$

and the field

$$E(x) = \sum_k \exp(ikna)\, E_k, \tag{2.6}$$

where the wave number k runs over the first Brillouin band in Eq. (2.5), and from $-\infty$ to $+\infty$ in Eq. (2.6). Making use of the Fourier transforms and combining Eqs. (2.1) and (2.3) one can arrive at the following expression for P_k

$$\left[\omega^2 - \Omega_0^2 - 2\Phi\cos(ka) - \frac{4\pi\alpha\omega^2}{ac^2}\sum_\kappa \frac{1}{\dfrac{\omega^2}{c^2} - \left(k + \dfrac{2\pi\kappa}{a}\right)^2}\right] P_k = \Delta\Omega^2 P_{n_0}\, e^{-ikn_0a}, \tag{2.7}$$

where k belongs to the first Brillouin band, $-\pi/a < k < \pi/a$, and κ is an arbitrary integer representing the number of a band. The sum over κ takes into account short wave components of the electromagnetic field, and can be calculated exactly in 1D situation. Finally, one obtains for the polarization the following equation

$$P_n = \Delta\Omega^2 P_{n_0}\frac{1}{N}G(n - n_0), \tag{2.8}$$

where $G(n-n_0)$ is a Green's function of a pure system describing the response of the system to the external excitation of the atomic component, and reads as

$$G(n-n_0)=\sum_k \frac{\left[\cos(ak)-\cos(\frac{a\omega}{c})\right]\ e^{ik(n-n_0)a}}{\left[\omega^2-\Omega_0^2-2\Phi\cos(ka)\right]\left[\cos(ak)-\cos(\frac{a\omega}{c})\right]-\frac{2\pi\alpha\omega}{c}\sin(\frac{a\omega}{c})}. \tag{2.9}$$

If one neglects the term responsible for the coupling with the electromagnetic field, the Green's function $G(n-n_0)$ is reduced to that of the pure atomic system. This fact reflects the nature of the defect in our model: it disturbs only mechanical (not related to interaction with the field) properties of the system. For $n=n_0$, Eq. (2.8) has a nonzero solution only if the following equation holds

$$\frac{a\,\Delta\Omega^2}{2\pi}\int_{-\pi/a}^{\pi/a}\frac{\cos(ak)-\cos(\frac{a\omega}{c})}{\left[\omega^2-\Omega_0^2-2\Phi\cos(ka)\right]\left[\cos(ka)-\cos(\frac{a\omega}{c})\right]-\frac{2\pi\alpha\omega}{c}\sin(\frac{a\omega}{c})}dk=1 \tag{2.10}$$

where we replaced the sum over k with an integral according to the standard rule: $(1/N)\sum \Rightarrow (a/2\pi)\int$. This is the sought equation for the eigenfrequency of the local mode. It has a real-value solution only if the solution falls into the gap between the upper and the lower polariton branches. This gap exists only if the parameter Φ in the dispersion equation of the polariton waves is positive, and the effective mass of the excitations in the longwave limit is, therefore, negative.

The integral in Eq. (2.10) can be calculated exactly, and yields the following form for the dispersion equation

$$1=\Delta\Omega^2\frac{1}{2\Phi D(\omega)}\left[\frac{\cos(\frac{a\omega}{c})-Q_2(\omega)}{\sqrt{Q_2^2(\omega)-1}}-\frac{\cos(\frac{a\omega}{c})-Q_1(\omega)}{\sqrt{Q_1^2(\omega)-1}}\right], \tag{2.11}$$

where $Q_{1,2}(\omega)$,

$$Q_{1,2}(\omega) = \frac{1}{2}\left[\cos(\frac{a\omega}{c})+\frac{\omega^2-\Omega_0^2}{2\Phi}\right]\pm\frac{1}{2}D(\omega), \tag{2.12}$$

$$D(\omega) = \sqrt{\left[\cos(\frac{a\omega}{c})-\frac{\omega^2-\Omega_0^2}{2\Phi}\right]^2-\frac{4\pi\alpha\omega}{\Phi c}\sin(\frac{a\omega}{c})}, \tag{2.13}$$

give the poles of the integrand in Eq. (2.10). The bottom of the polariton gap is determined by the condition $D(\omega)=0$ yielding in the longwave limit, $a\omega/c\ll 1$, for the corresponding frequency, ω_l,

$$\omega_l^2\simeq\tilde{\Omega}_0^2-2\tilde{\Omega}_0^2 d\frac{\sqrt{\Phi}a}{c}, \tag{2.14}$$

where we introduce the parameters $d^2=4\pi\alpha/a$, $\tilde{\Omega}_0^2=\Omega_0^2+2\Phi$, and take into account that the band width of the polarization waves, Φ, obeys inequality $\sqrt{\Phi}a/c\ll 1$. The last term in this expression is the correction to the bottom of the polariton gap due to the interaction with the transversal electromagnetic field. Usually this correction is small, but it has an important theoretical, and, in the case of strong enough spatial dispersion and the oscillator strength, practical significance [17]. Because of this correction the polariton gap starts at a frequency, when determinant $D(\omega)$ becomes imaginary valued, but functions $Q_{1,2}(\omega)$ are still less than 1. This leads to the divergency of the right-hand side of Eq. (2.11) at ω

approaching ω_l, and, hence, to the absence of the threshold for the solution of this equation. This divergency is not an 1D effect since the same behavior was also found in 3D isotropic model[17, 38]. An asymptotic form for Eq. (2.11) when $\omega \longrightarrow \omega_l$ in 1D situation reads

$$\sqrt{\omega^2 - \omega_l^2} \sim \frac{\Delta\Omega^2}{\sqrt{\Phi}} \tag{2.15}$$

and differs by the factor of $\left(d\omega_l a)/(c\sqrt{\Phi}\right)$ from the 3D case. Cancelation of the latter factor occurs because of the singular behavior of the density of state of the polarization waves in 1D situation. The upper boundary of the gap, ω_{up}, is determined by the condition $Q_1(\omega) = 0$, leading to

$$\omega_{up}^2 = \tilde{\Omega}_0^2 + d^2, \tag{2.16}$$

Eq. (2.11) also has a singularity at the $\omega \longrightarrow \omega_{up}$, but this singularity is exclusively caused by 1D nature of the system, and we will discuss local states that are not too close to the upper boundary in order to avoid manifestations of purely 1D effects.

For frequencies deeper inside the gap, Eq. (2.10) can be simplified in the approximation of the small spatial dispersion, $\sqrt{\Phi}a/c \ll 1$, to yield

$$\omega^2 = \tilde{\Omega}_1^2 - \Delta\Omega^2 \left[1 - \sqrt{\frac{\omega^2 - \tilde{\Omega}_0^2}{\omega^2 - \tilde{\Omega}_0^2 + 4\Phi}}\right] - d^2 \frac{\omega a}{2c} \frac{\Delta\Omega^2}{\sqrt{\left(\omega^2 - \tilde{\Omega}_0^2\right)\left(\tilde{\Omega}_0^2 + d^2 - \omega^2\right)}}, \tag{2.17}$$

where $\tilde{\Omega}_1^2 = \Omega_1^2 + 2\Phi$ is a fundamental ($k = 0$) frequency of a chain compounded from impurity atoms only. Two other terms in Eq. (2.17) present corrections to this frequency due to the spatial dispersion and the interaction with the electromagnetic field respectively. One can see that both corrections have the same sign and shift the local frequency into the region between $\tilde{\Omega}_0^2$ and $\tilde{\Omega}_1^2$. As we shall see below this fact is significant for transmission properties of the chain.

2.3 Resonant tunneling via LPM's

In order to consider transport properties of the model, one has to subject Eqs. (2.1) and (2.3) to the boundary conditions for the electromagnetic and polarization subsystems. We assume that an incident and transmitted electromagnetic waves propagate in vacuum so that the boundary conditions for Eq. (2.3) take the usual form

$$\begin{aligned} E(0) &= 1 + r; & \frac{dE}{dx} &= ik_\omega(1 - r) \\ E(L) &= t\exp(ik_\omega L); & \frac{dE}{dx} &= ik_\omega t\exp(ik_\omega L), \end{aligned} \tag{2.18}$$

where $k_\omega = \omega/c$ is a wave number of the electromagnetic wave in vacuum, $\mid t \mid^2$ and $\mid r \mid^2$ are transmission and reflection coefficients, respectively, and L is the length of the chain. The boundary conditions (BC) for dipole excitations can be chosen in the form

$$P_0 = P_N = \gamma, \tag{2.19}$$

where $0 \leq \gamma \leq 1$; $N = L/a$ is the number of sites in the chain. $\gamma = 1$ corresponds to the chain with relaxed boundary conditions; $\gamma = 0$ corresponds to the case with fixed terminal points, which in theory of exciton-polaritons is known as Pekar's boundary conditions[39]. In fact, after examining both types of BC, we found that the average (over different realizations) value of transmission coefficient is not sensitive to the particular choice of BC, but it convenient in the current context to choose it in the form $P_0 = P_N = 0$.

Our first goal in treating the problem of the resonance tunneling is to convert the differential equation (2.3) into a discrete form. We can do so considering separately free propagation of electromagnetic waves between sites and its scattering due to the interaction with a dipole moment at the site. Let E_n and E'_n be the magnitude of the electromagnetic field and its derivative right after scattering at the n-th site. The electric field, E, remains continuous at a scattering site, while its derivative undergoes the jump, which is equal to $-4\pi k_\omega^2 P_n$. Finally, one can derive the system of difference equations, that can be written with the use of the transfer matrix, T, in the form:

$$v_{n+1} = T_n v_n, \tag{2.20}$$

where we introduced the column vector, v_n, with components P_n, P_{n+1}, E_n, D_n ($D_n = E'_n/k_\omega$) and the transfer matrix, T_n, that describes the propagation of the vector between adjacent sites:

$$T_n = \begin{pmatrix} 0 & 1 & 0 & 0 \\ -1 & -\dfrac{\Omega_n^2 - \omega^2}{\Phi} & \dfrac{\alpha}{\Phi}\cos ka & \dfrac{\alpha}{\Phi}\sin ka \\ 0 & 0 & \cos ka & \sin ka \\ 0 & -4\pi k & -\sin ka & \cos ka \end{pmatrix}. \tag{2.21}$$

The dynamical state of the system at the right end of the chain, which is represented by the vector v_N, can be found from the initial state at the left end, v_0, by means of the repetitive use of the transfer matrix, T:

$$v_N = \prod_1^N T_n v_0. \tag{2.22}$$

Eigenvalues of the T-matrix determine the eigenfrequencies of the respective pure system. There exist four eigenvalues λ, which can be grouped in pairs with the product of the members of each pair being equal to one. The eigenvalues can be found as solutions of the following dispersion equation:

$$\left(\lambda + \lambda^{-1} - 2\cos ka\right)\left(\lambda + \lambda^{-1} + \frac{\Omega^2 - \omega^2}{\Phi}\right) + \frac{\alpha k}{\Phi}\sin(ka) = 0. \tag{2.23}$$

In the band of propagating states, the solutions of Eq. (2.23) are complex valued numbers with their absolute values equal to one. In this case the expression $\lambda + \lambda^{-1}$ can be presented in the form $2\cos(Qa)$, and with this replacement the dispersion equation (2.23) takes the same form as the equation for poles of the Green's function, obtained above, Eq. (2.9). In the band gap of the polariton spectrum, the eigenvalues λ become real valued and describe evanescent modes of the system.

Analytical calculation of the transmission coefficient in the considered situation is not feasible even in the case of a single impurity because of too cumbersome algebra. The problem, however, can be considerably simplified if one neglects spatial dispersion of the

polarization waves. In this case T-matrix can be reduced to a 2×2 matrix of the following form

$$\tau_n = \begin{pmatrix} \cos ka & \sin ka \\ -\sin ka + \beta_n \cos ka & \cos ka + \beta_n \sin ka \end{pmatrix}, \tag{2.24}$$

where the parameter β_n

$$\beta_n = \frac{4\pi\alpha\omega}{c\left(\omega^2 - \Omega_n^2\right)}; \tag{2.25}$$

represents the polarizability of the n-th atom due to its vibrational motion. When the spatial dispersion is absent one only needs the regular Maxwell boundary conditions given by Eq. (2.18) to express the complex transmission coefficient, t, in terms of elements of the resulting transfer matrix, $T^{(N)} = \prod_1^N \tau_n$,

$$t = \frac{2}{\left(T_{11}^{(N)} + T_{22}^{(N)}\right) - i\left(T_{12}^{(N)} - T_{21}^{(N)}\right)} e^{-ikL}. \tag{2.26}$$

In the case of a single impurity the product of the transfer matrices, τ, can be presented in the following form

$$T^{(N)} = \tau^{N-n_0} \times \tau_{def} \times \tau^{n_0-1}. \tag{2.27}$$

where the matrix τ_{def} describes the impurity atom with $\Omega_n = \Omega_1$. The matrix product in Eq. (2.27) is conveniently calculated in the basis, where the matrix τ is diagonal. After some cumbersome algebra one arrives at the following expression for the transmission coefficient, t:

$$t = \frac{2e^{ikL}\exp\left(-\kappa L\right)}{\left[1 - \frac{i}{\sqrt{D}}\left(2 - \beta\cot ka\right)\right]\left[(1+\varepsilon)\right] + 2i\exp\left(-\kappa L\right)\Gamma\cosh\left[\kappa a(N - 2n_0 + 1\right]}. \tag{2.28}$$

where $D = \beta^2 + 4\beta\cot(ak) - 4$, $\Gamma = \varepsilon\beta/(\sin(ka)\sqrt{D})$, $\kappa = |\ln(\lambda)|/a$ is the inverse localization length of the local state, and $\varepsilon = \left(\beta_{def} - \beta\right)/2\sqrt{D}$. The last parameter reflects the difference between host atoms and the impurity, and is equal to

$$\varepsilon = \frac{2\pi\alpha}{c\sqrt{D}}\omega\frac{\left(\Omega_1^2 - \Omega_0^2\right)}{\left(\omega^2 - \Omega_0^2\right)\left(\omega^2 - \Omega_1^2\right)}. \tag{2.29}$$

We have also neglected here a contribution from the second eigenvalue of the transfer matrix, which is proportional to $\exp(-2\kappa L)$, and is exponentially small for sufficiently long chains. For $\varepsilon = 0$ one has the transmission coefficient, t_0, of the pure system,

$$t_0 = \frac{2e^{ikL}\exp\left(-\kappa L\right)}{1 - \frac{i}{\sqrt{D}}\left(2 - \beta\cot ka\right)}, \tag{2.30}$$

exhibiting a regular exponential decay. At the lower boundary of the polariton gap, Ω_0, parameters β and κ diverge, leading to a vanishing transmission at the gap edge regardless the length of the chain. It is instructive to rewrite Eq. (2.28) in terms of t_0:

$$t = \frac{t_0}{(1+\varepsilon) + i\exp\left(-ikL\right)\Gamma t_0\cosh\left[\kappa a(N - 2n_0 + 1\right]} \tag{2.31}$$

This expression describes the resonance tunneling of the electromagnetic waves through the chain with the defect. The resonance occurs when

$$1 + \varepsilon = 0, \tag{2.32}$$

the transmission in this case becomes independent of the system size. Substituting the definition of the parameter ε given by Eq. (2.29) in Eq. (2.32) one arrives at the equation identical to Eq. (2.17) for the frequency of the local polariton state with the parameter of the spatial dispersion, Φ, being set to zero. The transmission takes a maximum value of unity when the defect is placed in the middle of the chain, $N - 2n_0 + 1 = 0$. The width of the resonance is proportional to Γt_0 and it exponentially decreases with an increase of the system's size. It is interesting to note that the transmission becomes exactly equal to one at frequency ω_T that is exponentially shifted from the frequency ω_{def} satisfying Eq. (2.32). The detailed consideration of this phenomenon we postpone until Chapter 6.

Having solved the transmission problem we can find the magnitude of the field inside the chain in terms of the incident amplitude E_{in} at the resonance frequency. Spatial distribution of the field in the local polariton state can be found from Eqs. (2.3), (2.8), and (2.9) to have the form $E = E_d \exp[-(n - n_0)\kappa a]$. Matching this expression with the outcoming field equal to $E_{in} t \exp(ikL)$ for the field amplitude at the defect atom we have

$$E_d = E_{in} t \exp(-ikL) \exp[(N - n_0)\kappa a]. \tag{2.33}$$

For $|t|$ being of the order of one in the resonance this expression describes the drastic exponential enhancement of the incident amplitude at the defect side due to the effect of the resonance tunneling.

2.4 One-dimensional dipole chain with macroscopical concentration of impurities: numerical simulations.

In this section we present the numerical simulations of the transport properties through the chain in the case of randomly distributed identical defects. The transfer matrix equation (2.20) along with the definition of the transfer matrix Eq. (2.21) and boundary conditions given by Eq. (2.18) and Eq. (2.19) provides a basis for our computations. However, it turns out that straightforward use of Eq. (2.20) in the gap region is not possible because of underflow errors arising when one pair of eigenvalues of the transfer matrix becomes exponentially greater than the second one. In order to handle this problem in Appendix we develop a new computational approach based upon the blend of the transfer-matrix method with the invariant embedding ideas [40].

In our simulations we fix the concentration of the defects and randomly distribute them among the host atoms. The total number of atoms in the chain is also fixed; the results presented below are obtained for a chain consisting of 1000 atoms. For a given choice of the defect frequency, Ω_1,the localization length of the local polariton state, l_{ind},is approximately equal to 150 interatomic distances. The transmission coefficient is found to be extremely sensitive to a particular arrangements of defects in a realization exhibiting strong fluctuations from one realization to another. Therefore, in order to reveal the general features of the transmission independent of particular positions of defects, we average the transmission over 1000 different realizations. We have also calculated the averaged Lyapunov exponent (the

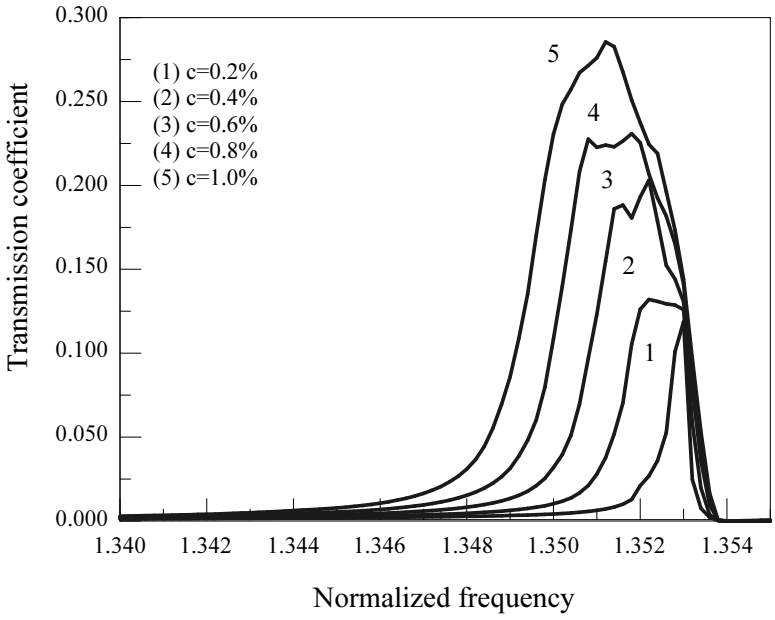

Figure 2.1: Frequency dependence of the averaged transmission coefficient for small concentrations of the defects. The frequency is normalized by the fundamental ($k = 0$) frequency of the pure chain, Ω_0. The low-frequency boundary of the polariton gap is at $\omega \approx 1.3$ and is not shown here.

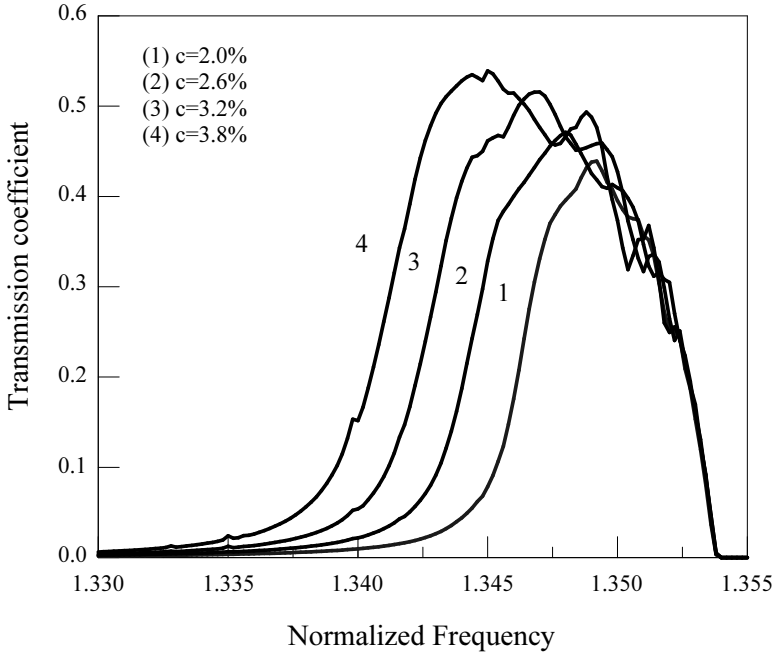

Figure 2.2: The same as in Fig. 2.1 but for intermediate concentrations.

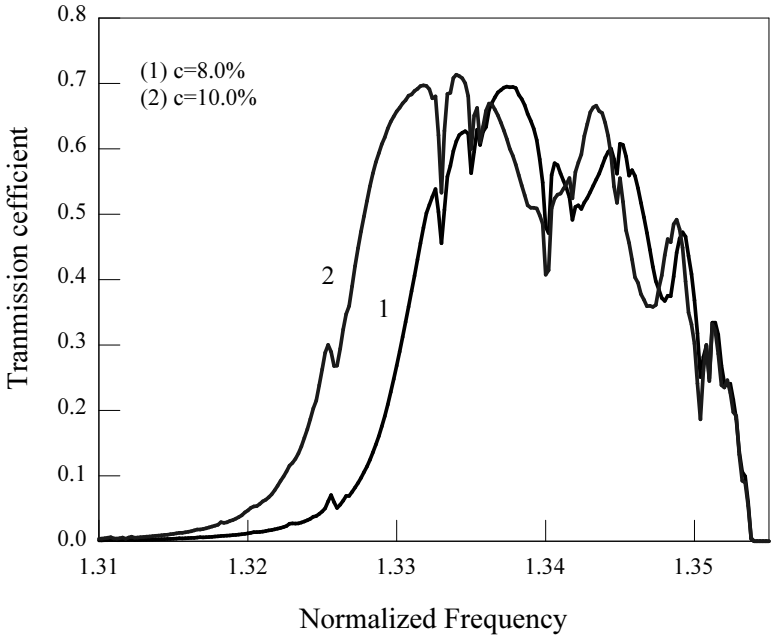

Figure 2.3: The same as in Fig. 2.1 but for large concentrations.

inverse localization length, l_{chain}, characterizing transport through the entire chain) to verify that the averaged transmission reveals a reliable information about transport properties of the system.

The results of the computations are presented in Figs. 2.1, 2.2, 2.3, 2.4, and 2.5. The first three figures show the evolution of the transmission with the increase of the concentration of the impurities. In Fig. 2.1 one can see the change of the transport properties at small concentrations up to 1%. The curve labeled (1) shows, basically, the single impurity behavior averaged over random positions of the defect. With an increase of the concentration there is a greater probability for two (or more) defects to form a cluster resulting in splitting a single resonance frequency in two or more frequencies. The double peak structure of the curves (2) and (3) reflects these cluster effects. With the further increase of the concentration the clusters' sizes grow on average leading to multiple resonances with distances between adjacent resonance frequencies being too small to be distinguished. Curve (5) in Fig. 2.1 reflects this transformation, which marks a transition between individual tunneling resonances and the defect induced band. The concentrations in this transition region is such that an average distance between the defects is equal to the localization length of the individual local states, l_{ind}. The collective localization length at the frequency of the transmission peak, $l_{chain}^{\max}$, becomes equal to the length of the chain at approximately the same concentration that allows to suggest the simple relationships between the two lengths: $l_{chain}^{\max} = cl_{ind}$, where c stands for the concentration. The numerical results presented in Fig. 2.4 clearly demonstrate this linear concentration dependence of $l_{chain}^{\max}$ at small concentrations. For larger concentrations as one can see from Figs. 2.2 and 2.3 the peak on the transmission coefficient is not so well defined marking further development of IPB. Curves in Fig. 2.2 show the transmission coefficient at intermediate concentrations, where localization length, l_{chain}, is bigger than

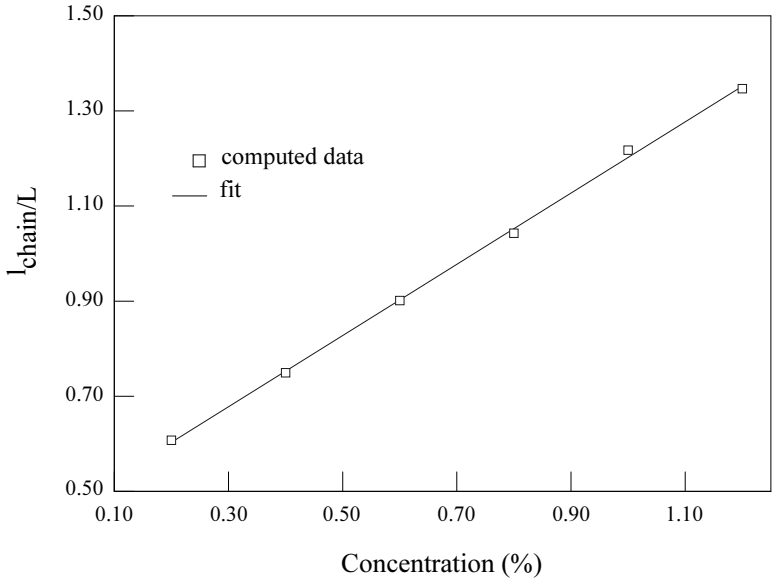

Figure 2.4: Concentration dependence of the collective localization length, l_{chain}, normalized by the system's size L.

the length of the system only in a small frequency region around the maximum of the transmission, and Fig. 2.3 presents well developed IPB with multipeak structure resulting from geometrical resonances at the boundaries of the system.

This figures reveal an important feature of the IPB: its right edge does not move with an increase of the concentration. The frequency of this boundary is exactly equal to the defect frequency, Ω_1, (which is normalized by Ω_0 in the figures), and the entire band is developing to the left of Ω_1 in complete agreement with the arguments based upon analytical solution of the single-impurity problem. Moreover, the magnitude of the transmission in the vicinity of $\Omega_1$decreases with an increase of the concentration also in agreement with our remarks at the end of the previous section. Fig. 2.5 presents the inverse localization length, l_{chain}, normalized by the length of the chain for three different concentrations. It can be seen that the inverse localization length at $\Omega_1$significantly grows with an increase of the concentration, reaching the value of approximately $17/L$ at the concentration as small as 3%. Such a small localization length corresponds to the transmission of the order of magnitude of 10^{-17}, which is practically zero in our computation. Further increase of the concentration does not change the minimum localization length. These results present an interesting example of the defects building up their forbidden gap.

From Fig. 2.5 it is also seen the development of the pass band to the left of Ω_1 presented above in Figs. 2.1, 2.2, 2.3, but at a larger scale. We can not distinguish here the details of the frequency dependence, but the transition from the single resonance behavior to IPB, marked by the significant flattening of the curve, is clear.

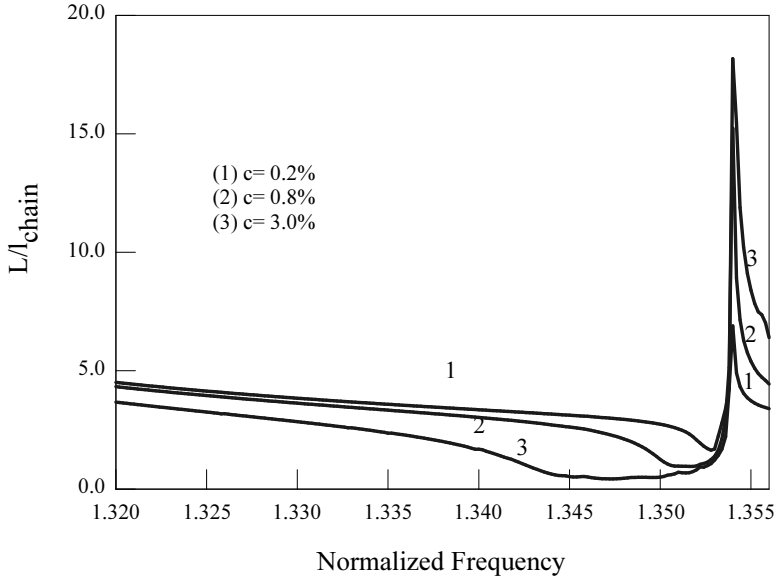

Figure 2.5: Frequency dependence of the Lyapunov exponent of the entire chain for several concentrations in the frequency region of the defect band.

2.5 Discussion

Equation (2.31) demonstrates that the resonance tunneling via local polariton states is remarkably different from other types of resonance tunneling phenomena, such as electron tunneling via an impurity state [41], or through a double barrier. The most important fact is that the frequency profile of the resonance does not have the typical symmetric Laurentian shape. At $\omega = \Omega_1$ the parameter ε diverges causing the transmission to vanish. At the same time the resonance frequency ω_T is very close to Ω_1 as it follows from Eq. (2.17). This results in strongly asymmetric frequency dependence of the transmission, which is skewed toward lower frequencies. Though the transmission vanishes precisely at two frequencies: at the low frequency band edge Ω_0 and at the frequency Ω_1 associated with the vibrational motion of the defect atom, the way it happens is remarkably different. At the band edge the transmission behaves as $(\omega^2-\Omega_0^2)^2 \exp\left(-1/\sqrt{\omega^2-\Omega_0^2}\right)$ while at the defect frequency it goes to zero simply as $(\omega^2-\Omega_1^2)^2$. These facts can be used to predict several effects that can occur with increase of the concentration of the defects. First, one can note that with the increase of the concentration of the impurities frequency Ω_1 eventually becomes the boundary of the new polariton gap when all original host atoms will be replaced by the defect atoms. One can conclude that the zero in the transmission at Ω_1 instead of being washed out by the disorder, would become more singular. In other words one should expect that the frequency dependence of the transmission in the vicinity of Ω_1 will exhibit a crossover from simple power decrease to more singular behavior associated with the band edge. Secondly, if factors preventing transmission from exact vanishing (spatial dispersion, damping) are taken into account, one should expect substantial suppressing of the transmission in the vicinity of Ω_1 with an increase of the concentration of the defects. Surprisingly enough, numerical calculations show that this effect does take place even at rather small concentration of the

defects. In Chapter 4 we will return to this problem when we will consider the formation of IPB in 3D mixed crystals.

Resonant tunneling is very sensitive to the presence of relaxation, which phenomenologically can be accounted for by adding $2i\gamma\omega$ to the denominator of the polarizability β. This will make the parameter ϵ complex valued, leading to two important consequences. First, the resonance condition becomes $Re(\varepsilon) = -1$, and it can be fulfilled only if the relaxation is small enough. Second, the imaginary part of ε will prevent the exponential factor t_0 in Eq.(2.31) from canceling out at the resonance. This restricts the length of the system in which the resonance can occur and limit the enhancement of the field at the defect. Since we only concern with a frequency region in the vicinity of Ω_1, real, ε_1, and imaginary, ε_2, parts of ε can be approximately found as

$$\varepsilon_1 \simeq d^2 \frac{\Omega_1 a}{2c} \sqrt{\frac{\Delta\Omega^2}{d^2 - \Delta\Omega^2}} \frac{\omega^2 - \Omega_1^2}{\left(\omega^2 - \Omega_1^2\right)^2 + 4\gamma^2\omega^2} \tag{2.34}$$

$$\varepsilon_2 \simeq \frac{2\gamma\omega}{\omega^2 - \Omega_1^2}\varepsilon_1 \tag{2.35}$$

It follows from Eq. (2.34) that the resonance occurs only if $(4\gamma c)/(ad^2) < 1$. This inequality has a simple physical meaning: it ensures that the distance between the resonance frequency, ω_T, and Ω_1, where the transmission goes to zero, is greater than the relaxation parameter γ. This is a strict condition that can only be satisfied for high frequency oscillations with large oscillator strength in crystals with large molecules in an elementary cell, and respectively large values of the interatomic spacing a. Another interesting opportunity can arise in so called atomic optical lattices, where atoms, trapped by a laser beam, form a lattice with spacing practically equal to the wavelength of the trapping field [42, 43, 44]. However, taking into account the spatial dispersion can lead to a more favorable situation for the tunneling resonance in our model. As one can see from numerical results of [19] and the present work, spatial dispersion does not change the transmission properties significantly. Therefore, one can rely upon Eq. (2.31) to estimate the effect of the dissipation in the presence of the spatial dispersion, assuming that it only modifies the parameter ε. According to Eq. (2.17), the interaction moves the resonance frequency farther away from Ω_1 undermining the influence of the damping and leading to weaker inequality $(\gamma\Omega_1)/\Phi < 1$. This condition can be fulfilled, even for phonons with a relatively small negative spatial dispersion, and becomes even less restrictive in the case of Frenkel excitons in molecular crystals.

For the imaginary part ε_2 at the resonance one can obtain from Eq. (2.35) the following estimate

$$\varepsilon_2 \sim \min[(4\gamma c)/(ad^2), (\gamma\Omega_1)/\Phi] \tag{2.36}$$

The requirement that ε_2 be much smaller than t_0 leads to the following restriction for the length of the system $L \ll (1/\kappa) \mid \ln[\varepsilon_2] \mid$, with ε_2 given above. The maximum value of the field at the defect site attainable for the defect located in the center of the chain is then found as $|E_d| \sim |E_{in}||t|/\sqrt{\varepsilon_2}$.

Chapter 3

Impurity polariton band in one dimension

3.1 The model of one-dimensional polaritons and the method of calculation

In the case of a single impurity with the resonance frequency Ω_1 we showed in Chapter 2 that the position of the local impurity state in the long-wave limit $a\omega/c \ll 1$ is determined by Eq. (2.17), where the last term describes the shift of the local frequency from the resonance frequency Ω_1 of the impurity due to coupling to the electromagnetic field. In the case of the atomic interpretation of the model, this radiative shift is very small, but taking into account the direct interaction between the atoms (the spatial dispersion of atomic excitations) moves the local frequency farther away from Ω_1. Eq. (2.17), however, can also be applied to MQW's in the case of so called short-period structures. In this case as we will show in Chapter 6 the radiative shift described by Eq. (2.17) can be made large enough to be observed experimentally. The transmission coefficient through the chain passes through the maximum at ω_T close to ω_{loc} and goes to zero at Ω_1. For experimental observation of this effect it is sufficient to have the radiative shift greater than homogeneous broadening of the QW exciton resonance at Ω_1.

The main object of interest in this Chapter is the properties of IPB in the case of finite concentration of impurities. It is characterized by Lyapunov exponent (LE), λ, which in our case can be defined as [20]

$$\lambda = \lim_{L\to\infty} \frac{1}{L} \ln \frac{\left\| \prod_1^N \hat{\tau}_n v_0 \right\|}{\|v_0\|}, \tag{3.1}$$

where L is the total length of the chain consisting of N atoms. It is well-known that the quantity defined by Eq. (3.1) is non-random (self-averages). It characterizes the spatial extent of the envelope of system eigenstates, all of which are localized in one dimension (see Ref. [45] and references therein). The same quantity also describes the typical value of the transmission coefficient, T, of an external excitation incident upon the system: $T_{typ} \simeq \exp(-\lambda L)$, and through the Thouless relation [46] it determines DOS of the system. Calculation of LE in the spectral region of the polariton gap of the pure system is the main task of this section.

3.1.1 The method of microcanonical ensemble

The major problem with calculating of LE or DOS in the region of impurity bands is that a simple concentration expansion is not able to describe the impurity band. Electron and phonon impurity bands have been intensively studied in the past (see, for example, Ref. [45]). In the limit of extremely small concentration of impurities, $(pl_0)/a \ll 1$, it was proved possible to provide a regular systematic of the arising states and use statistical arguments to describe their DOS [7]. Another method used for this type of calculations employed the so-called phase formalism (see Ref. [45] and references therein). This approach allowed one to calculate DOS of impurity bands in different spectral regions, including exponential behavior at the tails of the band for both small and large, $(pl_0)/a \gg 1$, concentrations. In the case of LPM's the localization length, l_0, of an individual local state can be so large that one has to deal with the situation described by the latter inequality even in the case of a rather small concentration of impurities. Therefore, in this Chapter we focus mainly upon the properties of the well-developed IPB when individual LPM's are overlapped. To this end we use the method of the microcanonical ensemble, which was first suggested for analytical calculations of LE in a one-dimensional single-band model of a disordered alloy [20]. The advantage of this method over other methods of DOS calculations is that it allows one to calculate simultaneously both DOS and the localization length. Its main shortcoming is that, as we shall see later, this method is a version of "effective media" methods, and as such it is unable to describe DOS near fluctuation boundaries of the spectrum. At the same time the results obtained allow a clear physical interpretation and, as follows from comparison with numerical simulations, they quite accurately describe properties of the bulk of the impurity band.

The starting point of our calculations is the general definition of LE given by Eq. (3.1). In spite of LE being a self-averaging quantity, it is convenient in practical calculations to perform averaging over the random configurations of the impurities. The regular ensemble of the realization is described by the fixed concentration of the impurities p, while their total number can vary from realization to realization. Therefore one can distinguish two causes for fluctuations: (1) local arrangements of the impurities and (2) the total number of the impurities. The main idea of the method of microcanonical ensemble is to reduce the finite size fluctuations in the system, eliminating the fluctuations of the total number of impurities. Such an ensemble with a fixed number of impurities is called the microcanonical ensemble in analogy with statistical physics. At the same time the result of the averaging in the limit $L \to \infty$ should not depend upon the type of ensemble used by virtue of the self-averaging nature of LE. The key idea of the microcanonical method is based on the assumption that with one cause of fluctuations eliminated, one can obtain reliable results when the microcanonical ensemble average of $\langle \ln(...) \rangle$ is replaced by $\ln\langle ... \rangle$. Such a substitution gives an exact result in the case of commutating matrices, and leads to an excellent agreement between analytical calculations and simulations in the case of 2×2 matrices with a single band spectrum [20].

Using the microcanonical ensemble, one can evaluate the average over all matrix sequences using the following expression derived in Ref. [20]:

$$\left\langle \prod_1^N \hat{\tau}_n \right\rangle = \binom{N}{pN}^{-1} \frac{1}{(pN)!} \cdot \frac{\partial^{pN}}{\partial x^{pN}} \left(\hat{\tau}_0 + x\hat{\tau}_1\right)^N \Big|_{x=0}, \tag{3.2}$$

where $\hat{\tau}_0$ and $\hat{\tau}_1$ are host and defect matrices, respectively and x is a free parameter. The

derivative in Eq. (3.2) then can be presented in the form of the Cauchy integral

$$\left\langle \prod_1^N \hat{\tau}_n \right\rangle = \binom{N}{pN}^{-1} \frac{1}{2\pi i} \int_C dx \frac{\nu^N(x)}{x^{pN+1}} \hat{D}(x), \tag{3.3}$$

where the contour of integration C is taken on the complex plane around $x = 0$, $\nu(x)$ is the largest eigenvalue of the matrix $\hat{\tau}_0 + x\hat{\tau}_1$, and the matrix $\hat{D}(x)$,

$$\hat{D}(x) = \nu^{-N}(x) \left(\hat{\tau}_0 + x\hat{\tau}_1\right)^N, \tag{3.4}$$

has eigenvalues not exceeding 1 in absolute value. In the limit of large N the above integral can be evaluated by the saddle point method. As the result we arrive at the following expression for the complex valued LE, $\widetilde{\lambda}$:

$$\begin{aligned} \widetilde{\lambda} &= \lim_{N\to\infty} \frac{1}{L} \ln \left[\text{largest eigenvalue} \left\langle \prod_1^N \hat{\tau}_n \right\rangle \right] \\ &= \frac{1}{a} \left[\ln \nu(x_0) - (1-p) \ln x_0 + p \ln p + (1-p) \ln(1-p) \right], \end{aligned} \tag{3.5}$$

where x_0 is defined by the saddle point equation

$$\left. \frac{\partial \ln \nu(x)}{\partial \ln x} \right|_{x=x_0} = p. \tag{3.6}$$

The real part of $\widetilde{\lambda}$ given by Eq. (3.5) represents LE, while its imaginary part according to Thouless [46] gives the integral density of states $N(\omega)$ in the impure system:

$$\lambda = \mathrm{Re}\left[\widetilde{\lambda}\right], \tag{3.7}$$

$$N(\omega) = -\frac{1}{\pi} \mathrm{Im}\left[\widetilde{\lambda}\right]. \tag{3.8}$$

The eigenvalues of the matrix $\hat{\tau}_0 + x\hat{\tau}_1$ can be found from the equation

$$\frac{\nu}{1+x} + \frac{1+x}{\nu} = \kappa(x) = 2\cos(ka) + \frac{\beta_0 + x\beta_1}{1+x}, \tag{3.9}$$

where β_0 and β_1 are polarizabilities of the host and defect atoms, respectively.

It is convenient to rewrite Eqs. (3.5) and (3.9) in terms of a new variable $y = x/(1+x)$:

$$\kappa(y) = (1-y)\nu(y) + \frac{1}{(1-y)\nu(y)} = \kappa_0(\omega) + yF(\omega), \tag{3.10}$$

$$\kappa_0(\omega) = 2\cos(ka) + d^2 ka \sin(ka) \frac{1}{\omega^2 - \Omega_0^2}, \tag{3.11}$$

$$F(\omega) = d^2 ka \sin(ka) \frac{\Omega_1^2 - \Omega_0^2}{(\omega^2 - \Omega_0^2)(\omega^2 - \Omega_1^2)}. \tag{3.12}$$

In the long-wave limit $\epsilon = ka \ll 1$ functions $F(\omega)$ and $\kappa_0(\omega)$ can be simplified and presented in the form, which clarifies their physical meaning:

$$\begin{aligned} F(\omega) &\simeq \epsilon^2 f(\omega), \\ \kappa_0(\omega) &\simeq 2 + \epsilon^2 \gamma(\omega), \end{aligned}$$

where $f(\omega)$ is defined according to

$$f(\omega) \simeq \frac{d^2(\Omega_1^2 - \Omega_0^2)}{(\omega^2 - \Omega_0^2)(\omega^2 - \Omega_1^2)} \tag{3.13}$$

and represents the difference $\beta_1 - \beta_0$ between polarizabilities (2.25) of the impurities and host atoms. Function $\gamma(\omega)$ defined as

$$\gamma(\omega) = 1 + \frac{d^2}{\Omega_0^2 - \omega^2} \tag{3.14}$$

is the longwave dielectric function of the pure chain.

Similarly, Eq. (3.5) transforms into

$$\widetilde{\lambda}(p) = \ln\left[(1 - y_0(p))\nu\left(y_0(p)\right)\right] - \left[p \ln \frac{y_0\,(p)}{p} + (1-p)\ln\frac{1 - y_0\,(p)}{1-p}\right], \tag{3.15}$$

with the saddle point equation reading as

$$\pm \frac{y(1-y)F}{\sqrt{\left(\kappa_0 + yF\right)^2 - 4}} + y \Bigg|_{y=y_0} = p, \tag{3.16}$$

The choice of the sign in Eq. (3.16) is determined by the requirement to use the greatest of the eigenvalues ν. Introduction of the new variable y turns $\kappa\,(y)$ in a linear function of y essentially simplifying future calculations.

3.2 The Lyapunov exponent and the density of states

3.2.1 Boundaries of IPB

Dielectric function $\gamma(\omega)$ determines the frequency region of the polariton gap: for $\Omega_0^2 < \omega^2 < \Omega_0^2 + d^2$ it is negative, and hence, propagating modes do not exist in this region. We shall assume that the defect frequency Ω_1^2 obeys the inequality $\Omega_0^2 < \Omega_1^2 < \Omega_0^2 + d^2$, so that IPB develops inside the gap of the original spectrum. As we already mentioned, the approach we use below belongs to the class of effective-medium approximations since we neglect here certain kinds of fluctuations in the system. It is natural to expect, therefore, that within this approach the impurity band would have well-defined spectral boundaries outside of which the differential DOS remains exact zero. Our first goal is to determine these boundaries and find the concentration dependence of the width of IPB. The differential DOS, $\rho(\omega) = dN(\omega)/d\omega$, takes on non-zero values when $\widetilde{\lambda}(\omega)$ acquires a non-constant imaginary part. Rewriting Eq. (3.15) in the form

$$\widetilde{\lambda}(\omega) = \frac{1}{a}\left\{\ln\left[\frac{1}{2}\left(\kappa_0 + y_0 F \pm \frac{y_0(1-y_0)F}{p - y_0}\right)\right] - \left[p\ln\frac{y_0}{p} + (1-p)\ln\frac{1-y_0}{1-p}\right]\right\}, \tag{3.17}$$

one can see that in the case of real y_0, $\operatorname{Im}\widetilde{\lambda}(\omega)$ can be either zero or π (the latter happens when the argument of ln is negative). In both cases differential DOS is obviously zero, and it can only take on a non-zero value when y_0 becomes complex. Eq. (3.16), which defines y_0, is formed by a polynomial of the third order with real coefficients; therefore it has either

three real roots or one real solution and a complex conjugated pair. In order to describe formation of IPB, one has to select the root, which has a complex component in a certain frequency interval and yields positive LE. Comparison with numerical simulations shows that the choice of only one of three saddle point, according to above mentioned criteria, produces the correct description of the impurity band. It is not difficult to show that at the frequency where $y_0(\omega)$ becomes complex, the derivative $\partial y_0/\partial\omega$ diverges. This fact gives us an explicit equation for the spectrum boundaries. From Eq. (3.16) one can find that the divergence occurs when y_0 satisfies the equation

$$\begin{aligned} y_0^3 F\left[F(1-p)+\kappa_0\right] &+ y_0^2\left[\kappa_0 F(1-3p)+k_0^2-4\right] \\ &+ y_0\kappa_0\left(F-2\kappa_0^2+4\right)+p(\kappa_0^2-4)=0. \end{aligned} \tag{3.18}$$

Eqs. (3.16) and (3.18) define the concentration dependence of the boundaries of IPB. An approximate solution of this equation can be obtained as a formal series in powers of parameter $\epsilon = ka$. It will be seen, however, from the results that the actual expansion parameter in this case is $1/pl_0 \ll 1$. The solution of Eq. (3.16) with the accuracy to ϵ^2 can be obtained in the form:

$$y = p - p(1-p)\frac{f}{2\sqrt{pf-\gamma}}\epsilon + p(1-p)\frac{2\left(pf-\gamma\right)f\left(1-2p\right)-fp\left(1-p\right)}{8\left(pf-\gamma\right)^2}f^2\epsilon^2, \tag{3.19}$$

where $y = p$ is the only non-vanishing zero order approximation for y. Since two other solutions, $y = 0$, correspond to a singular point of the integral (3.3), the chosen solution $y = p$ represents the only saddle point accessible within our perturbation scheme. Using additional criteria outlined above we verify that the solution given by Eq. (3.19) correctly reproduces the behavior of LE. Substituting Eq. (3.19) into Eq. (3.15) one finds the complex LE in the long wavelength approximation:

$$\widetilde{\lambda}(\omega) = \frac{\omega}{c}\left(\sqrt{pf(\omega)-\gamma(\omega)} - \frac{p(1-p)f^2(\omega)}{8[pf(\omega)-\gamma(\omega)]}\epsilon\right). \tag{3.20}$$

According to Eq. (3.20), $\widetilde{\lambda}(\omega)$ acquires an imaginary part at frequencies obeying the inequality

$$pf(\omega)-\gamma(\omega) \le 0, \tag{3.21}$$

The boundaries are determined by the respective equation $pf(\omega)-\gamma(\omega)=0$, which coincides with the long wavelength limit of Eq. (3.18). This equation determines two points where $pf(\omega)-\gamma(\omega)$ changes sign to negative:

$$\begin{aligned} \omega_{il}^2 &= \frac{(\Omega_0^2+\Omega_1^2+d^2)-\sqrt{(\Omega_0^2+d^2-\Omega_1^2)^2+4d^2(\Omega_1^2-\Omega_0^2)p}}{2}, \\ \omega_{pu}^2 &= \frac{(\Omega_0^2+\Omega_1^2+d^2)+\sqrt{(\Omega_0^2+d^2-\Omega_1^2)^2+4d^2(\Omega_1^2-\Omega_0^2)p}}{2}. \end{aligned} \tag{3.22}$$

The first of these solutions belongs to the initial polariton band-gap and as such represents the low-frequency boundary of the new impurity band. The second one lies outside of the gap and is a bottom frequency, modified by impurities, of the upper polariton branch of the initial spectrum. These two frequencies, however, are not the only points where the

expression $pf(\omega) - \gamma(\omega)$ turns negative. Two other points are

$$\begin{aligned} \omega_{pl}^2 &= \Omega_0^2, \\ \omega_{iu}^2 &= \Omega_1^2, \end{aligned} \tag{3.23}$$

and the change of the sign at these points occurs through infinity of $pf(\omega)-\gamma(\omega)$ rather than through zero. These two frequencies do not depend upon the concentration of impurities and present, therefore, stable genuine boundaries of the spectrum. This property of Ω_0 and Ω_1 is due to their resonance nature (they correspond to the poles of the respective polarizabilities) and disappears when, for example, the spatial dispersion is taken into account. At the same time, the numerical simulations from previous Chapter, in which the spatial dispersion was taken into consideration, indicate that the shift of these frequency from their initial values is negligibly small for realistic values of the inter-atom interaction parameter Φ, even for a relatively large concentration of impurities.

These four frequencies set the modified boundaries of the initial polariton spectrum of the pure system (ω_{pl}^2, ω_{pu}^2), and boundaries of the newly formed IPB (ω_{iu}^2, ω_{il}^2). The lower boundary of the forbidden gap of the crystal, Ω_0, is not affected by the impurities - the singularity in the polariton DOS at this point survives for any concentrations of defects. The upper boundary of the band gap, ω_{pu}, shifts toward higher frequencies with the concentration and when $p = 1$, it coincides with the upper band boundary of the new crystal, $\Omega_L^i = \sqrt{\Omega_1^2 + d^2}$. Frequencies ω_{il} and ω_{iu} give approximate values for the lower and upper boundaries of the impurity induced pass band which arises inside the original forbidden gap $\Omega_0 < \omega_{il} < \omega_{iu} < \sqrt{\Omega_0^2 + d^2}$. IPB grows asymmetrically with concentration: while its lower boundary moves towards Ω_0 with an increase of the concentration, the upper edge remains fixed at $\omega_{iu} = \Omega_1$. Such a behavior of IPB agrees well with our numerical results from Chapter 2.

The width of IPB defined in terms of squared frequencies $\Delta_{im}^2 = \omega_{iu}^2 - \omega_{il}^2$ can be found from Eqs. (3.22) and (3.23) as

$$\Delta_{im}^2 = \frac{\sqrt{(\Omega_0^2 + d^2 - \Omega_1^2)^2 + 4d^2(\Omega_1^2 - \Omega_0^2)p} - (\Omega_0^2 + d^2 - \Omega_1^2)}{2}. \tag{3.24}$$

For Ω_1 not very close to the upper boundary of the initial polariton gap, $\Omega_L = \sqrt{\Omega_0^2 + d^2}$, the linear in p approximation is sufficient to describe the concentration dependence of the band width

$$\Delta_{im}^2 \approx \frac{d^2(\Omega_1^2 - \Omega_0^2)p}{\Omega_0^2 + d^2 - \Omega_1^2}. \tag{3.25}$$

When Ω_1, however, happens to be close to Ω_L, a crossover is possible from the linear dependence (3.25) to the square root behavior:

$$\Delta_{im}^2 \approx \sqrt{d^2(\Omega_1^2 - \Omega_0^2)p}. \tag{3.26}$$

The condition for such crossover to occur is

$$1 \ll p \ll \frac{(\Omega_0^2 + d^2 - \Omega_1^2)^2}{4d^2(\Omega_1^2 - \Omega_0^2)}.$$

3.2.2 The Lyapunov exponent and the density of states far from the spectrum boundaries

Using Eqs. (3.7), (3.8) and (3.20) one can calculate LE and the integral DOS for different regions of the spectrum. For allowed bands, $(0,\Omega_0)$, (ω_{il},Ω_1), (ω_{pu},∞), one has

$$\begin{aligned} \lambda(\omega) &= -\frac{p(1-p)f^2}{8\,(pf-\gamma)}\frac{\omega}{c}\epsilon + O(\epsilon^2), \\ N(\omega) &= \frac{1}{\pi}\frac{\omega}{c}\sqrt{|pf-\gamma|} + O(\epsilon^2); \end{aligned} \tag{3.27}$$

for forbidden bands, $(\Omega_0,\omega_{il}),(\Omega_1,\omega_{pu})$, we obtain

$$\begin{aligned} \lambda(\omega) &= \frac{\omega}{c}\left\{\sqrt{pf-\gamma} - \left[\frac{p(1-p)f^2}{8\,(pf-\gamma)}\right]\epsilon\right\}, \\ N(\omega) &= 0. \end{aligned} \tag{3.28}$$

One can see from Eqs. (3.27) and (3.28) that within allowed bands, DOS appears in the zero order of the formal expansion parameter ϵ, while LE starts from the first order. For the forbidden bands the situation is reversed: LE contains a term of zero order in ϵ, while DOS in this order disappears. This observation suggests a simple physical interpretation of the microcanonical approximation in conjunction with the expansion over ϵ. Analysis of the series in this parameter shows that the actual small parameter is $a/(pl_0) = l_{def}/l_0$, where l_{def} is a mean distance between impurities. The zero order expansion in this parameter can be interpreted as a uniform continuous ($l_{def} \to 0$) distribution of impurities with concentration p. The results in this approximation then corresponds to IP which would exist in such a uniform system. The parameter l_{def}/l_0 in this case is a measure of disorder in the distribution of impurities, which leads to the localization of excitations described by DOS in Eq. (3.27) with the localization length, $l^{-1} = \lambda$, presented in the first line of the same equation.

Let us now consider frequencies in the interval $\omega \in (0,\Omega_0) \cup \left(\Omega_L^i,\infty\right)$, where pass bands of the pure chains composed of either host or impurity atoms overlap. The DOS in this region can be written in a physically transparent form

$$N(\omega) = \sqrt{(1-p)\,N_0^2(\omega) + pN_1^2(\omega)}; \tag{3.29}$$

where $N_0(\omega)$ and $N_1(\omega)$ are integral DOS in pure chains containing host atoms or impurities, respectively. In the remaining portion of the initial spectrum $\omega \in \left(\omega_{up},\Omega_L^i\right)$ (but not very close to the boundary ω_{up}, where the expansion ceases to be valid) DOS can be presented as $N(\omega) = \sqrt{(1-p)\,N_0^2(\omega) - pl_1^2(\omega)}$, where l_1 is the penetration length through the polariton gap of the 100% impure chain.

Our main goal, however, is obtaining DOS and LE of IPB, $\omega \in (\omega_{il},\Omega_1)$. Near the center of this region, DOS can be presented in the following form

$$N\left(\omega\right) = \frac{1}{\pi l_0}\left[1 + \frac{4|\gamma|\omega_c}{pd^2}\left(\omega-\omega_c\right) + O\left(\left(\frac{\omega-\omega_c}{d}\right)^2\right)\right], \tag{3.30}$$

where ω_c is the center of the impurity band, which in the linear in p approximation is

$$\omega_c^2 = \Omega_1^2 - \frac{1}{2}\Delta_{im}^2, \tag{3.31}$$

Figure 3.1: LE for a chain with a defect concentration of 10 % (solid line) in comparison to a pure system (dashed line).

where Δ_{im}^2 is the width of the band in terms of squared frequencies defined in Eq. (3.25). The first term in Eq. (3.30) represents the total number of states between ω_{il} and the center of the band; it is interesting to note that this number does not depend upon concentration of impurities. The coefficient at the second term gives the differential DOS at the center and can be rewritten as

$$\rho(\omega_c) = \frac{4\,|\gamma|\,\omega_c}{\pi l_0 p d^2} = \frac{2}{\pi l_0 \delta}, \tag{3.32}$$

where $\delta = \Delta_{im}^2/2\omega_c$ is an approximate expression for the impurity band width $\delta \simeq \Omega_1 - \omega_{il}$. This DOS has a simple meaning of the average density of states uniformly distributed through the entire band over the distance equal to $l_0/2$. In one dimensional uniform systems the wave number of the respective excitations, k, is simply connected to $N(\omega)$: $k = \pi N(\omega)$. The differential DOS would in this case be proportional to the inverse group velocity. Accordingly, $1/\pi\rho(\omega_c)$ given by Eq. (3.32) can also be viewed as a group velocity, v, of excitations in the center of our IPB in the case of the uniform distribution of impurities. The expression for v can also be presented as

$$v = \frac{d^2}{4\omega_c^2\,|\gamma|^{3/2}} pc \ll c, \tag{3.33}$$

which demonstrates that polariton excitations of the impurity band have much slower velocities not only compared to c but also to the velocities at both regular polariton branches.

Figure 3.2: Dependences of LE (solid line) and DOS (dashed line) on concentration for a frequency in the interval $\Omega_0 < \omega < \Omega_1$.

Expanding Eq. (3.27) for LE about the center of IPB, we obtain a parabolic frequency dependence of the localization length of the impurity polaritons

$$l(\omega) = \lambda(\omega)^{-1} = 2l_0(pl_0)\left[1 - \frac{20\gamma^2}{p^2}\left(\frac{\omega^2 - \omega_c^2}{d^2}\right)^2\right]. \tag{3.34}$$

One can see from this expression that $l(\omega)$ reaches its maximum value $2pl_0^2$ at the center of the band. It is important to note that the localization length here grows linearly with the concentration, whereas it is LE that grows with concentration for frequencies outside of IPB. An increase of the concentration of the impurities also results in fast ($\propto 1/p^2$) flattening of the maximum in the localization length, the fact we noticed in our numerical simulations in Chapter 2.

The frequency dependence of LE, defined by Eqs. (3.15) and (3.16), is shown in Fig. 3.1. For frequencies corresponding to the impurity band, LE drops sharply (the localization length increases); it then diverges at the upper boundary of IPB. This divergence has the same origin as LE divergence at the lower boundary of the band gap of the original crystal, where due to the specificity of the polariton spectrum, the wave vector becomes infinite. The concentration dependence of LE and integral DOS for some frequency $\omega_0 \in (\Omega_0, \Omega_1)$ is shown in Fig. 3.2. For $p = 0$ this frequency belongs to the forbidden gap, thus DOS is zero. With an increase of the concentration LE decreases (the localization length increases). For the concentration when the lower boundary of IPB crosses ω_0, DOS becomes non-zero and in $\lambda(\omega)$ the crossover between behaviors described by Eqs. (3.28) and (3.27) occurs. In

Figure 3.3: Comparison of LE calculated with (dashed line) and without (solid line) spatial dispersion in the vicinity of Ω_1. The concentration of defects for both curves is 1 %

Fig. 3.3 we compare the results of our analytical calculations with numerical simulations from previous Chapter. The comparison shows an excellent agreement between numerical and analytical results, confirming the validity of the microcanonical method in the considered limit. In addition, since numerical results were obtained with the spatial dispersion taken into account, the comparison shows that the model with dispersionless phonons produces reliable results for LE even not very far away from the spectrum boundaries.

3.2.3 The solution in the vicinity of the spectrum boundary. Non-analytic behavior.

The results obtained in the previous section are clearly not valid for frequencies close to the band boundaries ω_{il} and ω_{pu}, where $pf - \gamma = 0$ and the second term in the expansion (3.19) diverges. It is well known that perturbation expansions in disordered systems usually fail in the vicinity of boundaries of the initial spectrum of the system unperturbed by disorder [45]. The regions in the vicinity of these special frequencies ω_{il} and ω_{pu} require special consideration. Attempting to regularize our ϵ-expansion, we shall seek corrections to the zero order solution in the form

$$y = p + B\epsilon^{\alpha} \tag{3.35}$$

admitting a possibility of fractional values of α, and, hence, non-analytical behavior of the solution. We also introduce a new variable ζ which determines the proximity to either of

two frequencies ω_{il} or ω_{pu}:

$$pf - \gamma = \zeta \epsilon^{\alpha'}. \tag{3.36}$$

Substituting these expressions into Eq. (3.16) and equating the lowest order terms we see that the equation can only be satisfied for $\alpha = \alpha' = 2/3$. In this case we find that the parameter B introduced in Eq. (3.35) obeys the equation

$$\frac{p(1-p)f}{2\sqrt{\zeta + Bf}} + B = 0. \tag{3.37}$$

The substitution of y given by Eq. (3.35) in the condition for the spectral boundaries presented by Eq. (3.18) allows one to obtain an exact expression for the renormalized boundary

$$pf - \gamma = \left[3p^{2/3}(1-p)^{2/3} \left(\frac{-f}{2} \right)^{4/3} \right] \epsilon^{2/3}, \tag{3.38}$$

that modifies Eq. (3.21). The shift is small by virtue of smallness of $\epsilon^{2/3}$. In the lowest order in ϵ, the new positions of the band edges for small p are

$$\begin{aligned} \widetilde{\omega}_{il}^2 &= \Omega_1^2 - \frac{d^2\left(\Omega_1^2 - \Omega_0^2\right)}{d^2 - (\Omega_1^2 - \Omega_0^2)} p \left[1 + 3 \left(\frac{a}{4pl_0} \right)^{2/3} \right], \\ \widetilde{\omega}_{pu}^2 &= \Omega_L^2 + \frac{d^2\left(\Omega_1^2 - \Omega_0^2\right)}{d^2 - (\Omega_1^2 - \Omega_0^2)} p \left[1 - 3 \left(\frac{a}{16pl_0} \right)^{1/3} \right], \end{aligned} \tag{3.39}$$

where we again encounter $a/(pl_0)$ as a true small parameter of the expansion. It is interesting to note the different character of non-analytical corrections to the positions of the boundary of IPB $\widetilde{\omega}_{il}^2$ and the bottom of the upper polariton branch $\widetilde{\omega}_{pu}^2$. They have fractional concentration dependence with the correction to $\widetilde{\omega}_{pu}^2$ being much stronger in the limit $a/(pl_0) \ll 1$.

Now let us consider the modification of LE and the integral DOS due to the nonanalyticity. Substituting Eq. (3.35) into Eq. (3.15) the complex LE can be written as

$$\widetilde{\lambda} = -\frac{p(1-p)f}{2B} \epsilon^{4/3} = \sqrt{(pf - \gamma) + Bf\epsilon^{2/3}} \cdot \epsilon. \tag{3.40}$$

This expression explicitly demonstrates the crossover between analytical and nonanalytic behavior. When frequency ω lies far from the initial boundary $|pf - \gamma| \gg Bf\epsilon^{2/3}$, one recovers the term proportional to ϵ with the same coefficient as in Eq. (3.20), whereas in the opposite limit $|pf - \gamma| \ll Af\epsilon^{2/3}$, when we approach the boundary, the leading term gains fractional power and becomes $\propto \epsilon^{4/3}$.

At the vicinity of the renormalized spectral boundary, Eq. (3.39), DOS $\rho(\omega) \equiv 0$ to the left of $\widetilde{\omega}_{il}$ and for $\omega > \widetilde{\omega}_{il}$ it can be obtained as

$$\rho(\omega) = \frac{3}{\pi d} \left(\frac{\gamma}{l_0} \right)^{1/2} \frac{1}{(l_0 p)^{1/2}} \frac{\omega}{(\omega^2 - \widetilde{\omega}_{il}^2)^{1/2}}, \tag{3.41}$$

where γ and l_0 are evaluated at $\omega = \Omega_1$, and we have neglected the renormalization of the boundary when calculating the coefficient in $\rho(\omega)$. In this approximation the frequency and

concentration dependence of DOS does not change as compared to the one obtained from the non-renormalized expansion (3.27). It is interesting, however, that the renormalization brings about an additional numerical factor of 3 in Eq. (3.41), which is absent in the non-renormalized expression. This frequency dependence is typical for excitations with the quadratic dispersion law in the long-wave approximation. The main characteristics of this dispersion law is the effective mass m, which can be found from Eq. (3.41) as

$$m = \frac{9\gamma}{2pd^2l_0^2} = \frac{9\gamma^2}{2pc^2}\left(\frac{\omega_{il}}{d}\right)^2. \tag{3.42}$$

It is interesting to compare this expression with the effective mass of the upper polariton branch of the pure system at the bottom of the band $2m_0 = (\omega_L/dc)^2$. The two expressions have a similar structure if one introduces a "renormalized speed of light"

$$\tilde{c} = c\sqrt{p/9\gamma^2}. \tag{3.43}$$

Though the introduced parameter $\tilde{c}$ does not have a direct meaning of the speed of the excitations, it shows again that the excitations in IPB are considerably slower than their regular counterparts, with a similar dispersion law at the spectrum boundary as well as at the center of the band. Unlike, however, the center-of-band situation (3.33) the renormalized velocity at the edge is proportional to the square root of concentration.

LE in the vicinity of $\widetilde{\omega}_{il}$ is represented by different expressions for frequencies below and above $\widetilde{\omega}_{il}$ respectively

$$\begin{aligned} \lambda &= \frac{1}{2l_0}\left(\frac{1}{4pl_0}\right)^{1/3}\left[1+\frac{12}{d}\frac{(\gamma l_0)^{1/2}}{(4l_0p)^{1/6}}\left(\widetilde{\omega}_{il}^2-\omega^2\right)^{1/2}\right], \\ \lambda &= \frac{1}{2l_0}\left(\frac{1}{4pl_0}\right)^{1/3}\left[1-\frac{12}{d^2}\frac{\gamma l_0}{(4l_0p)^{1/3}}\left(\omega^2-\widetilde{\omega}_{il}^2\right)\right], \end{aligned} \tag{3.44}$$

reflecting a discontinuity of its frequency derivative at the spectrum boundary. LE itself is, of course, continuous at $\widetilde{\omega}_{il}$, giving rise to the localization length $l = 2l_0\,(4pl_0)^{1/3}$ at the edge of the band. It is interesting to compare this expression with the localization length at the center of IPB, Eq. (3.34). They both grow with the concentration but the latter one is much smaller and demonstrates slower fractional concentration dependence.

At the upper impurity band edge Ω_1 integral DOS, $N(\omega)$, diverges causing much stronger singularity in the differential DOS than at the lower boundary ω_{il}

$$\rho\,(\omega) = \frac{d\omega p^{1/2}}{\pi c\,(\Omega_1^2-\omega^2)^{3/2}}, \tag{3.45}$$

which is typical for DOS in the vicinity of resonance frequencies. Comparing this expression with a similar formula for a pure chain, one can again interpret this result as a renormalization of the velocity parameter c by the concentration of impurities, which is different from that presented by Eq. (3.43) by a numerical coefficient only.

The last spectrum boundary is the bottom of the upper polariton branch Ω_L. The spectrum in the vicinity of this frequency exists in the absence of the impurities, which are responsible for two effects in this region. First they move the boundary from Ω_L to higher

frequencies [Eq. (3.39)], and second, they increase the effective mass of the upper polariton branch, such that the differential DOS in the frequency region above $\widetilde{\omega}_{up}^2$ becomes

$$\rho(\omega) = \frac{1}{\pi dc} \frac{\omega}{\left(\omega^2 - \widetilde{\omega}_{up}^2(p)\right)^{1/2}} \left\{ 1 + \frac{p}{2} \left[\frac{d^2\left(\Omega_1^2 - \Omega_0^2\right)}{d^2 - \left(\Omega_1^2 - \Omega_0^2\right)} \right]^2 \right\}. \tag{3.46}$$

This expression can also be interpreted as a renormalization of the speed of light c.

3.3 Discussion

In this Chapter we presented a detailed study of IPB of excitations, which arise in the gap between lower and upper polariton branches of a linear chain with dipole active atoms. We have also studied impurity-induced effects on properties of the regular polariton branches.

We found that the dispersion law of the impurity band excitations at the lower frequency spectral boundary resembles that of the upper regular polariton band, but with a significantly (by a factor of $p^{1/2} \ll 1$) reduced effective mass. At the higher frequency edge of the band, the wave number diverges in a manner similar to the regular lower polariton branch with a velocity parameter again reduced by the same factor. The group velocity of the excitations near the center of the band, as well as is the localization length, is proportional to p. The latter, however, demonstrates a parabolic frequency dependence with the curvature of the parabola falling off with increase of the concentration as $1/p^2$. LPM's are drastically different from impurity-induced polaritons studied in Ref. [47]. The authors of the latter paper considered excitations of an ordered chain of two-level atoms embedded in a polar 1D crystal. Most significantly, the effective mass of polaritons of Ref. [47] is negative at the long-wave boundary of the spectrum while our excitations have a positive effective mass in this region; concentration dependencies of the effective mass and the band width also differ significantly.

The regular expansion in powers of the parameter l_{def}/l_0 produces diverging expressions at the boundaries of the zero order spectrum. Allowing for fractional powers in the expansion, we obtained a finite regularized expression for the density of states and the localization length at the boundaries. It is interesting to note that renormalized DOS at the lower boundary of IPB differs from its initial form only by a numerical factor of 3, while the position of the boundary is shifted toward lower frequencies.

The considered model gives us an insight on how to describe the properties of excitations that arise in 3D polar dielectrics with some special type of impurities. In this case an experimental significance of the results presented in this Chapter is affected by two factors: absorption due to different kind of anharmonic processes, and the one-dimensional nature of the considered model. Effects due to absorption were studied numerically with absorption introduced phenomenologically. We found that at low enough temperatures IPB survive the absorption and can be observed. As for the one-dimensionality of our model, it is generally accepted (see for instance Ref. [48]) that one-dimensional models give a fair description of tunneling in the limit of small concentrations ($l_{def}/l_0 \gg 1$). We deal with the opposite limit; however, our zero order results could describe the dispersion law of excitations in the real three dimensional medium propagating in one specified direction (for example, the direction with the highest symmetry). Disorder in this case would lead, of course, to scattering and deviation from one-dimensional geometry, but effects due to disorder are much weaker in three dimensions, and would not probably inhibit an observation of a defect induced

transparency in the frequency region of a polariton gap. Besides, as we have mentioned before, viability of one-dimensional models in describing dynamics of mixed crystals had been tested by enormous studies in the past [49]. In the next Chapter we will use the knowledge obtained here to build a model of IPB of a 3D mixed polar crystal.

Chapter 4

Concept of LPM and optical properties of mixed crystals

4.1 Introduction

The optical properties of mixed polar crystals have been attracting a great deal of interest since the 1950's. Main efforts have been directed to experimental and theoretical studies of the concentration dependencies of fundamental transverse (TO) and longitudinal (LO) phonon modes, and to the fine structure of spectra in the frequency region between them (*Restrahlen* band). Reviews of earlier experimental and theoretical works in this area can be found in Refs. [50, 51]. In spite of the disordered nature of mixed crystals, it is usually possible to observe both TO and LO modes of pure crystals at both ends of the concentration range, as well as features associated with disorder [50, 51, 52]. This is usually done in reflectance or transmittance experiments by identifying the maxima of $Im(\epsilon)$ and $-Im(1/\epsilon)$ with TO and LO modes respectively, where ϵ is the dielectric function [53].

The term mixed crystals is usually applied to materials in which the concentration of each component is large, so that no component can be considered as a system of independent impurities. At smaller concentrations the dynamics of impure systems is described in terms of defect states, which are either localized or quasilocalized depending on whether they fall into forbidden or allowed bands [7, 8, 9, 10] of the pure system. The transition from low to high concentration behavior occurs when the average distance between defects becomes of the same order as the localization length of the individual states. In the case of the local phonon states, the localization length is of the order of a few lattice constants, and the respective transition concentration is of the order of $\sim 10^{18}\ cm^{-3}$. Most of the studies of mixed crystals were focused upon combinations of alkali halides, II/IV and III/V group polar binary crystals $AB_{1-p}C_p$, where p is concentration. The B atoms are substituted with the atoms C from the same column of the Periodic Table. It was found that there were several patterns that TO and LO modes follow in mixed crystals [50, 51, 52, 54, 55]. In the type I mixed crystals, also called one-mode crystals, the frequencies of the TO and LO modes evolve smoothly and almost linearly with the composition parameter p from their values in AB to those in AC. In some one-mode systems (e.g., Ba/SrF_2, Ca/SrF_2 [56, 57]) an additional pair of weak modes inside the absorption band is observed.

Type II or two-mode mixed crystals exhibit qualitatively different behavior. Two dis-

tinct restrahlen bands are usually observed in the crystals of this category. For arbitrary concentration, the width of each of these bands, $\Omega_{LO} - \Omega_{TO}$, is approximately proportional to the composition parameter p for the dopant related band, and to $1 - p$ for that of the original material. Two-mode behavior is characteristic for the crystals formed by elements from III and V groups of the Periodic Table (e.g. $GaAs/P$ and the like).

Another mode behavior could not be fit experimentally either to one- or to two-mode patterns (e.g. Ga/InP [58], $PbSe/Te$ [59], K/RbI [60, 61], *etc.*). This group of mixed crystals was called Type I-II or one-two-mode systems. In these systems, one mode behaves as in Type I, while the other behaves as in Type II, which is why Type I-II is also called mixed mode.

To explain different types of behavior in mixed polar crystals, a number of theoretical models have been proposed. In the IR experiments, modes with wave numbers $q \sim 0$ are excited. The Random Element Isodispacement model (REI) [62, 63] takes advantage of this fact, assuming that the sublattices vibrate in phase with $q = 0$. With some modifications [52] after including the local field, and assuming a dependence of the force constants upon the composition, the modified REI model (MREI) was successfully used to fit two-mode crystals but encountered some problems in the one-mode materials. The fine structure of some mixed crystals was reproduced along the lines of REI by means of a considerable increase in the number of fitting parameters (cluster model [63]). A different approach made use of the Green's function formalism in order to treat vibrations in the mixed crystals; averaging over disorder was performed either in a simple virtual crystal approximation (VCA) or with the use of the much more elaborate coherent potential approximation [64] (CPA). Interaction with the electromagnetic field in these approaches was included after the averaging procedure was performed. The mean field approximation treats the crystal as if it has atoms of the same sort with some average properties. It reproduces well the one-mode behavior, but could not possibly explain the two-mode systems. CPA combined with an electrostatic treatment of the electric field was used to fit a broader range of experimental data (see, for instance, Ref. [65]).

An important theoretical problem many researchers have focused upon is to find a simple criterion for different mode behavior, based upon dynamical properties of the crystals. Lucovsky [54] originally considered the significance of whether the original absorption bands overlap or not, which turned out to be a rather rough criterion. Harada and Narita [55] proposed a criterion based on relations between MREI constants (see also review papers in Refs. [50, 51]). It turned out that one-mode and two-mode crystals can be described using quite simple models with only a few fitting parameter, such as VCA and MREI, respectively. Lucovsky *et al.* in Ref. [54] made an attempt to establish a connection between the behavior of a mixed crystal and the existence of the localized modes at small values of concentration parameters p or $1 - p$. It was suggested that the two-mode behavior is associated with the existence of local impurity states at both ends of the concentration range, while the one-mode regime occurs when such local states do not arise. These ideas, however, could not be applied to the mixed-mode behavior since the local phonon states arise either in the gap between acoustic and optic branches or above the optic branch of the phonon spectrum [7, 8, 9, 10]. Therefore, the mixed-mode crystals required much more elaborate models, where agreement with experimental data can only be achieved by increasing the number of fitting parameters. The same was true for weak features of spectra of the one-mode crystals.

One of the goals of this Chapter is to put forward a simple physical picture explaining the mixed-mode behavior based upon the concept of LPM's and IPB. A local polariton state within the *restrahlen* region was first observed experimentally in Ref. [66] as a weak feature

in reflectance and Raman spectra of $GaAs$ doped with Sn, Te or S. These states were found to be associated with the local change in susceptibility due to localization of an electron around the dopant. An interaction between the localized electron and LO vibrations of the crystal gives rise to local LO phonons, therefore these local states have a complicated structure that involves interactions between electrons, phonons and electromagnetic field. Theoretically these states, however, were only considered in the electrostatic approximation [66], and therefore these early observations did not lead to the concept of LPM's, which requires that the retardation be taken into account.

A new wave of interest in the optical properties of impure crystals in the *restrahlen* region occured recently and was due to a general interest in systems with depleted or altered electromagnetic density of states (DOS). The primary examples of such systems are photonic crystals [5], and microcavities [67]. The *restrahlen* region in polar crystals was considered from this new perspective independently in Refs. [17, 18, 19], where the concept of LPM's was introduced. The local state considered in Ref. [18] arises due to an impurity atom with optically active electronic transitions, which interacts with host atoms through the electromagnetic field only. With the transition frequency inside the *restrahlen* band, this atom forms a local atom-radiation bound state. To some extent these states are similar to the ones observed by Dean *et al.* [66], though an interaction with phonons was left out in Ref. [18]. A different type of LPM was considered in Refs. [17, 19], where it was shown that regular isotopic impurities can give rise to local states with frequencies inside the *restrahlen* region. The interaction with the retarded electromagnetic field is responsible for the localized electromagnetic component of the states. The detailed analysis of the LPM in a three dimensional sodium-chloride-like structure (BCC) crystal in the case of diagonal and off-diagonal disorder was carried out in Ref. [38]. It was proven that, because of retardation effects, a LPM splits off the bottom of the TO-LO gap for an arbitrarily small strength of the defects even in three dimensional systems.

When considering local polaritons, the authors of Refs. [17, 19, 38] assumed that the *restrahlen* is a spectral gap not only for electromagnetic excitations but for phonons as well. This is indeed the case for some polar crystals. It occurs more frequently, however, that the *restrahlen* region is devoid of transverse optic phonons, but is still filled with LO modes. In this case the interaction between LPM's and LO phonons would make the former quasi-stationary. Whether the local polaritons survive this interaction depends upon their life-time, and we shall address this question in this study. At the same time it is useful to note that the states observed in Ref. [66] reside in the frequency region where the density of LO modes is especially large. The fact that they remained observable allows for optimism that LPM's of Refs. [17, 19, 38] could also survive provided that DOS of LO is not too large. If this is the case, then local polaritons due to isotopic impurities can be invoked to explain the mixed-mode behavior of mixed crystals and weak features in the one-mode systems without having to introduce tens of fitting parameters.

These ideas can be used to discuss the one-two-mode mixed crystal $Ga_{0.70}In_{0.30}P$. Pure GaP has a complete polariton gap in all directions, and experiments of Ref. [68] clearly demonstrated the polariton band associated with In atoms inside the *restrahl* of GaP even at room temperature. Polariton branches inside *restrahlen* were also observed in pure $CuCl$ [68]. This material demonstrates a very peculiar behavior because Cu atoms can occupy several non-equivalent positions, thereby producing defects even in a pure material [54, 69]. These defects were shown to be responsible for a new TO mode with a frequency in the main *restrahlen* [54, 69]. These experiments were originally described using a phenomenological two-oscillator model, but they perfectly fit to the idea of LPM's.

Local polaritons, however, can take us further than an explanation of the old reflectivity experiments. When retardation is taken into account, LPM's give rise to a new transmitting channel for electromagnetic excitations, via IPB. Experimentally, such a band can be observed in transmission steady-wave and time-resolved experiments. The majority of the old experiments mentioned above dealt with reflection spectra. Dips in the reflection coefficient in those experiments were associated with impurity-induced absorption, while they could have actually occured because of enhanced transmission via IPB. The effect of the enhanced transmission inside the *restrahlen* region of a polar crystal was observed in $CuCl$ [70].

4.2 Model

In previous Chapter we considered development of IPB in a one-dimensional model, and used the so-called microcanonical method [20] in order to analytically calculate the complex Lyapunov exponent of the system. Used approximation was shown to be equivalent to a continuous medium approximation. The latter can easily be generalized to 3D systems, and below we develop an approach to IPB in 3D mixed polar crystal using the following fundamental assumptions.

In order to model optic vibrations of the system under study, we introduce two subsystems of oscillators with different frequencies. One subsystem represents an optic mode of the host atoms. The interaction between this mode and light leads to the polariton gap between TO and LO frequencies of the pure crystal. The second subsystem introduces vibrations of impurities, and it is assumed that its frequency belongs to the *restrahlen* of the host crystal. This is a crucial assumption of the model, since interaction between light and this mode brings about LPM's. The significance of this assumption rests upon two ideas. The first one goes back to Lucovsky [54], who was the first to connect modes of mixed crystals with local impurity modes. The second one is the concept of LPM's, which are local states with frequencies in the restrahlen of the host. As it was shown in Chapters 2,3, the presence of LPM's gives rise to IPB, when the concentration of impurities grows.

The frequencies of both oscillators are, in general, complex-valued. The imaginary part of host vibrations is due to anharmonicity, while the impurity mode has two sources of decay. Besides usual relaxation, local polaritons can acquire an additional imaginary part due to interaction with LO phonons which in some cases can fill the *restrahlen*. We will consider the contribution of this interaction into the life-time of LPM's in the next section, and the general effects of relaxation upon reflection spectra of mixed crystals will be discussed in Section 4.5.

It was found in Refs. [17, 19, 38] and Chapter 3 that for all frequencies outside of the immediate vicinity of the TO boundary of the *restrahlen*, the localization length l_0 of LPM's is of the order of magnitude of the wavelength of the incident light $\sim 10^{-3}\ cm$. Even for residual concentration $n \sim 10^{12}\ cm^{-3}$ of the impurities, nl_0^3 is large. The individual states significantly overlap and a macroscopic volume containing many impurities can still be much smaller than the localization length. This fact allows us to develop a continuous medium approximation similar to the usual one used to treat long-wave excitations [71], but this time we use it to treat the sub-system of impurities. We would like to emphasize again that this consideration is reasonable for the polariton band only because of the long-range nature of the localized electromagnetic component of the local polaritons.

The microscopical Hamiltonian describing optic modes of our system is:

$$H = \sum_{\mathbf{r}} \frac{\mu_0}{2} \left(\frac{d\mathbf{u_r}}{dt} \right)^2 + \sum_{\mathbf{r}'} \frac{\mu_1}{2} \left(\frac{d\mathbf{v_{r'}}}{dt} \right)^2 + \frac{1}{2} \sum_{\mathbf{r},\mathbf{r}'} \Phi \left(\mathbf{u_r}, \mathbf{v_{r'}} \right), \tag{4.1}$$

where μ_0, μ_1 and $\mathbf{u_r}$, $\mathbf{v_{r'}}$ are the reduced masses and relative displacements of the ions in pure AB and AC crystals, respectively. We will assume that the presence of atoms C does not affect the order in the A sublattice. The summation runs over spatial index $\mathbf{r}$ for host atoms and over $\mathbf{r}'$ for the impurities. The third term in the above expression is the potential energy. In the harmonic approximation it can be written as

$$\begin{aligned} \Phi \left(\mathbf{u_r}, \mathbf{v_{r'}} \right) &= \Phi^{(0)}_{i,j} \left(\mathbf{r} - \mathbf{r}_1 \right) u^i_{\mathbf{r}} u^j_{\mathbf{r}_1} + \Phi^{(1)}_{i,j} \left(\mathbf{r}' - \mathbf{r}'_1 \right) v^i_{\mathbf{r}'} v^j_{\mathbf{r}'_1} \\ &+ \Phi^{(01)}_{i,j} \left(\mathbf{r} - \mathbf{r}' \right) u^i_{\mathbf{r}} v^j_{\mathbf{r}'}. \end{aligned} \tag{4.2}$$

In order to avoid unnecessary complications, we assume no spatial dispersion in our model Hamiltonian (4.1) and isotropy of force constants

$$\Phi \left(\mathbf{u_r}, \mathbf{v_{r'}} \right) = \Phi_0 \mathbf{u}^2_{\mathbf{r}} + \Phi_1 \mathbf{v}^2_{\mathbf{r}'}, \tag{4.3}$$

where Φ_0 and Φ_1 are force constants describing the interaction of the ions in the AB and AC lattices, respectively. As follows from the form of expression (4.3), the contributions due to host and impurity ions in the Hamiltonian (4.1) can be separated

$$\begin{aligned} H &= \sum_{\mathbf{r}} \left[\frac{1}{2} \mu_0 \left(\frac{d\mathbf{u_r}}{dt} \right)^2 + \frac{1}{2} \Phi_0 \mathbf{u}^2_{\mathbf{r}} \right] \\ &+ \sum_{\mathbf{r}'} \left[\frac{1}{2} \mu_1 \left(\frac{d\mathbf{v_{r'}}}{dt} \right)^2 + \frac{1}{2} \Phi_1 \mathbf{v}^2_{\mathbf{r}'} \right]. \end{aligned} \tag{4.4}$$

We have several parameters of the dimension of length in our system: a lattice constant, a; an average distance between defects, $l \sim n^{-1/3}$, which depends on concentration; and the localization length and the wavelength of the incident light, which are of the same order, $l_0 \sim \lambda \sim 10^{-5}\ m$. We shall assume that the concentration is such that $n \gg l_0^{-3}$. When this condition is satisfied, the individual defect states overlap, and the dynamical properties, apart from those at the fluctuation band-edge, do not depend significantly upon the particular arrangement of the defects in the crystal. Hence, one can introduce a smoothing parameter $l_{\delta V}$ such that $l \ll l_{\delta V} \ll l_0$. The macroscopic volume associated with this parameter is such that it contains macroscopically many impurities, but there are still no significant changes in spatial distribution of vibrations over this length: $\mathbf{u_{r+R}}, \mathbf{v_{r+R}} \approx \mathbf{u_r}, \mathbf{v_r}$ for $R \sim l_{\delta V}$. Taking advantage of this fact one can sum over the volume $\delta V(\mathbf{R}) \sim l^3_{\delta V}$ in the vicinity of $\mathbf{R}$ in the Hamiltonian (4.4):

$$\begin{aligned} &\sum_{\mathbf{r} \in \delta V(\mathbf{R})} \left[\frac{1}{2} \mu_0 \left(\frac{d\mathbf{u_r}}{dt} \right)^2 + \frac{1}{2} \Phi_0 {\mathbf{u_r}}^2 \right] \quad \rightarrow \\ &\rightarrow \left[\frac{1}{2} \mu_0 \left(\frac{d\mathbf{u_R}}{dt} \right)^2 + \frac{1}{2} \Phi_0 {\mathbf{u_R}}^2 \right] \cdot \quad n_0 \quad [1 - p(\mathbf{R})]\, \delta V(\mathbf{R}), \end{aligned} \tag{4.5}$$

$$\sum_{\mathbf{r}'\in\delta V(\mathbf{R})}\left[\frac{1}{2}\mu_0\left(\frac{d\mathbf{u}_{\mathbf{r}'}}{dt}\right)^2+\frac{1}{2}\Phi_0{\mathbf{u}_{\mathbf{r}'}}^2\right]\;\rightarrow$$

$$\rightarrow\left[\frac{1}{2}\mu_0\left(\frac{d\mathbf{u}_{\mathbf{R}}}{dt}\right)^2+\frac{1}{2}\Phi_0{\mathbf{u}_{\mathbf{R}}}^2\right]\;\cdot\;n_0p(\mathbf{R})\delta V(\mathbf{R}), \tag{4.6}$$

where we assume that the change in lattice constants of two end crystals is negligible, $a\simeq n_0^{1/3}$, and $p(\mathbf{R})=n(\mathbf{R})/n_0$. Thus the Hamiltonian (4.4) can be rewritten in the continuous medium approximation as

$$H=\frac{n_0}{2}\int\Big[(1-p(\mathbf{R}))\,\mu_0\,\dot{\mathbf{u}}_{\mathbf{R}}^2+(1-p(\mathbf{R}))\Phi_0\mathbf{u}_{\mathbf{R}}^2$$

$$+p(\mathbf{R})\mu_1\,\dot{\mathbf{v}}_{\mathbf{R}}^2+p(\mathbf{R})\Phi_1\mathbf{v}_{\mathbf{R}}^2\Big]\,dV. \tag{4.7}$$

The ion polarization at $\mathbf{R}$ is

$$\begin{aligned}\mathbf{P}_{ion}(\mathbf{R}) &= \frac{1}{\delta V(\mathbf{R})}\left[\sum_{\mathbf{r}\in\delta V(\mathbf{R})}q\mathbf{u}_{\mathbf{r}}+\sum_{\mathbf{r}'\in\delta V(\mathbf{R})}q\mathbf{v}_{\mathbf{r}'}\right]\\ &\rightarrow (1-p(\mathbf{R}))qn_0\mathbf{u}_{\mathbf{R}}+p(\mathbf{R})qn_0\mathbf{v}_{\mathbf{R}}\;,\end{aligned} \tag{4.8}$$

where we assume for simplicity the same effective charges for both oscillators, and again use the fact that $l_{\delta V}\ll l_0$ and consequently $\mathbf{u}_{\mathbf{r}}$, $\mathbf{v}_{\mathbf{r}'}$ do not change significantly over such distances. The interaction of the polarization with the electromagnetic field gives rise to an additional term in the Hamiltonian:

$$U_{int}=\int\mathbf{P}\cdot\mathbf{E}dV=n_0\int[(1-p(\mathbf{R}))\mathbf{u}_{\mathbf{R}}+p(\mathbf{R})\mathbf{v}_{\mathbf{R}}]\cdot\mathbf{E}dV. \tag{4.9}$$

Combining Eqs. (4.7) and (4.9) and writing out the resulting Hamilton equations for $\mathbf{u}_{\mathbf{R}}$, $\mathbf{v}_{\mathbf{R}}$, one obtains

$$\begin{aligned}\mu_0\,\ddot{\mathbf{u}}_{\mathbf{R}} &= \Phi_0\mathbf{u}_{\mathbf{R}}+q\mathbf{E},\\ \mu_1\,\ddot{\mathbf{v}}_{\mathbf{R}} &= \Phi_1\mathbf{v}_{\mathbf{R}}+q\mathbf{E}.\end{aligned} \tag{4.10}$$

These equations of motion should be accompanied by the Maxwell equation for the electromagnetic field in the medium

$$\nabla\times\nabla\times\mathbf{E}=\frac{1}{c^2}\frac{d^2\left(\mathbf{E}+4\pi\mathbf{P}_{ion}+4\pi\mathbf{P}_{el}\right)}{dt^2}, \tag{4.11}$$

where the last term describes an electron contribution to the polarization that determines the high-frequency value of the dielectric parameter. Another effect to be taken into account is that the local electric field on atoms that induces polarization is different from the macroscopic field entering the Maxwell equations. The effective local field in a high symmetry crystal can be written in the form [71, 65]:

$$\mathbf{E}_{loc} = \mathbf{E}+\frac{4\pi}{3}\left(\mathbf{P}_{ion}+\mathbf{P}_{el}\right), \tag{4.12}$$

$$\mathbf{P}_{el} = n_0\alpha_\infty\mathbf{E}_{loc}. \tag{4.13}$$

Substituting the effective local field into Eq. (4.10) and total polarization of the volume $\mathbf{P} = \mathbf{P}_{ion} + \mathbf{P}_{el}$ into Eq. (4.11), one obtains the closed system of equations of mechanical coordinates, the polarization and the electric field. Eqs. (4.10), (4.11), (4.12), and (4.13) formally resemble equations of MREI used in many papers. There are, however, important differences. First, the concentration parameter $p(\mathbf{r})$ entering our equations is still a random function of coordinates. The statistics of this parameter, however, are significantly different from the original statistics of the microscopic distribution of impurities. The spatial inhomogeneity of the continuous function $p(\mathbf{r})$ reflects the fluctuations in the number of impurities in the macroscopic volume δV, which are significantly reduced as compared to the fluctuations in the original microscopic distribution of impure atoms. More detailed consideration of the statistical properties of $p(\mathbf{r})$ will be presented in the last Section. Second, the derivation of Eqs. (4.10), (4.11), (4.12), and (4.13) is explicitly based upon existence of a macroscopic length scale – the localization length of LPM's. A similar procedure cannot be applied to the regular phonon states, because the localization length of the local phonon states is usually microscopic. Finally, the requirements that the impurity-induced oscillator has its frequency within *restrahlen* replaces conditions for local phonon modes that appear in regular MREI [52]. In this section we will assume that the fluctuation of the number of defects in the chosen volume is negligible and, therefore, $p(\mathbf{R}) \equiv p$. Excluding the polarization and lattice displacements from the system yields the following equation for the Fourier components of the electric field

$$\mathbf{k} \times \mathbf{k} \times \mathbf{E}_\omega = \frac{\omega^2}{c^2}\epsilon(\omega)\mathbf{E}_\omega. \tag{4.14}$$

In this equation, $\epsilon(\omega)$ denotes the effective dielectric function of the mixed polar crystal $AB_{1-p}C_p$

$$\epsilon(\omega) = \epsilon_\infty \frac{1 + \frac{2}{3}\left((1-p)\frac{d_0^2}{\Omega_0^2 - \omega^2} + p\frac{d_1^2}{\Omega_1^2 - \omega^2}\right)}{1 - \frac{\epsilon_\infty}{3}\left((1-p)\frac{d_0^2}{\Omega_0^2 - \omega^2} + p\frac{d_1^2}{\Omega_1^2 - \omega^2}\right)}, \tag{4.15}$$

where $\Omega_{0,1}^2 = (\Phi_{0,1}/\mu_{0,1})^{1/2}$ are the lattice eigenfrequencies and parameters

$$d_{0,1}^2 = 4\pi\frac{\epsilon_\infty + 2}{3\epsilon_\infty}\frac{q^2}{\mu_{0,1}}$$

determine the width of the polariton gaps of the end crystals. We assume that the high frequency dielectric constant does not depend upon the concentration. ϵ_∞ can be expressed in terms of polarizability α_∞ as

$$\epsilon_\infty = 1 + \frac{4\pi\alpha_\infty n_0}{1 - \frac{4\pi}{3}\alpha_\infty n_0}.$$

From Eq. (4.14) one can separate the transverse and longitudinal modes as

$$k^2\mathbf{E}_\omega^\perp = \frac{\omega^2}{c^2}\epsilon(\omega)\mathbf{E}_\omega^\perp\ , \tag{4.16}$$

$$\epsilon(\omega)\mathbf{E}_\omega^\parallel = 0\ . \tag{4.17}$$

A similar expression for the dielectric function was obtained previously in Ref. [55] within the MREI. Nobody, however, assumed before that the Ω_1 lies within the *restrahlen* of the

host. It is only the concept of LPM's that justifies using this dielectric function in the case when the frequency of the defect oscillator falls into the polariton band gap. Comparing Eq. (4.15) with the respective expression obtained in the previous Chapter, one can see that Eq. (4.15) is a zero-order approximation in a series expansion in terms of the small parameter $l/l_0 \ll 1$. In the last Section of this Chapter we shall demonstrate this fact implicitly.

4.3 Long-living quasistationary LPM's in restrahlen band

The model developed in the previous section is implicitly based upon the assumption about the existence of local states with frequencies within the *Restrahlen*. In this section we shall provide additional justifications for this assumption.

In the original papers [17, 19] where local polaritons were introduced, it was assumed that within the restrahlen there is a genuine spectral gap with the phonon DOS being equal to zero over some frequency region. Such situations are, indeed, possible in some crystals (GaP, ZnS, $CuBr$, *etc* [72]). It is more common, however, that the *restrahlen* is filled with LO phonons, which are linearly coupled to LPM's. This coupling results in the "phonon radiative decay" of the local polaritons (compare to radiative decay of local phonons due to coupling to light). It is important to emphasize, however, that the electromagnetic component of the LPM's remains localized even when there is leakage through the phonon component. The phonon radiative decay broadening of local polaritons (and the respective life-time) is determined by the density of LO phonon states within the *restrahlen*. In some cases this DOS is large enough to suppress LPM's. At the same time, there exists a broad range of materials (for instance, NaF,$NaBr$, RbF, *etc.* [72]) that have a relatively low DOS inside the *restrahlen*, so one could expect that local polaritons can survive the presence of LO phonons and affect significantly the transport properties of the system. In fact, the local states inside the *restrahlen* observed in Ref. [66] resided in the frequency region with a rather large DOS, and still could be observed both in reflection and Raman spectra.

Since the fundamental assumptions incorporated into the model presented in this Chapter are based upon existence of long-living LPM's, it is of great importance to study their life-time in realistic polar crystals. Our consideration of the question about the "phonon radiative decay" time of the local polaritons is based upon results of Ref. [38]. It was shown that the frequency of LPM is determined by

$$\begin{aligned} 1 &= -\frac{\delta m}{m}\omega^2 \int \frac{\rho_{\parallel}(z) + 2\rho_{\perp}(z)}{\omega^2 - z^2} dz \\ &= -\frac{\delta m}{m}\left[\omega^2 \int \frac{\rho_{\parallel}(z) + 2\rho_{\perp}(z)}{\omega^2 - z^2} dz\right], \end{aligned} \tag{4.18}$$

where $m = \frac{m_- + m_+}{m_-/m_+}$, m_+ and m_- are the masses of positive and negative ion sublattices respectively, δm is the difference between masses of the defect and the host atom replaced by the defect, and $\rho_{\parallel}(\omega)$ and $\rho_{\perp}(\omega)$ are densities of states of TO and LO phonons, respectively. If the LO DOS differs from zero in the *restrahlen* region where we expect the local state to reside, the respective integral in Eq.(4.18) acquires an imaginary part equal to $i\pi\omega\rho_{\parallel}(\omega)$. For a light impurity ($\delta m < 0$) this equation would have a real solution ω_l if $\rho_{\parallel}(\omega) = 0$.Podolsky The presence of LO modes makes the solution complex valued, $\omega_l' = \omega_l - i\gamma$. The phonon component becomes delocalized, although the electromagnetic component remains localized.

If, as we assume, $\gamma/\omega_1 \ll 1$, then ω_1 can be considered to be the solution of Eq. (4.18)

with the imaginary part dropped and γ can be found as the first order correction to it

$$\frac{\gamma}{\omega_1} = \frac{\pi\omega_1\rho_{\parallel}(\omega_1)}{2\omega_1^2 R(\omega_1) + \omega_1^3 \frac{dR(\omega_1)}{d\omega_1}}, \tag{4.19}$$

where $R(\omega_1)$ is a principal value of the integral entering Eq.(4.18). The derivative of $R(\omega_1)$ can be estimated using the explicit form of this function as $\omega_1 \frac{dR(\omega_1)}{d\omega_1} = 2R(\omega_1) + O\left((\omega_1 a/c)^2\right)$. Finally one obtains

$$\frac{\gamma}{\omega_1} = \frac{\pi}{4}\left(\frac{-\delta m}{m_- + m_+}\right)\frac{m_-}{m_+}\omega_1\rho_{\parallel}(\omega_1). \tag{4.20}$$

It follows from Eq. (4.20) that there are three factors affecting the life-time of the polariton states. First of all, it is the density of LO phonon states $\omega_1\rho_{\parallel}(\omega_1)$ in the *restrahlen*. As mentioned above, due to the strong dispersion of the LO branch, the density of states in many alkali halides [72] between $\Omega_{(TO)}(0)$ and $\Omega_{(LO)}(0)$ can be less then 10% of the maximum DOS at TO frequency. Unfortunately, the experimental data on the phonon DOS known to us do not provide its value in absolute units, and in order to obtain an estimate for this quantity in the region of interest, we have to rely upon some assumptions. To this end we use the Debye model for DOS of the *acoustic* phonons in order to establish a scale for the experimental results listed in Ref. [72]. This choice seems reasonable because the Debye model gives a fairly good description of low-temperature thermodynamic properties of crystals, and parameters of the model for most of the crystal of interest are established with good accuracy. Having the scale for the phonon DOS, one can assess the numerical value of the dimensionless quantity $\omega_1\rho_{\parallel}(\omega_1)$. Our estimates show that this parameter in the spectral region of interest can take values between 0.2 and 0.6 in different systems.

The next factor affecting the life-time of LPM's is the defect parameter δm. This parameter cannot be assumed to be too small since we would like to have our local state farther away from the TO boundary of the *restrahlen*, and as it was shown in Refs. [17, 38], the frequency of LPM state moves deeper into the *restrahlen* with increase of the defect strength δm. At the same time, it is clear that the factor $-\delta m/(m_- + m_+)$ is at least less then unity. The third factor $m_-/m+$ (or $m_+/m-$ when the negative atom is replaced), can be as small as 0.2 for RbF or even 0.06 in the case of LiI. Combining all terms we find that in a number of crystals ($NaBr$, $NaCl$, RbF, *etc*,) the dissipation of the local polariton state is rather small $\gamma/\omega_1 < 0.1$. In fact, it appears to be of the same order of magnitude as anharmonic absorption, and later in the Chapter we will introduce both these relaxation channels phenomenologically using just one parameter of relaxation. The presented estimates show that LPM's can actually survive even in materials with *restrahlen* filled with LO phonons, and provide, therefore, a foundation for the model presented in the previous section. Now we can start discussing the results following from this model.

4.4 IPB in mixed polar crystals

4.4.1 Dispersion laws of impurity polaritons

In this section we discuss properties of polariton excitations in our system neglecting relaxations. Effects of the dissipation will be incorporated in our treatment of reflection spectra in

the next section. The dispersion of the transverse polaritons is determined by the equation

$$k = \sqrt{\epsilon(\omega)}\frac{\omega}{c}, \tag{4.21}$$

while the longitudinal excitations obey the equation $\epsilon(\omega) = 0$ and are dispersionless within the present model. The sign of $\epsilon(\omega)$ determines the structure of the spectrum. The bands of propagating electromagnetic waves coupled to the lattice vibration appear at frequencies where $\epsilon(\omega)$ is positive, and bandgaps arise where the dielectric function (4.15) is negative. The change of the sign of $\epsilon(\omega)$ occurs when $\epsilon(\omega) = 0$ and when $1/\epsilon(\omega) = 0$. In the electrostatic approximation, the first of these conditions determines the LO frequencies ω_{LO}, while the second gives the frequencies of TO phonon modes, ω_{TO}. With retardation taken into account for regular polaritons in pure crystals, the latter becomes the short wave limit of the lower transverse polariton branch, while ω_{LO} determines the $k = 0$ frequency of the upper polariton transversal branch degenerate with the longitudinal phonon mode. As we shall see in this section for the impurity induced polaritons, the interpretation of the boundary frequencies is quite different.

In the absence of defects, $p = 0$, the *restrahlen* polariton band stretches between transverse ,

$$\Omega_0^{(TO)2} = \Omega_0^2 - \frac{\epsilon_\infty}{3}d_0^2,$$

and longitudinal,

$$\Omega_0^{(LO)2} = \Omega_0^2 + \frac{2}{3}d_0^2,$$

frequencies. Introducing defects with $\Omega_0^{(TO)2} < \Omega_1^2 < \Omega_0^{(LO)2}$ in the system with concentrations significant enough to satisfy the condition $l/l_0 \ll 1$ yet still small in the sense that $p \ll 1$, one can rewrite Eq. (4.15) in the linear in p approximation:

$$\epsilon(\omega) \simeq \epsilon_\infty \left(\frac{\Omega_0^{(LO)2} - \omega^2}{\Omega_0^{(TO)2} - \omega^2}\right)\frac{\omega_{il}^2 - \omega^2}{\omega_{iu}^2 - \omega^2}. \tag{4.22}$$

It can be directly seen from this expression that the impurities give rise to the band of propagating excitations inside the *restrahl* of the original crystal, with boundaries given by

$$\begin{aligned}
\omega_{il}^2 &= \Omega_1^2 - p\left(\frac{\frac{2}{3}d_0^2(\Omega_1^2 - \omega^2) - \frac{2}{3}d_1^2(\Omega_0^2 - \omega^2)}{\Omega_0^{(LO)2} - \Omega_1^2}\right), \\
\omega_{iu}^2 &= \Omega_1^2 + p\left(\frac{\frac{\epsilon_\infty}{3}d_1^2(\omega^2 - \Omega_0^2) - \frac{\epsilon_\infty}{3}d_0^2(\omega^2 - \Omega_1^2)}{\Omega_1^2 - \Omega_0^{(TO)2}}\right).
\end{aligned} \tag{4.23}$$

The width of the band (in terms of squared frequencies) is linearly proportional to the concentration

$$\Delta_{imp}^2 \simeq d_1^2(\Omega_1^2 - \Omega_0^2)\frac{\frac{4\epsilon_\infty}{3}d_0^2 - \frac{\epsilon_\infty+2}{3}(\Omega_1^2 - \Omega_0^2)}{\left(\Omega_0^{(LO)2} - \Omega_1^2\right)\left(\Omega_1^2 - \Omega_0^{(TO)2}\right)} \cdot p \ > 0 \ , \tag{4.24}$$

provided that the impurity frequency Ω_1 is not too close to $\Omega_0^{(LO)}$ such that

$$\Omega_0^{(LO)\ 2} - \Omega_1^2 < \frac{2}{3}d_0\, d_1\sqrt{p}. \tag{4.25}$$

The lower band boundary, given by Eq. (4.23), corresponds to a dispersionless longitudinal polariton branch

$$\omega_i^{(LO)}(\mathbf{k}) = \omega_{il}, \tag{4.26}$$

while the upper one is the short wave limit of the branch of transversal excitations. An approximate dispersion law for these excitations can be obtained from Eq. (4.21) if one substitutes $\omega = \Omega_1$ everywhere except in terms containing IPB boundaries:

$$\omega_i^{(TO)}(\mathbf{k}) = \omega_{il} + \delta_{imp}\frac{k^2 l_0^2}{1 + k^2 l_0^2}. \tag{4.27}$$

Parameter l_0 in this equation is the localization length of a single LPM with the frequency equal to Ω_1:

$$l_0^{-1} = \left(\frac{\Omega_1^2}{c^2}\epsilon_\infty \frac{\Omega_0^{(LO)2} - \Omega_1^2}{\Omega_1^2 - \Omega_0^{(TO)2}}\right)^{1/2}. \tag{4.28}$$

Excitations described by Eqs. (4.26) and (4.27) demonstrate a number of peculiarities. First, one can note that the mutual positions of longitudinal and transverse modes are reversed compared to the regular polaritons: the longitudinal mode has lower frequency than the transverse one. However, if one takes the original polariton branches of the host crystal into consideration, the normal sequence of transverse and longitudinal modes is restored: the host transverse polariton branch is followed by the impurity longitudinal mode, which is followed by the impurity transverse mode. The last modes in the sequence are the LO mode and upper transverse polariton branch of the host. Second, the single transverse impurity polariton mode combines properties of lower and upper regular polariton modes. Indeed, at $k = 0$ this mode becomes degenerate with the impurity longitudinal mode akin to the upper branch of regular polaritons. At the same time the short wave limit $k \to 0$ of the same mode corresponds to the TO frequency of the electrostatic approximation, and sets the upper boundary of the propagating band similar to the regular lower polariton branch.

The dispersion curves of the transverse excitations, obtained from general equation (4.21) for several concentrations, are shown in Fig. 4.1. The similar dispersions were observed experimentally by means of Raman spectroscopy in mixed crystal Ga/InP in Ref. [68]. Originally, the interpretation of these observations was based upon a phenomenological dielectric function with multiple resonances, while it seems clear now that they provide a solid support for the concept of impurity polaritons.

From the dispersion law described by Eq. (4.27) one can obtain an expression for the group velocity of the respective excitations:

$$\frac{v_g(\omega)}{c} = \frac{l_0}{\lambda}\frac{\left(\omega^2 - \omega_{il}^2\right)^{1/2}\left(\omega_{iu}^2 - \omega^2\right)^{3/2}}{\omega^2 \Delta_{imp}^2}, \tag{4.29}$$

which reaches its maximum value of

$$\frac{v_g(\omega_{max})}{c} = \frac{l_0}{\lambda}\frac{3^{3/2}}{8}\frac{\delta_{imp}}{\omega} \sim \frac{\delta_{imp}}{\omega}, \tag{4.30}$$

at

$$\omega_{max}^2 = \omega_{il}^2 + 1/4\Delta_{imp}^2.$$

We introduced here a new parameter, δ_{imp}, characterizing the width of IPB in terms of frequencies themselves: $\delta_{imp} \simeq \Delta_{imp}^2/2\omega$. The group velocity is linear in concentration and is

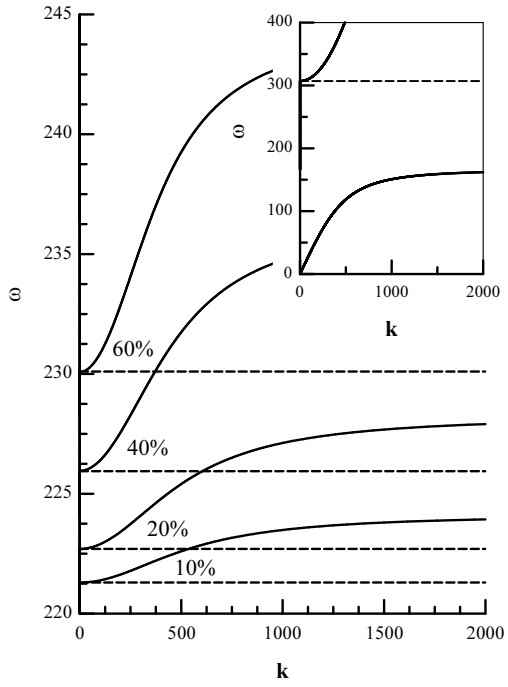

Figure 4.1: Dispersion curves of the transverse (solid) and longitudinal (dashed) optic defect modes in the *restrahl* for four different concentrations. The insert depicts the dispersion curves of the pure crystal. Frequency and wavenumber are given in the same units, cm^{-1}.

significantly smaller than the speed of light in vacuum. This is an interesting result showing that propagation of light through mixed crystals can be significantly (and controllably) slowed down. The smallness of the group velocity is also reflected in the flatness of the dispersion curves presented in Fig. 4.1, as well as in experimental results of Ref. [68]

The density of polariton states in the impurity band (IPDOS) can also be obtained from the dispersion equation, Eq. (4.27),

$$D(\omega) \simeq \frac{1}{2\pi^2 l_0^3}\omega\Delta_{imp}^2 \frac{\left(\omega^2-\omega_{il}^2\right)^{1/2}}{\left(\omega_{iu}^2-\omega^2\right)^{5/2}}. \tag{4.31}$$

At the low-frequency boundary of the band this DOS reproduces the singular behavior characteristics for the lower polariton band of pure polar crystals, while at the high frequency edge it resembles the behavior of the regular upper polariton band. At the center of the impurity band IPDOS can be expressed in compact form in terms of the localization length l_0 and the linear width of the band δ_{imp}:

$$D(\omega_c) \simeq \frac{1}{\pi^2 l_0^3 \delta_{imp}}. \tag{4.32}$$

The dependence of IPDOS upon concentration is different at the edges of the band and at the center. The boundary of IPDOS depends linearly upon p, and tends to zero when p decreases. At the band center IPDOS is inverse proportional to p, and goes to infinity when $p \to 0$. Such a behavior has a simple meaning – it describes the collapse of the band into a single local state with an infinite density.

The linear in concentration approximation for IPB fails when the defect frequency Ω_1 falls close to the band edge, $\Omega_0^{(LO)}$, of the pure crystal, so that Eq. (4.25) does not hold anymore. In this case, one can obtain approximate expressions for characteristics of the impurity band using an expansion of Eq. (4.15) in powers of $\Omega_0^{(LO)} - \Omega_1$. The zeroth order in this parameter leads to a square root dependence of the band width upon concentration:

$$\Delta_{imp}^2 \simeq \frac{2d_0 d_1}{3}\sqrt{p}. \tag{4.33}$$

It is interesting to note that this situation was probably observed in one-two-mode mixed crystal $Ga/InAs$ [73]. In that system at small concentration of In the frequencies $\omega_{il}(p)$ and $\Omega^{(LO)}(p)$ could not be fit with linear in p expressions, while $\omega_{iu}(p)$ remained linear. This is exactly what our model predicts in the case when Ω_1 approaches $\Omega_0^{(LO)}$:

$$\begin{aligned} \omega_{il}^2 &= \Omega_0^{(LO)2} - \frac{2d_0 d_1}{3}\sqrt{p}, \\ \omega_{iu}^2 &= \Omega_0^{(LO)2} + \frac{2}{3}\frac{\epsilon_\infty}{2+\epsilon_\infty} d_1^2 p, \\ \Omega^{(LO)\ 2} &= \Omega_0^{(LO)\ 2} + \frac{2d_0 d_1}{3}\sqrt{p}. \end{aligned} \tag{4.34}$$

DOS in this case is given by the expression

$$D(\omega) \simeq \frac{\Omega_0^{(LO)}}{2\pi^2\lambda^3} \frac{(\omega^2-\Omega_0^{(LO)\ 2})^2+\Delta_{imp}^4}{\left(\frac{2+\epsilon_\infty}{3\epsilon_\infty}d_0^2\right)^{3/2}} \frac{\left(\omega^2-\omega_{il}^2\right)^{1/2}}{\left(\omega_{iu}^2-\omega^2\right)^{5/2}}, \tag{4.35}$$

which has the regular polariton behavior at the boundaries similar to one described by Eq. (4.31), but with a different pre-factor. This pre-factor significantly modifies IPDOS at the center of the band,

$$D(\omega_c) \simeq \frac{3^{1/2}5}{\pi^2} \frac{1}{\lambda^3 \Omega_0^{(LO)}} \left(\frac{\Omega_0^{(LO)\ 2}}{\frac{2+\epsilon_\infty}{3\epsilon_\infty} d_0^2} \right)^{3/2} \left(\frac{\delta_{imp}}{\Omega_0^{(LO)}} \right)^{1/2}, \tag{4.36}$$

which is now proportional to $p^{1/4}$. At very small concentrations, however, this dependence will change over to the one described by Eq. (4.32) as the condition given by Eq. (4.25) becomes valid again.

The dispersion relation for the impurity TO branch becomes in this limit more complicated:

$$\begin{aligned} \omega_i^{(TO)\ 2}(\mathbf{k}) &= \omega_{il}^2 + \frac{1}{2} \left[2\Delta_{imp}^2 + k^2\lambda^2 \left(\frac{2+\epsilon_\infty}{3\epsilon_\infty} d_0^2 \right) \right. \\ &- \left. \sqrt{k^4\lambda^4 \left(\frac{2+\epsilon_\infty}{3\epsilon_\infty} d_0^2 \right)^2 + 4\Delta_{imp}^4} \right], \end{aligned} \tag{4.37}$$

while it still has the same limits $\omega_i^{(TO)}(\mathbf{k}) - \omega_{il} \sim k^2$ for small k and $\omega_i^{(TO)}(\mathbf{k}) = \omega_{iu}$ for large k. The crossover parameter, however, is no longer the localization length l_0, but rather a vacuum wavelength of light at frequency Ω^{LO}: $\lambda = \Omega^{LO}/c$. The effective mass of the branch at the longwave boundary is much larger than in Eq. (4.27) and does not depend upon concentration. The LO frequency of the impurity polariton branch does not show any dispersion:

$$\omega_i^{(LO)}(\mathbf{k}) = \omega_{il}, \tag{4.38}$$

similar to the situation considered before, for $k^2 > \Delta_{imp}^2/(\lambda^2 d_0^2)$ two branches of IPB run almost parallel showing a very small dispersion.

The group velocity at the boundaries approaches zero at the same rate as before, but at the center of the band, the dependence upon the concentration is different:

$$\frac{v_g(\omega_c)}{c} \simeq \frac{3^{1/2}}{5} \left(\frac{2+\epsilon_\infty}{3\epsilon_\infty} \frac{d_0^2}{\Omega_0^{(LO)\ 2}} \right)^{1/2} \left(\frac{\delta_{imp}}{\Omega_0^{(LO)}} \right)^{1/2}. \tag{4.39}$$

It is much larger than the respective quantity, when the linear in p expansion is valid, and increases much faster $\sim p^{1/4}$ with the concentration.

4.4.2 Evolution of IPB boundaries with composition parameter

Further increase of concentration leads to more complicated dependencies of the bandwidth, DOS, *etc.* on concentration and other parameters. In this subsection we shall focus upon concentration dependencies of band boundaries, which are experimentally identified with TO and LO phonon frequencies of the electrostatic approximation. These dependencies were extensively studied experimentally, as we have already discussed in the Introduction, and the objective of this subsection is to show how the concept of impurity induced polaritons provides a simple and physically transparent explanation for the weak mode in one-mode crystals, and for one-two-mode behavior. Analysis of poles and zeroes of the dielectric

function (4.15) shows that the evolution of the modes with concentration is determined in our model by a relative position of the characteristic frequencies Ω_0, Ω_1, Ω_0^{TO}, Ω_0^{LO}, Ω_1^{TO}, and Ω_1^{LO}. The first pair of these frequencies are the initial phonon frequency of the host crystal, and LPM of the impurity, respectively. The electrostatic interaction, and the local field changes Ω_0 to actual TO and LO host frequencies Ω_0^{TO} and Ω_0^{LO}. The last pair of the frequencies, Ω_1^{TO} and Ω_1^{LO}, corresponds to TO and LO modes of the crystal made up of impurity atoms only. The local field, which induces the difference between initial frequencies, $\Omega_{0,1}$, and actual TO, LO frequencies, is very important. In pure crystals (made of initial host atoms or initial impurities) the relation between $\Omega_{0,1}$ and $\Omega_{0,1}^{TO}$ and $\Omega_{0,1}^{LO}$,

$$(2+\epsilon_\infty)\Omega_{0,1}^2 = 2\Omega_{0,1}^{(TO)\ 2} + \epsilon_\infty \Omega_{0,1}^{(LO)\ 2}, \tag{4.40}$$

was originally derived in Ref. [71], and its importance was stressed in Ref. [65]. The same relation exists in our model as well. At small concentrations, $p \ll 1$, the initial impurity related frequency Ω_1 is not renormalized by local-field corrections because this renormalization is caused by the interaction with like atoms. At small concentrations an impurity atom is mostly surrounded by atoms of the host crystal, and the renormalization does not occur. Similarly, for $1-p \ll 1$, the local field turns Ω_1 into Ω_1^{TO} and Ω_1^{LO}, while leaving Ω_0 unchanged as a characteristic frequency of former host atoms. Eqs. (4.23) demonstrate that at small p IPB inside the *restrahlen* of the host arises when Ω_1 falls inside the host *restrahlen*, see Fig. 4.2a,c,d. For $1-p \ll 1$, host and impurity atoms exchange their roles. In this case, should Ω_0 falls in between $\Omega_1^{(TO)}$ and $\Omega_1^{(LO)}$, it gives rise to IPB induced now by the "host" atoms. Hence, if both $\Omega_0^{(TO)} < \Omega_1 < \Omega_0^{(LO)}$ and $\Omega_1^{(TO)} < \Omega_0 < \Omega_1^{(LO)}$ conditions are satisfied at the same time, then IPB exists in both $p \to 0$ and $p \to 1$ limits. This situation is shown in Fig. 4.2a. This is one-mode behavior with a "weak" mode. One observes strong TO and LO modes of the original crystal smoothly evolving into those of the end crystal, while inside the *restrahlen* a weak additional TO and LO impurity polariton modes arise with vanishing TO-LO splitting at both ends of the impurity range. This peculiar behavior occurs due to the interplay between the external electric field and the polarization, affecting the local field (4.12). Experimentally, this type might be realized in the materials where the polariton gap is sufficiently wide, which may be the case for many alkali halides. However, because of the weakness of these modes they are vulnerable to any kind of dissipation, as we shall see in the next section. This fact can explain the absence of the defect mode in "classical" (no weak mode inside the *restrahlen*) one-mode mixed crystals. At the same time, we can relate the features presented in Fig. 4.2 to the weak mode observed in the $Ba/SrF_2, Ca/SrF_2$ and some other one-mode crystals (see Discussion). Previously, in order to reproduce the weak feature observed in spectra of these crystals, one had to use models with tens of fitting parameters (see Refs. [50, 51] and references therein). The concept of IPB, presented here, gives a transparent and quite general explanation of this type of spectra.

If IPB exists only in one limit, for example, $\Omega_0^{(TO)} < \Omega_1 < \Omega_0^{(LO)}$ for small p, but Ω_0 lies outside the interval $(\Omega_1^{(TO)}, \Omega_1^{(LO)})$ when $p \sim 1$, our model predicts the one-two-mode behavior (Fig. 4.2c,d). Two types of one-two-mode mixed crystals appear depending upon whether Ω_0 falls below the interval $(\Omega_1^{(TO)}, \Omega_1^{(LO)})$ (Fig. 4.2c), or above it (Fig. 4.2d). In the first case, the lower mode weakens with the concentration, while in the second case, the upper one does. At $p \simeq 0$ the situation remains qualitatively the same as in the one-mode case. At $p \to 1$, the splitting between new modes does not vanish, and they form the new *restrahlen* of the pure crystal at $p = 1$. Strictly speaking, in this limit we cannot justify our

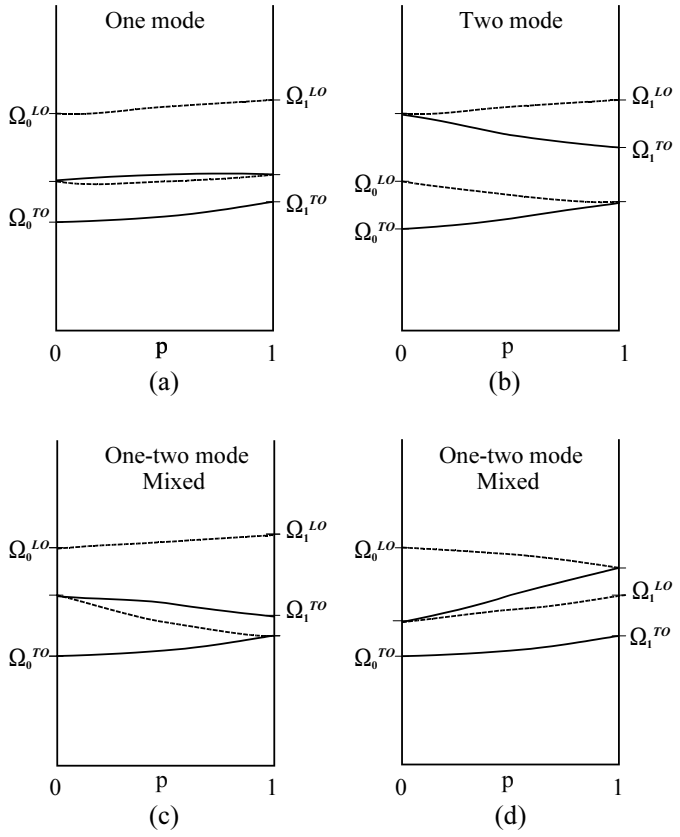

Figure 4.2: Four different types of the evolution of the transverse (solid lines) and longitudinal (dashed lines) optic mode frequencies of the mixed polar crystals with composition parameter. The leftmost and rightmost composition parameters correspond to pure end crystals.

model, since there are no local modes at this end of the concentration range. Quantitatively however, we can still explain the one-two-mode behavior as a result of the presence of LPM's at small p, and the absence of them at p close to one. If in neither limit IPB appears inside the gap ($\Omega_1 \not\subset (\Omega_0^{(TO)}, \Omega_0^{(LO)})$ and $\Omega_0 \not\subset (\Omega_1^{(TO)}, \Omega_1^{(LO)})$), our approach is not applicable at any concentration. Although the absence of the impurity bands at end concentrations, in our opinion, suggests two-mode behavior (Fig. 4.2d).

4.5 Transmittance and reflectance of EM waves from mixed polar crystals

Having obtained the effective dielectric function of the mixed polar crystal, one can study their reflection and transmission spectra for a number of different geometries. Among them, the normal reflection spectrum from a semi-infinite sample and normal transmission and reflection from a slab of finite dimensions are of particular interest since they are a primary source of information about optical properties of crystals studied in numerous experiments [50, 51].

4.5.1 Reflection spectrum of semi-infinite mixed polar crystals

In this section we phenomenologically incorporate damping in the dielectric function (4.15) substituting $\omega + i\gamma$ for ω in the resonance terms of Eq. (4.15). As we already discussed it is sufficient for our qualitative purposes to assume that the damping parameter is the same for both host and impurity related modes. We can note, however, that as numerical calculations demonstrated, properties of each mode are determined primarily by its own relaxation parameters, and effects due to damping in the other subsystem are usually negligible. This means that, in principle, it is possible to experimentally determine relaxation parameters for each of the participating oscillators independently. For our calculations we chose the value of γ such that $\gamma/\Omega_0 \sim 0.1$, which is a rather conservative estimate. For typical polar crystals the relaxation parameter ranges from γ/Ω_0 less than 0.01 to 0.1, and since the relaxation in the impurity subsystem due to coupling to LO phonons inside the *restrahlen* was estimated in Section 4.3 as less than 0.1, our choice for this parameter seems quite reasonable.

After accounting for the dumping, the effective dielectric function (4.15) becomes

$$\epsilon(\omega) = \epsilon_\infty \frac{1 + \frac{2}{3}\left[(1-p)\frac{d_0^2}{\Omega_0^2 - \omega^2 + 2i\gamma\omega} + p\frac{d_1^2}{\Omega_1^2 - \omega^2 + 2i\gamma\omega}\right]}{1 - \frac{\epsilon_\infty}{3}\left[(1-p)\frac{d_0^2}{\Omega_0^2 - \omega^2 + 2i\gamma\omega} + p\frac{d_1^2}{\Omega_1^2 - \omega^2 + 2i\gamma\omega}\right]}. \tag{4.41}$$

For normal incidence, the reflection coefficient from the semi infinite crystal is equal to

$$R(\omega) = \left|\frac{1 - \epsilon^{1/2}(\omega)}{1 + \epsilon^{1/2}(\omega)}\right|^2. \tag{4.42}$$

In the absence of damping, the original dielectric function (4.15) has a peculiar property, which is specific only for the model with IPB within the *restrahlen* of the host. Inside this band, the dielectric function goes from zero to infinity, and hence, necessarily passes through

unity. At a frequency where this happens, the reflection coefficient must become zero, since for this frequency the medium becomes transparent. At small concentrations, this frequency, $\omega_{T=1}$, is determined by the equation:

$$\omega_{T=1}^2 = \frac{\lambda_1^2\omega_{il}^2 + l_0^2\omega_{iu}^2}{\lambda_1^2 + l_0^2}, \tag{4.43}$$

and since l_0 is less or of the order of $\lambda_1 = \Omega_1/c$ it lies slightly off the center of the band, closer to ω_{il}. When relaxation is accounted for, the zero of reflection is not reached, but the reflection still can have a minimum at a certain frequency. The magnitude of reflection at this frequency is determined by relaxation, and can be used for independent measurements of the latter.

We used typical values of the parameters in Eq. (4.41) to plot normal reflection spectra for semi-infinite mixed crystals. The optic frequencies $\Omega_{0,1}^{(TO,LO)}$ of such systems are about a few hundred cm^{-1}, the widths of their polariton gaps range from $\sim 10\%$ for III/V group polar crystals, up to $\sim 30\%$ for alkali halides. The high limit dielectric constant lies within the range of $\sim 3-5$. Fig. 4.3 presents three graphs corresponding to three different types of spectra, which can be described within the model of impurity polaritons. Each graph shows curves obtained for $p = 0\%,\ 25\%,\ 50\%,\ 75\%,\ 100\%$. Fig. 4.3a depicts the reflection spectrum of the one-mode crystal. As it can be seen from the plot, for all concentrations there is one dominating absorption band. Nevertheless, for intermediate concentrations one can notice a weak mode inside this band. This mode is quite weak in accord with the discussion of the previous section, and can be smoothed away by the absorption. Whether this mode will be observed in a concrete material depends upon the interplay of several parameters. At the same time, since we have used realistic values of parameters characteristic for one-mode group of mixed crystals, our calculations show that the impurity polaritons can indeed be used to explain this feature of one-mode type spectra. Reflection spectra corresponding to one-two-mode behavior are shown in Figs. 4.3b,c. There are two types of such spectra, which are very much alike. At small p, the spectra look akin to the one-mode type, but with an increase of the concentration two modes appear, with one-mode growing stronger and the second one diminishing. Spectra Figs. 4.3b,c correspond to phase diagrams shown in Figs. 4.2c,d respectively. It is seen that the presence of damping does not prevent one-two-mode behavior predicted by our model to be observed in reflectance experiments.

4.5.2 Slab of finite dimensions

In this subsection we consider normal reflection and transmission spectra of a mixed crystal slab. The width of the slab is assumed to be much greater than the average distance between the impurities, so that our averaging procedure can be applied. At the same time we do not consider samples thicker than several wavelength, so that the damping does not suppress transmission completely.

The transmission coefficient through a slab of width L for normal incidence is given by

$$T(\omega) = \left| 1 - \frac{(\epsilon^{1/2}-1)^2 \cos\left(\frac{\omega}{c}\epsilon^{1/2}L\right)}{2\epsilon^{1/2}\cos\left(\frac{\omega}{c}\epsilon^{1/2}L\right) - i(\epsilon+1)\sin\left(\frac{\omega}{c}\epsilon^{1/2}L\right)} \right|^2 . \tag{4.44}$$

In the absence of damping, the transmission coefficient turns to unity when either $\epsilon = 1$ or $\omega\epsilon^{1/2}L/c = \pi(m+1/2)$, where m is an integer. The first case corresponds to the frequency

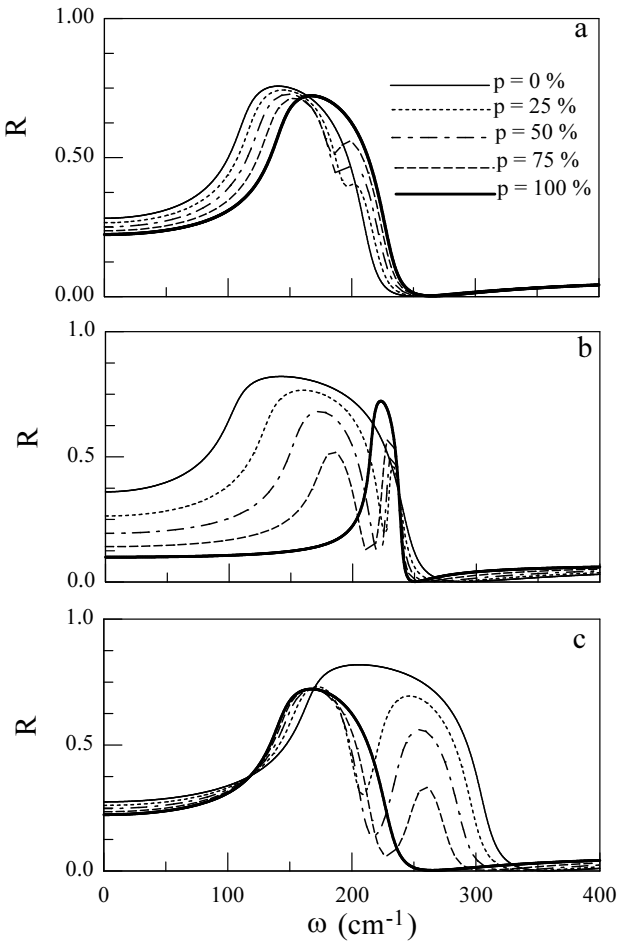

Figure 4.3: Normal reflection spectra from semi infinite mixed crystals. Three graphs correspond to one-mode (graph (a) in Fig. 4.2) and two types of one-two-mode (graphs (c) and (d) in Fig. 4.2) behaviors. The parameters used to generate these graphs (including absorption) are typical parameters for polar crystals.

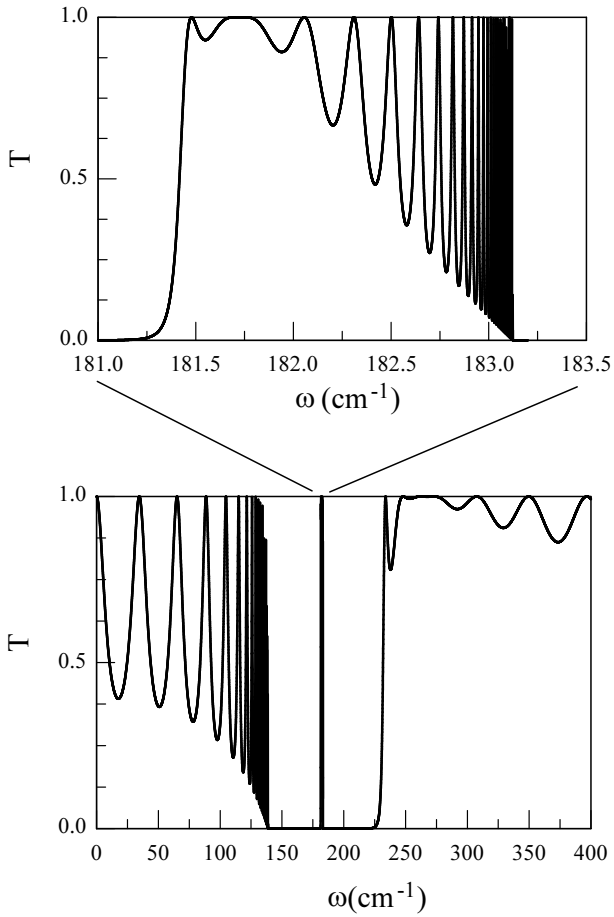

Figure 4.4: Transmittance spectrum through a slab of one wavelength width with typical parameters, plotted as a function of frequency. The lower graph shows the full frequency range, while the upper one is restricted to the polariton defect band at $p = 10\%$.

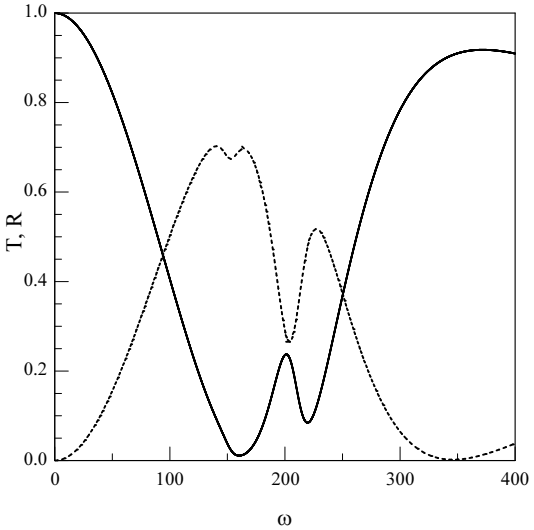

Figure 4.5: Transmission (solid) and reflection (dashed) coefficients of a thin mixed crystal at $p = 20\%$ in the presence of absorption.

determined by Eq. (4.43), when the medium becomes optically transparent, while the second condition corresponds to the usual geometrical resonances.

The width of geometrical resonances decreases as $1/\epsilon(\omega)$ with $\omega \to \omega_{iu}$ because of the divergence of the dielectric function at this frequency. Fig. 4.4 depicts the transmission spectrum of the 10% impure slab of the width $L = \lambda$ in the absence of absorption, where the lower plot shows the broader frequency interval covering the entire *restrahlen* of the host crystal. One can see IPB inside the forbidden gap at the frequency $\sim 180\ cm^{-1}$. The wide flat-top resonance at 181.7 cm^{-1} corresponds to the frequency (4.43), where the dielectric function becomes one, and all the other peaks represent geometrical resonances.

Different natures of the resonances affect their response to damping. The narrow comb of geometrical resonances washes out first even when damping is relatively small. This occurs due to the fact that the geometrical resonances are in essence standing waves that experience multiple reflections and therefore are strongly damped. The $\epsilon = 1$ resonance, to the contrary, is much less affected by the relaxation because polaritons pass through the sample only once. Fig. 4.5 depicts the transmission (solid line) and reflection (dashed line) coefficients for a narrow slab with 20% impurities and the same set of parameters, which was used to generate Fig. 4.3c. It is clearly seen, that even despite of high absorption rate $\gamma/\Omega_0 = 0.1$, the peak in the transmission coefficient survives, and can be associated with the minimum in reflection. It allows us to suggest that reflection anti-resonance observed in many systems can be associated not only with the impurity induced absorption, but also with the impurity induced transmission. A similar transmission maximum was observed experimentally in $CuCl$ [70], where the role of defects was played by some Cu atoms occupying off-center positions. The maximum in the transmission is direct evidence of IPB. It would be of great interest to

carry out transmission measurements for different groups of mixed crystals in order to verify predictions of the current Chapter. We believe that time-resolved measurements could also provide important information, particularly regarding group velocities of these excitations.

4.6 Scattering in IPB

In previous sections we considered optical properties of mixed polar crystals neglecting fluctuations of concentration function $p(\mathbf{r})$. Results obtained for 1D model considered in our previous Chapter suggests that this approximation is a zero-order term in the series expansion in terms of the parameter $l/l_0 \ll 1$, where l is an average distance between defects and l_0 is the localization length of the single LPM. In this section we take into account fluctuations of concentration in the first non-vanishing order in terms of the parameter $\delta p = p(\mathbf{r}) - p$, and show that the actual small parameter of this approximation is indeed $l/l_0 \ll 1$. The main result of this section is to demonstrate that the scattering of impurity polaritons induced by concentration fluctuations is decreasing with an increase of the average concentration, and is actually negligible on the background of absorption. This fact provides a justification for the results obtained in the previous sections of this Chapter, where these fluctuations are neglected.

We shall employ the Green's function formalism in order to calculate the scattering length of the impurity-induced polaritons due to concentration fluctuations. The Green's function of the inhomogeneous dielectric medium can be presented as

$$\left[G^{(0)\ -1}_{\alpha\gamma}(\mathbf{r},\mathbf{r}') - \frac{\omega^2}{c^2}\left[\epsilon(\omega,p(\mathbf{r})) - \epsilon(\omega,p)\right]\delta_{\alpha\gamma}\right] G_{\gamma\beta}(\mathbf{r},\mathbf{r}') = \delta_{\alpha\beta}\delta(\mathbf{r}-\mathbf{r}'), \tag{4.45}$$

where $G^{(0)}_{\alpha\gamma}$ is the Green's function of the system with homogeneous dielectric function $\epsilon(\omega,p)$ given by Eq. (4.15). This zeroth order Green's function can be written down in k-space in terms of the projection operators $\hat{\mathbf{e}}^{\perp}_{\alpha\beta} = \delta_{\alpha\beta} - k_\alpha k_\beta/k^2$ and $\hat{\mathbf{e}}^{\parallel}_{\alpha\beta} = k_\alpha k_\beta/k^2$ as

$$G^{(0)}_{\alpha\beta}(\mathbf{k}) = \frac{\hat{\mathbf{e}}^{\perp}_{\alpha\beta}}{k^2 - k_0^2} - \frac{\hat{\mathbf{e}}^{\parallel}_{\alpha\beta}}{k_0^2}. \tag{4.46}$$

where $k_0^2(\omega) = \omega^2\epsilon(\omega)/c^2$. Since we search for the leading corrections to the Greens' function of the system, we expand $\epsilon(\omega,p(\mathbf{r}))$ in terms of $\delta p(\mathbf{r})$ and keep only the linear term

$$\epsilon(\omega,p(\mathbf{r})) - \epsilon(\omega,p) = \frac{\omega^2}{c^2}\frac{\delta\epsilon(\omega,p+\delta p(\mathbf{r}))}{\delta p(\mathbf{r})}\bigg|_{\delta p(\mathbf{r})\equiv 0}\delta p(\mathbf{r}) = \kappa^2(\omega,p)\delta p(\mathbf{r}).$$

Statistical properties of the random function $\delta p(\mathbf{r})$ can be described in this approximation by its momenta up to the second order:

$$\begin{aligned} \langle\delta p(\mathbf{r})\rangle &\equiv 0\ , \\ \langle\delta p(\mathbf{r})\delta p(\mathbf{r}')\rangle &= K(|\mathbf{r}-\mathbf{r}'|). \end{aligned} \tag{4.47}$$

The second order correlator depends only upon the distance between two points in space, since the system is assumed to be homogeneous and isotropic on average. After standard transformations to k-representation one obtains

$$G^{-1}_{\alpha\beta}(\mathbf{k}) = (k^2 - k_0^2)\hat{\mathbf{e}}^{\perp}_{\alpha\beta} - k_0^2\hat{\mathbf{e}}^{\parallel}_{\alpha\beta} - \tag{4.48}$$

$$
\begin{aligned}
- \quad & \kappa^4 \int \frac{d^3k'}{(2\pi)^3} \left(\frac{\hat{\mathbf{e}}^{\perp}_{\alpha\beta}}{k'^2 - k_0^2} - \frac{\hat{\mathbf{e}}^{\parallel}_{\alpha\beta}}{k_0^2} \right) S(\mathbf{k} - \mathbf{k}') \\
= \quad & (k^2 - k_0^2 - \Sigma^{\perp}(k))\hat{\mathbf{e}}^{\perp}_{\alpha\beta} - (k_0^2 + \Sigma^{\parallel}(k))\hat{\mathbf{e}}^{\parallel}_{\alpha\beta},
\end{aligned}
$$

where $S(\mathbf{k})$ is the Fourier transform of the correlator (4.47). The new Green's function can be expressed using transverse and longitudinal mass operators $\Sigma^{\perp}(k), \Sigma^{\parallel}(k)$:

$$
G_{\alpha\beta}(\mathbf{k}) = \frac{\hat{\mathbf{e}}^{\perp}_{\alpha\beta}}{k^2 - k_0^2 - \Sigma^{\perp}(k)} - \frac{\hat{\mathbf{e}}^{\parallel}_{\alpha\beta}}{k_0^2 + \Sigma^{\parallel}(k)}. \tag{4.49}
$$

Real parts of the mass operators determine the renormalization of the spectrum, and are neglected below. We shall only consider imaginary parts of the transverse mass operators, which determine the scattering length (mean-free-path) of the transverse modes, and in the lowest approximation read as

$$
Im\ \Sigma^{\perp}(k_0(\omega), \omega) = i\frac{\kappa^4}{2\pi} k_0 \int S\left(2k_0 \sin\frac{\theta}{2}\right)\ d\cos\theta, \tag{4.50}
$$

where θ is scattering angle between $\mathbf{k}$ and $\mathbf{k}'$. The explicit form of the integral scattering cross section depends on the particular choice of the correlator (4.47). In our case however, when the wavelength of the considered excitations is assumed to be much greater than the characteristic size of the inhomogeneities, the difference between different choices of the correlation function is mostly reduced to a numerical factor of the order of unity. One can choose the correlator, for example, in the standard Gaussian form [74]:

$$
K(|\mathbf{r} - \mathbf{r}'|) = \left\langle \delta p^2 \right\rangle\ e^{-|\mathbf{r}-\mathbf{r}'|^2/l_c^2} \tag{4.51}
$$

with its respective Fourier transform

$$
S(k) = \frac{\left\langle \delta p^2 \right\rangle \pi^{3/2} l_c^3}{8}\ e^{-k^2 l_c^2/4}. \tag{4.52}
$$

In the spirit of our general approach, the concentration fluctuations must be considered with regard to the smoothing volume δV, so that the respective variance $\left\langle \delta p^2 \right\rangle$ is calculated using the Poisson distribution of independent impurities inside the volume δV:

$$
\left\langle \delta p^2 \right\rangle = \frac{p(1-p)}{N(\delta V)}, \tag{4.53}
$$

The correlation length l_c, then should be identified with the $l_{\delta V}$-smoothing length we employed in Eqs. (4.5) and (4.6). However, as will be seen below, the same results can be obtained if one considers initial distribution of discrete impurities and chooses the interatomic distance a as the correlation length. In any case, $k_0 l_c \ll 1$, and the expression for the complex wave number $k(\omega)$ determined from the pole of the respective Green's function takes the form:

$$
k(\omega) = k_0(\omega) + i\frac{\sqrt{\pi}}{16}\ \left\langle \delta p^2 \right\rangle \kappa^4 l_c^3. \tag{4.54}
$$

Using Eq. (4.53) and the identification of l_c one can obtain for the scattering length:

$$
l_s^{-1} \simeq \frac{\pi^{1/2}}{16}\ p(1-p)a^3\ \left[\frac{\omega^2}{c^2}\frac{\delta\epsilon(\omega, p(\mathbf{r}))}{\delta p(\mathbf{r})}\right]^2. \tag{4.55}
$$

In the limit of small concentrations, $p \ll 1$, the derivative of $\epsilon(\omega, p)$ with respect to p can be evaluated in different regions of the spectrum.

To assess the value of the scattering length inside the impurity band we pick the center of the defect band $\omega_c^2 = (\omega_{il}^2 + \omega_{iu}^2)/2$. For small concentration one obtains

$$l_s^{-1}(\omega_c) \simeq \frac{\pi^{1/2}}{4} \frac{l^3}{l_0^4(\Omega_1)} \alpha_1^2 \sim \frac{1}{p}, \tag{4.56}$$

where

$$\alpha_1 = \frac{\Omega_1^2 - \Omega_0^2}{\frac{4\epsilon_\infty}{3(2+\epsilon_\infty)} d_0^2 + \frac{2-\epsilon_\infty}{2+\epsilon_\infty}(\Omega_1^2 - \Omega_0^2)}$$

does not depend upon the concentration. In the last expression the anticipated small parameter l/l_0 has appeared raised to the third power. Taking into account typical values of this parameter for realistic mixed crystals, one can see that this scattering is completely negligible. One may also note that this scattering length increases with concentration, which has a simple physical explanation – the greater the concentration the greater the overlap of individual local states, and the closer the system is to a uniform continuous medium.

For frequencies from host bands, the situation is qualitatively different:

$$\begin{aligned} l_s^{-1}\left(\omega \le \Omega^{(TO)}\right) &\simeq \left[\frac{\pi^{1/2}}{16}\alpha_2^2 \left(\frac{\Omega_0^{(TO)\,2}}{\omega^2 - \Omega^{(TO)\,2}}\right)^4\right] \frac{pa^3}{\lambda^4\left(\Omega_0^{(TO)}\right)} \sim p \\ l_s^{-1}\left(\omega \ge \Omega^{(LO)}\right) &\simeq \left[\frac{\pi^{1/2}}{16}\alpha_3^2\right] \frac{pa^3}{\lambda^4\left(\Omega_0^{(LO)}\right)} \sim p \end{aligned} \tag{4.57}$$

where

$$\alpha_2 = \epsilon_\infty \frac{\frac{\epsilon_\infty}{3} d_0^2 \left(\Omega_0^{(LO)\,2} - \Omega_0^{(TO)\,2}\right)\left(\Omega_1^{(TO)\,2} - \Omega_0^{(TO)\,2}\right)}{\Omega_0^{(TO)\,4}\left(\Omega_1^2 - \Omega_0^{(TO)\,2}\right)}$$

and

$$\alpha_3 = \epsilon_\infty \frac{\frac{2}{3} d_0^2 \left(\Omega_1^{(LO)\,2} - \Omega_0^{(LO)\,2}\right)}{\left(\Omega^{(LO)\,2} - \Omega^{(TO)\,2}\right)\left(\Omega_0^{(LO)\,2} - \Omega_1^2\right)}$$

are constants. This scattering length is much smaller then for impurity polaritons, and is decreasing with the increase of concentration, which is quite a regular behavior. Indeed, the perfectly ordered at $p = 0$ system experiences increasing scattering due to the impurities. This difference between scattering properties of regular and impurity polaritons explains why our approach can be justified to describe properties of the former, while the latter requires more elaborate treatment of disorder.

4.7 Discussion

In this Chapter we suggested that certain features of optical spectra of mixed crystals in the *restrahlen* region can be explained if, along with standard optical phonon vibrations, one introduces additional impurity induced oscillators with the frequency falling into the

restrahlen of the host crystal. Justification for this assumption comes from the concept of LPM's introduced earlier in Refs. [17, 18, 19, 38] and the results obtained here for 1D models which show how local polaritons develop into IPB. LPM's are significantly different from local phonons, which were extensively studied in connection with optical properties of mixed crystals. First, they are assumed to exist in the *restrahlen* region, which in many cases is filled with phonons. Therefore, it is not exactly a spectral gap, which is necessary for local states to exist. However, the dielectric function within the *restrahlen* remains negative, which means that electromagnetic excitations cannot exist in this frequency region, which is therefore a gap for electromagnetic excitations. This situation is reversed compared to the case of pure phonon gaps, which are deprived of phonon states, but contain electromagnetic ones. Because of non-zero electromagnetic DOS, local phonons acquire their electromagnetic radiation width, and because of non-zero phonon DOS, LPM's acquire their phonon "radiation" width. A significant difference between these two situations is that the density of electromagnetic states in the phonon gap is so small that the radiative broadening of local phonons is negligible, while the density of phonon states in the *restrahlen* is large, and local polaritons may or may not survive it. Analyzing known phonon DOS, we found that for some crystals like GaP, ZnS, $CuBr$, $ZnTe$, CuI, SrF_2, BaF_2, PbF_2, UF_2, CaF_2 [72], GaN, AlN,AsN [75], there are actually frequency regions with zero phonon DOS, though often quite narrow ones. Therefore, the right impurity could in principle give rise to a local state considered in Refs. [17, 18, 19, 38]. However, *restrahlen* region of a much broader class of crystals like $NaCl$, $NaBr$, KCl, $RbCl$ and many others [72] are filled with LO phonons whose DOS within certain regions is relatively small. In the present Chapter we studied the life-time of LPM's due to interaction with these LO phonons, and found that under regular circumstances this life-time is no shorter than the one due to anharmonicity. We argued, therefore, that LPM's can actually survive interaction with *restrahlen* phonon states, and contribute to the optical properties of the crystals. Moreover, the presence of some local states within the *restrahlen* was confirmed experimentally in Ref. [66], where neutral dopants (S, Sn, Te) give rise to the local electron-phonon state at the frequency slightly below LO of GaP. What is interesting is that the region where these states reside, has a relatively high density of phonon states, which obviously did not preclude them from existence. All these arguments justify the use of local polaritons to describe properties of the *restrahlen* of mixed crystals.

The second important property of LPM's is that their spatial extent is of the order of optic wavelengths in the *restrahl* ($\sim 10^{-3}\ cm$), which is much larger than the size of local phonons (several interatomic distances). This fact means that even at residual concentrations of impurities, local polaritons overlap, forming a well developed band. We showed in this Chapter that this band can be described using the continuous medium approximation for the impurity subsystem. Neglecting fluctuations of impurity concentration, we derived an effective dielectric function for our model, and used it to analyze the structure of optical spectra of mixed crystals. This dielectric function describes new IPB's, which arise inside the *restrahlen* of the host crystal.

The first problem we set out to consider using the concept of impurity polaritons was weak features in the spectra of so called one-mode crystals Ba/SrF_2, Ca/SrF_2 [56, 57], $ZnCdS$, $Mn/ZnTe$ [51], and the one-two-mode behavior of a different group of crystals In/GaP [58], $PbSe/Te$ [59], K/RbI [60, 61], $RbBr/Cl$, $GaAs/Sb$, $InAs/Sb$, $AgBr/Cl$ [51], $In/GaAs$ [73]. The existing descriptions of these types of spectrum [51] require a great number of fitting parameters. Our model allowed us to explain these types of spectra naturally as manifestations of the impurity polariton mode, which reveals itself differently depending

upon the relation between fundamental frequencies of crystals at both ends of the concentration range, and the frequency of LPM. Introducing relaxation in a phenomenological way, we considered reflection and transmission spectra, and demonstrated that our model survives rather strong damping, and reproduces spectra closed to experimental observations. For rather thin samples our model predicts a resonant enhancement in the transmission at the frequency of the impurity polaritons, which accompanies an anti-resonance in reflection. The latter was observed in many papers [50, 51], but was mostly attributed to the impurity induced absorption. The only transmission measurements known to us were performed on pure $CuCl$ [70], where transmission was found to exhibit the maximum similar to the one predicted in our work. $CuCl$ is a peculiar material, since Cu atoms at low temperature can occupy several non-equivalent positions, thereby creating internal defects [68, 69]. These off-center Cu atoms can be responsible for IPB, and therefore, transmission spectra of $CuCl$ can be considered as the first evidence of this band.[1]

Since we took the retardation into account, we were able consider not only boundaries of the spectra but also dispersion laws, DOS, and group velocities of the impurity induced polaritons. One of the most remarkable properties of these excitations is that their group velocity is proportional to the concentration, and can be thousands of times smaller than the speed of light in vacuum. The smallness of the group velocity makes dispersion curves of the excitation look almost flat. Rather similar dispersion curves were measured experimentally in Ref. [68] in one-two-mode mixed crystal $Ga_{0.70}In_{0.30}P$ with the use of Raman spectroscopy. It would be interesting to carry out additional steady state and time-resolved experiments in this material, which could verify predictions of our theory and provide more solid support for our concept of impurity-induced polaritons. Our approach also allowed us to study scattering of impurity polaritons due to fluctuations of concentrations. We found that their scattering length is significantly different from the similar characteristics of regular polaritons of the host material. The scattering length of impurity polaritons is proportional to the concentration, making the scattering less efficient with an increase of concentration. Quantitatively, the scattering length is very large, much larger than the attenuation length due to inelastic damping, making scattering due to concentration fluctuations negligible for impurity polaritons. This finding is in agreement with the results obtained in Chapter 3 and provides a firm foundation for our approach. The scattering length for regular host polaritons, at the same time, is inversely proportional to the concentration, and is rather short. Therefore, studying optical properties related to these excitations requires more elaborate theoretical approaches used in many papers on the subject (see, for instance, Ref. [65]).

We hope that the present results will revive an interest of experimentalists in the properties of *restrahlen* of mixed crystals. In our opinion, it would be interesting to study transmission spectra through thin slabs of one-two mode crystals in both CW and time resolved experiments. Such experiments could provide additional insight into properties of impurity polaritons, and elucidate their dynamic properties, such as group velocities. Comparing experiment and present theoretical results, one can obtain additional information about the material parameters of these systems.

[1] A.J. Sievers drew our attention to an alternative explanation of the IR reflection spectra of *CuCl*. In Refs. [39], an additional absorption line inside the gap was attributed to the interaction of TO phonons with acoustic phonons arise from by strong anharmonic terms in the potential of *Cu* atoms, rather than due to an additional polariton band associated with the off-center ions. Although there exists strong evidence in favor of the model discussed in Refs. [76], it does not explain, however, the enhanced transmission observed in Ref. [70].

Chapter 5

Tunable LPM's in semiconductors

5.1 Introduction

Capture of non-equilibrium charge carriers by a deep defect center provides an important channel of energy dissipation in wide-bandgap semiconductors and insulators [77]. A significant amount of energy, at least equal to the binding energy, $\epsilon_T \simeq 1eV$, of the electron (or the hole) to the center, should be released in each capture event, is usually accompanied by a substantial lattice relaxation. Several mechanisms can be responsible for the electron transitions involving deep levels in semiconductors. The energy lost by the captured carrier can be transferred either to photon(s) in the radiative transition [78], or to nearby carrier in the Auger effect [79], or to a series of long-wavelength acoustic phonons when the carrier descends a staircase of the excited states in the cascade mechanism [80], or to the local vibration quanta when multi-phonon emission [81] takes place. There are some indirect [82, 83, 84] and direct [85, 86, 87, 88, 89, 90, 91, 92, 93, 94] evidence that capture or release of the charge carrier is associated not only with the lattice relaxation but, more importantly with the alteration of local vibrational modes (LVM's), i.e. with changes in the local elastic constants.

In this Chapter we show that (LPM's) are sensitive to the charge-state induced changes in local elastic constants and should, therefore, exhibit the effect similar to charge-state-dependent LVM's.

5.2 Local polariton states in 3D

The system under consideration is a polar 3D crystal where dynamics of the atoms can be described by the classical Newton equations. Polaritons in the system arise as collective excitations of the polarization waves related to optical phonons of "right" symmetry, coupled to the electromagnetic field by means of a coupling parameter α proportional to the oscillator strength of the respective oscillations. The electromagnetic subsystem is described by Maxwell equations that include the polarization density related to phonons [38].

In a perfect crystal, the solution of the system of the Maxwell and atomic equations in the long-wave approximation yields the dispersion equation. The dispersion curves, of course,

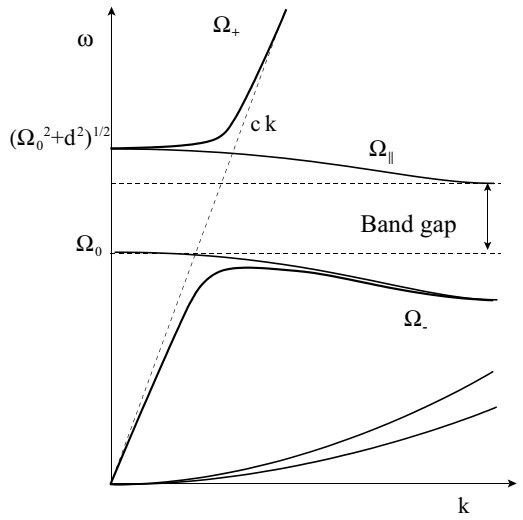

Figure 5.1: Schematic phonon dispersion curves in a polar crystal.

depend on the symmetry of the crystal. For our consideration, however, the particular form of the dispersion is not important as long as the polariton gap exists. Therefore, in the long-wave approximation we can present the upper, $\Omega_+(k)$, and lower, $\Omega_-(k)$, polariton branches in the following isotropic form [38] (see Fig. 5.1):

$$\Omega^2_{\pm}(k) = \frac{1}{4}\left(\sqrt{[\Omega_\perp(k)+ck]^2+d^2} \pm \sqrt{[\Omega_\perp(k)-ck]^2+d^2}\right)^2 . \tag{5.1}$$

Here $\Omega^2_\perp(k)$ is the TO branch of the phonon spectrum, which in the long-wave limit can be approximated as $\Omega_0^2 - v_\perp^2 k^2$, where $v_\perp$ determines the spatial dispersion of TO phonons, c is the speed of light in the crystal, and k is the wave vector. The width of the polariton bandgap, $(\Omega_0, \sqrt{\Omega_0^2+d^2})$, is determined by a parameter d, related to the coupling constant α.

In ideal crystals, LO phonons do not interact with transverse excitations. In the presence of defects, however, restrictions due to momentum conservation are relaxed, and the energy of LPM can leak via LO phonons, if the latter have a nonzero density of states at the frequency of LPM. In this case, the phonon component of LPM becomes delocalized, but its electromagnetic component remains localized. There are few crystals where the dispersion of the LO branch, $\Omega^2_{||}(k) = \sqrt{\Omega_0^2+d^2} - v^2_{||}k^2$, is not large enough to fill the entire bandgap and LPM can exist as truly localized states. In most cases, the LO modes have rather large dispersion with a non-zero density of the phonon states throughout the entire gap. However, as it was shown in the previous Chapter the large dispersion leads to a relatively small density of the LO states, and the lifetimes of LPM's in certain materials can be large enough for their survival.

The equation for the frequency of LPM, Ω_{loc}, in the presence of a substitutional defect in a two-sublattice crystal was obtained in Ref. [38]. Assuming that the defect replaces an ion in the negatively charged sublattice, one can write this equation in the following

approximate form

$$\frac{4}{3\pi}\frac{(\Omega_0 a)^3}{v_\perp^2 c}\frac{d}{\sqrt{\Omega_{loc}^2-\Omega_0^2}}\left[\frac{\delta\beta}{\beta}-\left(\frac{m_+}{M}\right)^2\frac{\delta m}{\mu}\right]=1, \tag{5.2}$$

where δm is the deviation of the mass of the defect from that of the host atoms, $\delta\beta$ is the local change in the elastic constant, M is the total mass of the positive (m_+) and negative (m_-) ions, $\mu = m_+m_-/(m_+ + m_-)$ is their reduced mass, and a denotes the lattice constant. This equation describes the LPM arising in the vicinity of the TO long-wavelength limiting frequency Ω_0. Obviously, the real-value solution, Ω_{loc}, of Eq. (5.2) exists when the expression in the braces is positive.

The results obtained in earlier Chapters show that the profile of electromagnetic-wave transmission is shown to have an asymmetric shape (Fano resonance) where the maximum is followed by a closely spaced zero. The maximum value of the transmission exponentially depends on the position of the defect in the crystal and, without absorption, it reaches unity for the defect placed at the center of the system. The width of the resonance decreases exponentially with an increase of the size of the system.

Because of the large spatial size of the local-polariton states, even at a very low impurity concentration, $\sim 10^{12}\ cm^{-3}$, they significantly overlap. As a result, IPB is formed inside the polariton band gap (see Chapters 3,4). This band has a number of interesting properties. For instance, the group velocity of electromagnetic excitations, propagating via such a band, has been found proportional to the concentration of the impurities, and it can be significantly smaller than the speed of light in vacuum. As we saw earlier, for a large range of defect concentrations, the position of the boundaries of the IPB linearly depends on the frequency Ω_{loc} of the "seed" LPM. Therefore, one can expect that the charge-state induced changes in the local elastic constants of the deep centers, that generate the IPB, will affect its boundaries in the same way as they affect the frequency of LPM at smaller concentrations. In the next section, we will explore this idea in reference to the well studied substitutional oxygen defect in gallium phosphide.

5.3 Charge-state induced changes in local elastic constants: O_P center in gallium phosphide

A striking alteration of the local elastic constants was established by Henry and Lang [82] in their detailed experimental studies of the charge states of the O_P center in GaP. This deep donor center has two bound states, 1 and 2, with one or two bound electrons, correspondingly. Henry and Lang concluded that a significant decrease in the local lattice frequency after capture of the first or second electron is needed in order to consistently explain a variety of experimental data on photoionization and thermal emission (deep level transient spectroscopy) involving the two states in question. For state 2, where the second electron is trapped by or released from the electrically neutral center with a short-range attraction potential, this effect can be understood in the framework of the so called "zero-radius potential" model [83, 95, 96]. (Such a model can be justified if the depth of the impurity potential well for the second electron at the center is small compared to its binding energy, ϵ_{T2} [83]) It can be shown [95, 96] that for the "zero-radius potential" center the adiabatic potential curves $U(q)$, corresponding to bound and extended (continuum) electron states, would rather contact than intersect each other at the point q_c (Fig. 5.2) where the electron

binding energy goes to zero [83]. (Here q represents the configurational coordinate corresponding to a single mode of local vibrations that is coupled to the localized carrier(s).) Let us demonstrate that this rather general requirement accounts for the alteration of LVM of the O_P center in GaP introduced *ad hoc* in Ref. [82].

In the adiabatic harmonic single-mode approximation, the potential energy of the heavy ion, which itself is an eigenvalue of the light-electron Hamiltonian, can be presented as

$$U_N(q) = \frac{\beta_0 q^2}{2} + N\epsilon(q) + U_c n_\uparrow n_\downarrow + (2-N)E_c. \tag{5.3}$$

The first term in this equation describes the elastic energy in the absence of the localized electrons with β_0 being the elastic constant, and

$$\epsilon(q) = \epsilon_0 - \lambda q - \frac{\gamma q^2}{2} \tag{5.4}$$

is the localized-electron energy with electron-phonon coupling taken into account by expanding the electron energy in powers of q about the equilibrium point in the absence of electrons. U_c is the Hubbard repulsion energy for two electrons localized at the center, and the last term in Eq. (5.3) is the energy of the electron in the conduction band. $n_\sigma = 0, 1$ is the occupation number of a one-electron localized state with a spin σ, and $N = \sum_\sigma n_\sigma = 0, 1, 2$ is the number of electrons trapped by the center. (In Eq. (5.4), we have chosen the negative sign at the quadratic term to assure the *internal* contact of terms $U_1(q)$and $U_2(q)$; the sign of λ is irrelevant.)

By using the contact condition at the point q_c,

$$U_1(q_c) = U_2(q_c), \quad \left(\frac{dU_1}{dq}\right)_{q_c} = \left(\frac{dU_2}{dq}\right)_{q_c}, \tag{5.5}$$

it is easy to show that $E_c - \epsilon_0 - U_c = \lambda^2/2\gamma$ and therefore the binding (thermal ionization) energy of state 2 is

$$\epsilon_{T2} = U_1(q_1) - U_2(q_2) = \frac{\lambda^2}{2\gamma(1-x)(1-2x)}. \tag{5.6}$$

Here q_N is the equilibrium configuration coordinate of the center with N trapped electrons, and $x = \gamma/\beta_0$. By the same token, the optical ionization energy of state 2 is

$$\epsilon_{opt2} = U_1(q_2) - U_2(q_2) = \frac{\lambda^2}{2\gamma(1-2x)^2}. \tag{5.7}$$

Then with experimentally measured values of $\epsilon_{T2} = 0.89\ eV$ and $\epsilon_{opt2} = 2.03\ eV$ for the O_P center in GaP [82], Eqs. (5.6) and (5.7) yield $x = \gamma/\beta_0 = 0.36$. This allows us to immediately evaluate the ratios of the LVM frequencies for different charge states of the O_P center in GaP:

$$\frac{\omega_2}{\omega_1} = \sqrt{\frac{1-2x}{1-x}} \simeq 0.66; \quad \frac{\omega_1}{\omega_0} = \sqrt{1-x} \simeq 0.80 \tag{5.8}$$

in fairly good agreement with ratios $\omega_2/\omega_1 = 0.65$ and $\omega_1/\omega_0 = 0.78$ extracted by Henry and Lang [82] from numerous experimental data.

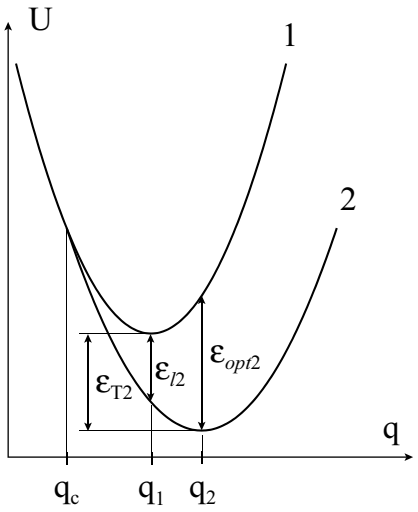

Figure 5.2: Configuration coordinate diagram for the charge states $N = 1, 2$ of the O_P deep center in GaP.

The goal of the above simple exercise is to show that if a multi-charge deep center in one of its states ($N = 2$) can be described by the "zero-radius potential" model, then non-linear electron-phonon coupling may result in a substantial change in the local elastic constants associated with this center when it captures or releases charge carriers. If the second electron is captured by the neutral center as a result of the radiative transition, the energy of the emitted photon is

$$\epsilon_{l2} = U_1(q_1) - U_2(q_1) = \frac{\lambda^2}{2\gamma(1-x)^2}. \tag{5.9}$$

From Eqs. (5.6), (5.7), and (5.9), the following criterion of applicability of the "zero-radius potential" model can be derived (see also Ref. [83]):

$$\epsilon_{T2} = \sqrt{\epsilon_{opt2}\epsilon_{l2}}, \tag{5.10}$$

as opposed to the standard relation [81]

$$\epsilon_{T2} = (\epsilon_{opt2} + \epsilon_{l2})/2, \tag{5.11}$$

held for deep centers with linear electron-phonon coupling when no change in the local frequencies is expected.

If the parameters of a deep center satisfy relation (5.10), as it happens for the O_P center in GaP [83], the capture (release) of the first or second electron will diminish (increase) the local elastic constants in the vicinity of this center. To evaluate the effectiveness of such a rearrangement of the LVM's, let us consider a simple case of the p-type semiconductor doped by shallow acceptors with the concentration N_A and partially compensated by the

deep multi-charge donors of the type considered above with a concentration $N_D \ll N_A$. At equilibrium, all the deep donors will be free of electrons (state 0), i.e. positively charged. Then, incident light with photon energy close to $E_g - \epsilon_{opt1}$ will transfer electrons from the valence band to the states with $N = 0$, thus recharging the deep centers ($+ \rightarrow 0$). (Here E_g is the electron bandgap and ϵ_{opt1} is the optical ionization energy of state 1.) Further evolution of the system depends on the sign of the effective two-electron correlation energy [97, 98]

$$U_{eff} = U_0(q_0) + U_2(q_2) - 2U_1(q_1) = \epsilon_{T1} - \epsilon_{T2}, \tag{5.12}$$

where $\epsilon_{T1} = U_0(q_0) - U_1(q_1)$ is the thermal ionization energy of state 1.

By using experimental values [82] of $\epsilon_{T1} = 1.14\,eV$ and $\epsilon_{T2} = 0.89\,eV$, it is easy to find that $U_{eff} \simeq 0.26\ eV > 0$ for the O_P center in GaP. This means that, in this case, the electrically neutral state 1 generated by photons with energy $(E_g - \epsilon_{opt1})$, which is close to $1.5\ eV$ [82, 84], remains metastable under constant illumination conditions and will not be further converted into negatively charged state 2. Then the electro-neutrality condition,

$$p + N_D^+ = N_A^-, \tag{5.13}$$

combined with the standard rate equations for the concentration $N_D^0 \simeq N_D - N_D^+$ of the deep neutral donors

$$\partial N_D^0/\partial t = \sigma_{p1}^{opt} J N_D^+ - p\,\langle v_p\rangle\,\sigma_{p1}^{th} N_D^0 \tag{5.14}$$

and for the concentration $N_A^0 = N_A - N_A^-$ of shallow neutral acceptors,

$$\partial N_A^0/\partial t = p\,\langle v_p\rangle\,\sigma_{pA}^{th} N_A^- - e_{pA} N_A^0, \tag{5.15}$$

allow one to evaluate the percentage of recharged deep centers. Here p is the concentration of free holes, $\langle v_p\rangle$ is their mean thermal speed; σ_{p1}^{th} (σ_{pA}^{th}) is the non-radiative capture cross-section of the free holes by the deep neutral donors (shallow negative acceptors); σ_{p1}^{opt} is the cross-section of the optical photo-neutralization of state 0; J is the flux of incident photons; $e_{pA} = N_v\,\langle v_p\rangle\,\sigma_{pA}^{th}\exp(-I_A/k_BT)$ is the rate of thermal emission of the holes by the shallow acceptors with the ionization energy I_A; N_v is the valence-band density of states; k_B is the Boltzmann constant.

From Eq. (5.15) it follows that at not very low temperatures such that $T > I_A\,[k_B \ln(N_v/N_A)]^{-1}$, all the shallow acceptors are ionized, i.e. the concentration of the free holes [see Eq. (5.13)] p is approximately N_A ($N_A \gg N_D$). Then for the steady-state illumination conditions, Eq. (5.14) yields

$$\frac{N_D^0}{N_D} \simeq \left[1 + \frac{N_A\,\langle v_p\rangle\,\sigma_{p1}^{th}}{J\sigma_{p1}^{opt}}\right]^{-1}. \tag{5.16}$$

This means that the deep donors will be almost completely photo-neutralized ($+ \rightarrow 0$), if the flux of the incident sub-bandgap photons, $J \geq 10^{19}\ cm^{-2}s^{-1}$. (For this estimate, we take $\sigma_{p1}^{th} = 5 \times 10^{-21}\ cm^{-2}$, $\sigma_{p1}^{opt} = 1.3 \times 10^{-16}\ cm^{-2}$, $N_A = 10^{17}\ cm^{-3}$, $\langle v_p\rangle = 10^7\ cm/s$ [82, 84]). Such a photon flux can be easily generated by a $1W$-source for a spot area of the order of $1\ cm^2$. In a p-type semiconductor with positive-U_{eff} centers, this will convert a high-frequency LVM associated with these centers into a low-frequency one ($\omega_0 \rightarrow \omega_1$). However, for a n-type material the photo-neutralization of the deep positive-U_{eff} centers will have the opposite effect: it converts the low-frequency LVM into the high-frequency one

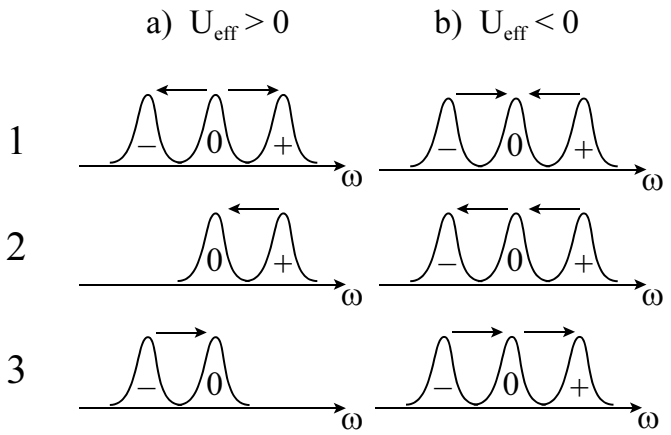

Figure 5.3: Sub-bandgap light-absorption-induced modification of LVM's for the different charge states of a deep center with (a) positive and (b) negative effective two-electron correlation energy in the semi-insulating (1), p-type (2), and n-type (3) semiconductors.

($\omega_2 \to \omega_1$). If the concentration of the deep centers is high enough ($N_D \gg N_A$), then the light from the sub-bandgap or fundamental regions will convert the intermediate-frequency LVM into the high and low-frequency LVM's: $\omega_1 \to \omega_0$, $\omega_1 \to \omega_2$ [see Fig. 5.3a and Eq. (5.8)].

For materials with negative-U_{eff} centers, the continuous sub-bandgap (impurity) illumination should, in principle, have more a profound effect on LVM due to the so called disproportionation [85], i.e. thermodynamically driven spontaneous decay of the metastable electron state 1 into the states with the next higher, state 2, and the next lower, state 0, number of electrons. In p-type materials, it will initially convert the high-frequency LVM, ω_0, into the low-frequency one, ω_1, associated with the neutral donors, which later on due to $U_{eff} < 0$ will be further spontaneously converted into the lower one, ω_2. For n-type materials, as in the previous case of positive U_{eff}, the effect will be opposite: $\omega_2 \to \omega_1 \to \omega_0$ (Fig. 5.3b). And, finally, in semi-insulating material, when the Fermi level is pinned by the negative-U_{eff} defects [97, 98], the illumination should convert the lowest and highest energy LVM into the intermediate one: $\omega_2 \to \omega_1$, $\omega_0 \to \omega_1$ (Fig. 5.3b).

5.4 Centers and materials perspective for alteration of LPM's

It is interesting to compare predictions based on our simple model with the observed optically induced conversion of the charge-state dependent LVM bands in the oxygen doped $GaAs$ [85]. It has been proven that the off-center substitutional O_{As} in $GaAs$ represents one of the few negative-U_{eff} systems in compound semiconductors [85, 86]. And indeed, during illumination with sub-bandgap light with photon energy around 1.37 eV, the high-energy 730.7 cm^{-1} band A is almost completely converted into the low-energy 714.9 cm^{-1}

band B through the other low-energy 714.2 cm^{-1} band B'. These bands were attributed, correspondingly, to the unoccupied, singly, and doubly occupied electron states of the O_{As} center in certain semi-insulating samples of $GaAs$, where the Fermi level was pinned *below* the lowest, doubly occupied, state 2 of O_{As} [85, 86]. The material in question is analogous to p-type semiconductors with the negative-U_{eff} centers in our classification. We conclude that, though in accordance with our model $\omega_0 > \omega_2$, the frequency of the singly occupied state, ω_1, is almost the same as that of the doubly occupied one, ω_2, as opposed to the case of the O_P center in GaP for which $\omega_0^2 - \omega_1^2 = \omega_1^2 - \omega_2^2 > 0$. An extensive discussion of the electronic structure of O_{As} in $GaAs$ can be found in Ref. [86]. According to Skowronski [86], oxygen in $GaAs$ creates a complex off-center defect with dangling gallium hybrids involved, whose coupling strongly depends on the charge state of the center. The adiabatic potentials of the coupled dangling bonds in tetrahedrally bonded and amorphous semiconductors are shown to have a complex multi-well structure that is extremely sensitive to parameters of the structural defects in question [99, 100, 101]. For instance, a stretched bond of the type, participating in the formation of O_{As} in $GaAs$, with one or three electrons, will be strongly coupled to at least two LVM's with charge-state dependent frequencies [100]. Though such a defect is not described by the above single-mode model, it can be responsible for photo-induced changes in the local elastic constants.

Let us now return to O_P in GaP. The elastic constants for the three different charge states, β_N ($N = 0, 1, 2$ enumerates the charge states of the center), of this center are directly related to the frequency of the correspondent LVM's given by Eq. (5.8):

$$\frac{\beta_2}{\beta_1} = \left(\frac{\omega_2}{\omega_1}\right)^2; \qquad \frac{\beta_1}{\beta_0} = \left(\frac{\omega_1}{\omega_0}\right)^2.$$

We want to check if this defect can give rise to LPM's in any of its charge states. According to Eq. (5.2), the criterion for the appearance of LPM's is set by

$$\frac{\delta\beta_N}{\beta} - \left(\frac{m_+}{M}\right)^2 \frac{\delta m}{\mu} > 0, \tag{5.17}$$

where $\delta\beta_N = \beta_N - \beta$ with β being the elastic constant of the host atom. Therefore, it is not sufficient just to know the ratios of the local elastic constants, we need to establish their values. It is equivalent to finding the frequencies of LVM's since $\beta_N \simeq m_O\omega_N^2$, where m_O is the mass of the oxygen atom. Direct experimental measurements of these frequencies are not available to us; however, it is possible to determine them from the configuration coordinate diagram of this center (Fig. 5.2). Calculated by means of the "zero-radius potential" model, the multi-phonon emission electron-capture cross-sections were compared in Ref. [83] with the experimental data from deep level transient spectroscopy [82]. It gave $\omega_1 \simeq 195\ cm^{-1}$ for the O_P defect in GaP. This value differs from the one ($\omega_1 \simeq 155\ cm^{-1}$) obtained in the original paper (Ref. [82]), where fitting is believed to be somewhat inconsistent [83]. Later, in Ref. [102] it was argued that because of a strong field dependence of the thermal emission energy, ϵ_{T1}, of the electron from the singly occupied state, the deep level transient spectroscopy data should be re-evaluated. This led to a modified value of the local-phonon energy $\omega_1 \simeq 290\ cm^{-1}$. We believe that the above re-evaluation of ω_1 should not affect the ratios of the frequencies given by Eq. (5.8), for in the framework of the model developed, it is based on the value of parameter $x = \gamma/\beta_0 = 0.36$. The latter, in turn, was obtained by means of the ratio $\epsilon_{opt2}/\epsilon_{T2}$ involving experimentally measured ionization energies of the state $N = 2$ with a short-range potential that can hardly be affected by the electric field in the area of the p-n junction.

Examining criterion (5.17) for LPM's to occur, one can see that in the most favorable case $\delta\beta_N$ should be positive while δm should be negative. This has a simple physical explanation. As the frequency of the TO mode is defined by $\omega_{TO} = (\beta/\mu)^{1/2}$, in order to make the defect frequency $\Omega_{loc}^{(N)}$ advance into the polariton bandgap (above the TO frequency) one should either make β_N larger than β ($\simeq$ 175 N/m in gallium phosphide) of the host atoms, or decrease the mass of the defect.

For the case of the oxygen center in gallium phosphide where $\delta m < 0$, we examined three values of β_1 obtained by means of all three values of ω_1 from Refs. [82, 83, 102]. Then we used ratios (5.8) between the rest of the LVM frequencies to determine the local elastic constants β_N of the defect in three charge states. We find that using the data from Refs. [82, 83], it is not possible to satisfy our condition Eq. (5.17). On the other hand, $\omega_1 \simeq 290\ cm^{-1}$, obtained in Ref. [102], results in $\beta_0 \simeq 160\ N/m$, $\beta_1 \simeq 95\ N/m$, and $\beta_2 \simeq 40\ N/m$. Even though for all three charge states $\delta\beta_N < 0$, $\beta_{N=0}$ still satisfies Eq. (5.17). Thus, we predict that in the p-type (semi-insulating) GaP:O, the LPM associated with $N = 0$ charge-state will be eliminated (created) by illuminating the sample with the light with a photon energy close to 1.48 eV (0.96 eV) (see Ref. [82] for details), and as it was shown for the charge-state dependent LVM's, this process is reversible. We also stress that the LPM's arise/disappear between TO (365 cm^{-1}) and LO (405 cm^{-1}) frequencies, in contrast to the LVM's that occur either below or above this region.

The oxygen defect in GaP cannot, by any means, be considered as a single candidate for tunable LPM's to be observed. Semiconductors and insulators that possess a complete (omnidirectional) polariton gap include well known materials such as GaP, SiC, ZnS, $ZnTe$, CuI, CaF_2, SrF_2, BaF_2, PbF_2 [103, 104], as well as extensively studied nitrides AlN, GaN, InN [75]. In these materials many impurities form deep centers [77, 50, 105, 106]. The charge-state dependent LVM's, which can be considered as precursors of tunable LPM's, remain relatively unstudied. In a recent paper by Wetzel *et al,*[89] the charge-state dependent triplet of LVM's generated by oxygen in GaN has been reported, which is similar to the GaP:O deep center. Even though this defect does not satisfy our condition for LPM's, Eq. (5.17), ($\delta\beta < 0$ and $\delta m > 0$ for this defect), it gives us confidence that some defects can give rise to LPM's in crystals with the complete polariton bandgap. Our optimism is also supported by the fact that there are many defects that satisfy this criterion but occur in materials without a polariton gap, namely: $GaAs$:O, [85, 86] $EL2$ center in $GaAs$ [90], $GaAs$:Si [92], Si:H [93], and $AlAs$:Be [94], Si:C [87, 88].

Chapter 6

LPM's in multiple quantum well heterostructures

6.1 Introduction

Equations describing dynamics of the light-exciton interaction in multiple quantum well (MQW) heterostructures are essentially equivalent to a model of 1D chain of dipoles used in Chapter 2,3. Similar equations also appear in the theory of atomic optical lattices [107]. The essential difference between results presented in this Chapter and previous studies stems from the peculiarities of the Bragg arrangement. Using Greens' function and transfer matrix formalisms, we study both eigenfrequencies of LPM's for different types of defects and transmission properties of the defect structures. Using parameters of the system studied experimentally in Ref. [26, 27], we predict which defects will produce the most significant changes in transmission and reflection properties of realistic MQW structures.

Optical properties of MQW's have attracted a great deal of interest recently [21, 22, 23, 24, 26, 27, 108, 109]. Unlike other types of superlattices, excitons in MQW are confined in the planes of the respective wells, which are separated by relatively thick barriers. Therefore, the only coupling between different wells is provided by the radiative optical field. The coupling results in MQW polaritons – coherently coupled quasi-stationary excitations of quantum well (QW) excitons and transverse electromagnetic field. The spectrum of short MQW structures consists of a number of quasi-stationary (radiative) modes with finite life-times. This spectrum is conveniently described in terms of super- or sub-radiant modes [21, 23, 108]. When the number of wells in the structure grows, the life-time of the former decreases, and the life-time of the latter increases. In longer MQW structures, however, this approach becomes misleading, as discussed in Ref. [110], and a more appropriate description is obtained in terms of stationary modes of an infinite periodic structure. The spectrum of MQW polaritons in this case consists of two branches separated by a gap with a width proportional to the exciton-light coupling constant Γ [21, 23]. The length at which this description becomes preferable, usually depends upon a problem at hand. For instance, even though the discrete structure of the sub-radiant modes of 100 long MQW in Refs. [26, 27] could be resolved, the description of the gap region in terms of the super-radiant mode leads to an apparent contradiction with the absence of significant luminescence in this region. If one is interested in properties of the gap region, a "long system" usually means that it is

longer than the penetration length of radiation into the sample. The latter length depends upon the frequency, therefore the system can be long enough for frequencies close to the center of the gap, and still "short" for frequencies in the vicinity of the band edges. Systems similar to those studied in Ref. [27] can be considered sufficiently long for 90% of the gap region when the number of wells becomes close to 200.

In a number of papers [22, 26, 27, 109] it was shown that the width of the polariton bandgap can be significantly increased by tuning the interwell spacing, a, to the Bragg condition, $a = \lambda_0/2$, where λ_0 is the wavelength of the light at the exciton frequency Ω_0. Under this condition, boundaries of two adjacent gaps become degenerate, and one wider gap with the width proportional to $\sqrt{\Gamma}$ is formed. Detuning of the lattice constant from the exact Bragg condition removes the degeneracy and gives rise to a conduction band in the center of the Bragg gap [110]. A well-pronounced Bragg polariton gap was observed in recent experiments [27] with $InGaAs/GaAs$ Bragg structures with the number of wells up to 100. These experiments convincingly demonstrate that despite homogeneous and inhomogeneous broadening, the coherent exciton-photon coupling in long MQW is experimentally feasible. Polariton effects arising as a result of this coupling open up new opportunities for manipulating optical properties of quantum heterostructures.

One such opportunity is associated with introducing defects in MQW structures. These defects can be either QW's of different compositions replacing one or several "host" wells, or locally altered spacing between elements of the structure. It is well known in the physics of regular crystals (see, for instance, Ref. [9]) that local violations of otherwise periodic structures can lead to the appearance of local modes with frequencies within spectral gaps of host structures. This idea was first applied to MQW in Ref. [111], where it was shown that different defects can indeed give rise to local exciton-polariton modes in infinite MQW. Unlike regular LPM's in 3D periodic structures, these modes are localized only in the growth direction of the MQW, while they can propagate along the planes of the wells. Therefore, one should clearly distinguish these defect polariton modes from well known interface modes in layered systems or non-radiative two-dimensional polariton modes in ideal MQW [28, 29, 112]. The latter exist only with the in-plane wave numbers, $k_{||}$, exceeding certain critical values, while LPM in a defect MQW structure exists at $k_{||} = 0$ and can be excited even at normal incidence.

In this Chapter we present results of detailed studies of LPM's produced by four different types of individual defects in Bragg MQW structures. The peculiar structure of Bragg MQW's results in a wider than usual polariton gap, which is actually formed by two gaps with degenerate boundaries. This property has a profound effect on the properties of local modes, leading, for instance, to emergence of two local states from a single defect. The similar effects of doubling the number of local modes was also predicted in the case of braggoritons - excitations arising inside photonic band gaps of periodic structures made of a dispersive material, if the resonance frequency of the dielectric functions happens to belong to the gap [113].

We neglect in-plane disorder in individual QW's, and assume that apart from a deliberately introduced single defect, the structure remains ideally periodic. We consider LPM's with zero in-plane wave vector only. Such modes can be excited by light incident in the growth direction of the structure, and can result in the resonance transmission of light with gap frequencies. This effect is studied both analytically and numerically with the nonradiative decay taken into account phenomenologically. The rate of the non-radiative decay may include contributions from homogeneous as well as from non-homogeneous broadening; such an approach was shown in Ref. [114] to give a good description of high quality MQW

structures.

6.2 Defect modes in Bragg MQW

In order to describe optical properties of QW's one has to take into account the coupling between retarded electromagnetic waves and excitons. This is usually done with the use of the non-local susceptibility determined by energies and wave functions of a QW exciton [21, 112]. The treatment of the exciton subsystem can be significantly simplified if the interwell spacing is much larger than the size of a well itself. In $InGaAs/GaAs$ MQW structures studied in Ref. [27], on which we base our numerical examples, the width of the QW layer amounts only to about 10% of the period of the structure. In this case, one can neglect the overlap of the exciton wave functions from neighboring wells and assume that an interaction between well excitons occurs only due to coupling to the light. It is also important that the width of the wells is also considerably smaller than the exciton's Bohr radius, and, therefore, one can neglect spatial extent of the wells, and describe them with polarization density of the form: $\mathbf{P}(\mathbf{r}, z) = \mathbf{P}_n(\mathbf{r})\delta(z - z_n)$, where $\mathbf{r}$ is an in-plane position vector, z_n represents a coordinate of the n-th well, and $\mathbf{P}_n$ is a surface polarization density of the respective well. Optical response of the system even in the presence of inhomogeneous broadening is successfully described by the linear dispersion theory (see, for instance, Ref. [114]) based upon a single oscillator phenomenological expression for the exciton susceptibility

$$\chi = \frac{d^2}{\Omega_0^2 - \omega^2 - 2i\gamma_{nr}\omega}, \tag{6.1}$$

where Ω_0 and γ_{nr} are $1s$ exciton frequency and relaxation parameter respectively, d is a parameter describing the light-exciton coupling. For our purposes, however, it is more convienient to consider explicitely equations of exciton dynamics coupled with Maxwell equations for the electromagnetic field. In the case of waves propagating along the growth direction of the structure, which is considered here, only excitons with the zero in-plane wave number are coupled to light, and the equations of motion can be presented in the form similar to Eqs. (2.1,2.3):

$$\left(\Omega_n^2 - \omega^2 - 2i\gamma_{nr}\omega\right) P_n = \frac{1}{\pi} c\Gamma_n E(z_n), \tag{6.2}$$

$$\frac{\omega^2}{c^2} E(z) + \frac{d^2 E(z)}{dz^2} = -4\pi \frac{\omega^2}{c^2} \sum_n P_n \delta(z - z_n), \tag{6.3}$$

where Ω_n is the exciton frequency of the n-th QW. The strength of the exciton-photon coupling in Eq. (6.2) is described by the parameter Γ_n equal to the radiative decay rate of a single n-th well. This parameter is related to the parameter d of Eq. (6.1) according to $d^2 = (c\Gamma)/(\pi w)$, where w characterizes the spatial extent of exciton wave functions in the growth direction (we assumed it to be zero when we described the exciton polarization by the δ-function). In what follows, we refer to Γ_n as to a coupling parameter. The relation of Γ_n to the radiative life time can be established, for instance, if one uses Eqs. (6.2) and (6.3) to obtain the reflection coefficient for a single n-th QW, r_n,

$$r_n = \frac{2i\omega\Gamma_n}{\Omega_0^2 - \omega^2 - 2i\omega(\gamma_{nr} + \Gamma_n)} \approx \frac{i\Gamma_n}{\Omega_0 - \omega - i(\gamma_{nr} + \Gamma_n)} \tag{6.4}$$

which in the resonance approximation (the last expression in Eq. (6.4)) coincides with the standard linear dispersion theory expression used in Refs. [22, 27] and others.

In an infinite pure system, all $\Gamma_n = \Gamma_0$, $\Omega_n = \Omega_0$, $z_n = na$, where $a = \lambda_0/2$ is the Bragg's interwell separation. Eq. (6.3) describes an electromagnetic wave of one of the degenerate transverse polarizations, propagating in the growth direction of the structure. This equation coincides with equations used in Refs. [19, 107] and here, in Chapters 2,3, for one-dimensional chains of atoms. The spectrum of ideal periodic MQW's with homogeneous broadening parameter $\gamma_{nr} = 0$ has been studied in many papers [21, 23, 110, 107, 115, 116]. In the specific case of Bragg structures, the exciton resonance frequency, Ω_0, is at the center of the bandgap determined by the inequality $\omega_l < \omega < \omega_u$, where $\omega_l = \Omega_0 \left(1 - \sqrt{2\Gamma_0/\pi\Omega_0}\right)$ and $\omega_u = \Omega_0 \left(1 + \sqrt{2\Gamma_0/\pi\Omega_0}\right)$ [110]. In the formed bandgap the electromagnetic waves decay with the penetration (localization) length,

$$l_0^{-1} = a^{-1} \ln \left(\cos(k_0 a) + \frac{\beta}{2} \sin(k_0 a) - \sqrt{\left[\cos(k_0 a) + \frac{\beta}{2} \sin(k_0 a)\right]^2 - 1} \right), \tag{6.5}$$

where $k_0 = \omega/c$ and

$$\beta = \frac{4\Gamma_0 \omega}{\omega^2 - \Omega_0^2}. \tag{6.6}$$

As in Chapter 2, parameter β is proportional to the susceptibility of the well in the absence of exciton relaxation, Eq. (6.1), and is the main quantity used in our theory to characterize the optical response of the single well. The homogeneous broadening can be taken into account by adding $2i\gamma_{nr}\omega$ in the denominator of Eq. (6.6); we, however, neglect it until the last section of this Chapter, where transmission and reflection spectra of defect MQW structures are discussed.

As it was mentioned earlier, for structures, which are longer than the penetration length, l_0, for the most of the band-gap, consideration based upon modes of the infinite periodic structure is more appropriate. Using Eq. (6.5) one can show that in the case of 140 (for GaAs/AlGaAs) or 200 (for InGaAs/GaAs) wells long MQW's of the type considered in Refs. [26, 27], $l_0 > Na$ for 90% of the bandgap of the infinite structure characterized by the boundaries ω_l and ω_p. This bandgap is the frequency region where we look for new local states associated with the defects. In this Chapter, we consider four types of such defects. First of all, one can replace an original QW with a QW with different exciton frequency (Ω-defect). This can be experimentally achieved by varying the composition of the semiconductor in the well. Another possibility is to change the coupling constant (Γ-defect) at one of the wells. Even though an experimental realization of this defect in its pure form is not straightforward, it is still methodologically important to consider such an idealized situation in order to be able to estimate how changes in Γ could effect optical properties of the systems with real defects. The third possibility is to perturb an interwell spacing between two wells. Here we distinguish two defects, which we call a- and b-defects. The former is realized when the interwell spacing between a pair of wells is changed (Fig. 6.1a). It can be seen that this induces a shift in the position of all wells that follow the defect, making it significantly nonlocal. The b-defect is produced when one shifts just one well keeping positions of the rest unchanged (Fig. 6.1b). Experimental realizations of these two defects is simple and can be done at the sample growth stage. In the following section we show that each of these types affects the optical properties of the MQW lattice in remarkably different ways.

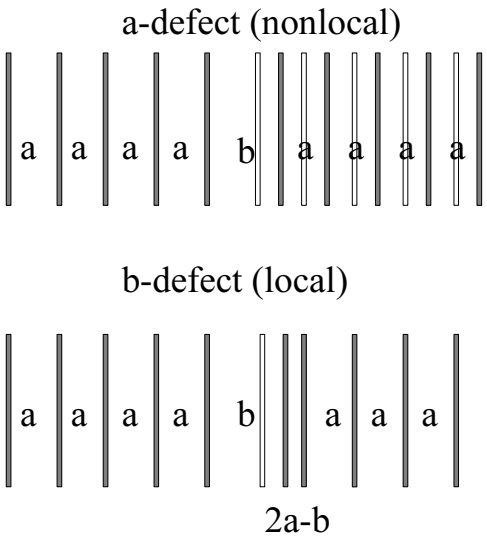

Figure 6.1: Two types of interwell spacing defects. The nonlocal a-defect (a) as opposed to the local b-defect (b). Solid bars represent locations of QW's in the defect lattice. The empty bars represent what would have been a perfectly ordered MQW lattice.

We start with Ω- and Γ-defects which are similar in a sense that they both introduce perturbations in the equation of motion, Eq. (6.2), which are localized at one site (the diagonal disorder). Therefore, they can be studied by the usual Green's function technique like the one used to treat the localized phonon states in impure crystals (see, for instance, Ref. [9]). Using the polarization Green's function defined in a standard way by adding δ_{n,n_0} to Eq. (6.2), we can express the polarization of the n-th QW in terms of the polarization of the defect QW, P_{n_0} as

$$P_n = G(n - n_0)P_{n_0}.$$

(see details of the derivation, as well as an expression for $G(n-n_0)$ in Chapter 2). Allowing $n = n_0$, and using expression for the Green function from Eq.(2.9) one obtains the equation for eigenfrequencies of LPM:

$$F_{\Omega,\Gamma} = \frac{\frac{\beta}{2}\sin(k_0 a)}{\sqrt{\left[\cos(k_0 a) + \frac{\beta}{2}\sin(k_0 a)\right]^2 - 1}}, \tag{6.7}$$

where the function $F_\Omega = \left(\Omega_1^2 - \omega^2\right) / \left(\Omega_1^2 - \Omega_0^2\right)$ corresponds to the Ω-defect and the function $F_\Gamma = \Gamma_0 / (\Gamma_1 - \Gamma_0)$ describes the Γ-defect; Ω_1 and Γ_1 denote respective parameters of the defect layer. Eq. (6.7) is an exact consequence of Eqs. (6.2) and (6.3), and was first derived in Chapter 2 for the Ω-defect. There, in the longwave approximation, we found that the equation had one real valued solution for any $\Omega_1 > \Omega_0$. We find that in the case of the Bragg structures, there are always two solutions for both types of defects, one below Ω_0 and one above. This is a manifestation of the fact that the bandgap consists of two gaps positioned one right after the other. The above equations can be solved approximately when

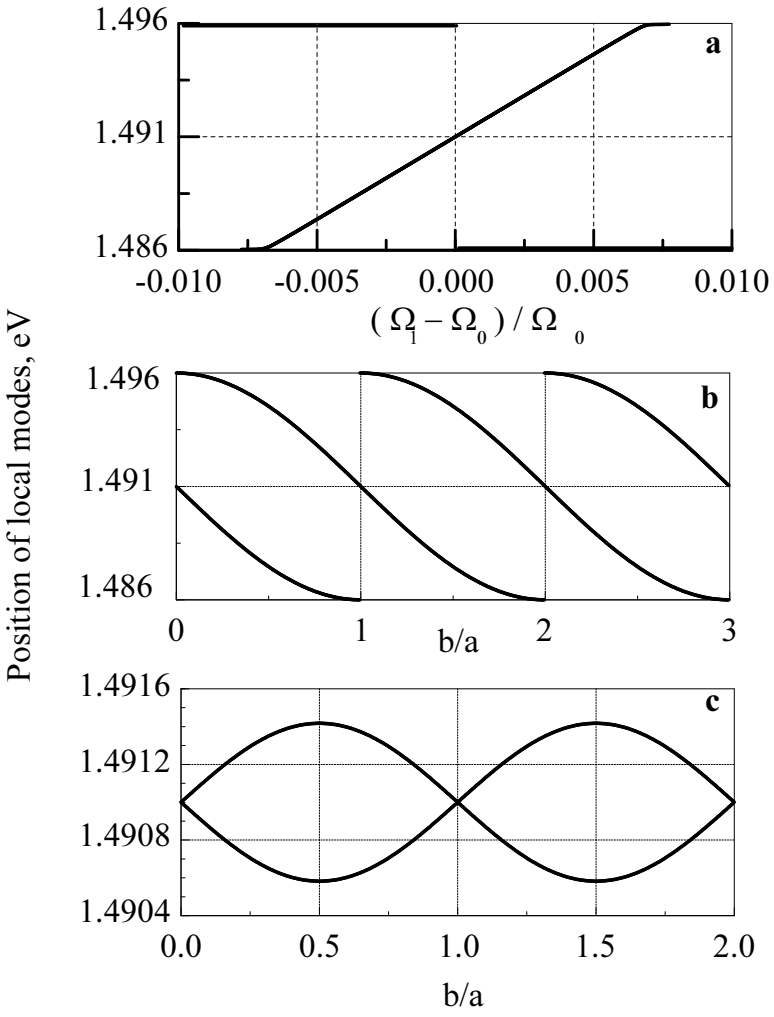

Figure 6.2: Positions of the local modes in the bandgap (1.486 - 1.496 eV) for the Ω-defect (a), a-defect (b), and b-defect (c) as functions of the defect strengths. Numerical values of the exciton resonant frequency and the exciton-light coupling constant were taken the same as in $InGaAs/GaAs$ structures studied in Ref. [27].

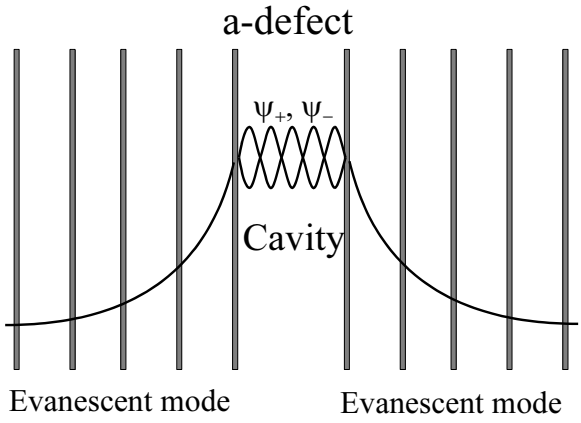

Figure 6.3: Matching the solutions for half-infinite perfect MQW with cavity modes $\psi_{\pm}$ one can obtain the dispersion equation for (quasi)local modes (in finite systems) of such a system with the defect.

$\Gamma_0 \ll \Omega_0$, which is the case for most materials. For the Ω-defect, one solution demonstrates a radiative shift from the defect frequency Ω_1,

$$\omega_{def}^{(1)} = \Omega_1 - \Gamma_0 \frac{\Omega_1 - \Omega_0}{\sqrt{(\omega_u - \Omega_1)(\Omega_1 - \omega_l)}}, \tag{6.8}$$

while the second solution splits off the upper or lower boundary depending upon the sign of $\Omega_1 - \Omega_0$:

$$\omega_{def}^{(2)} = \omega_{u,l} \pm \frac{1}{2}(\omega_u - \omega_l)\left(\frac{\pi}{2}\frac{\Omega_1 - \Omega_0}{\Omega_0}\right)^2, \tag{6.9}$$

where one chooses ω_u and "$-$" for $\Omega_1 < \Omega_0$, and ω_l and "$+$" in the opposite case. This is illustrated in Fig. 6.2a. It can be seen that the shift of $\omega_{def}^{(1)}$ from the defect exciton frequency Ω_1 is negative for $\Omega_1 > \Omega_0$ and positive for $\Omega_1 < \Omega_0$. The magnitude of the shift is of the order of the coupling constant Γ_0, which is usually rather small, and this fact, as it is shown in the next section, is crucial for the optical properties of the defect. The second local mode $\omega_{def}^{(2)}$ lies very close to the edges of the bandgap, and it would be, therefore, very difficult to distinguish it from the modes making up the allowed bands even for negligible dissipation.

In the case of the Γ-defect, one again finds two solutions of Eq. (6.7):

$$\omega_{def}^{(1,2)} = \omega_{u,l} \pm 2\left(\Gamma_1 - \Gamma_0\right)^2 (\omega_u - \omega_l)\,. \tag{6.10}$$

which exist only for $0 < \Gamma_1 < \Gamma_0$ and are very close to the gap boundaries. The situation is similar to the second solution for the Ω-defect, and one can conclude, therefore, that the Γ-defect would not affect significantly the optical spectra of the system.

The next defect we consider, the *a*-defect, is shown in Fig. 6.1a. One can see that this defect differs from the other two in a fundamental way. An increase in an interwell distance

between any two wells automatically changes the coordinates of an infinite number of wells: $z_n = na$ for $n \leq n_d$ and $z_n = (b-a)+na$ for $n_d < n$, where b is the distance between the n-th and $(n+1)$-th wells. Therefore, this defect is non-local and cannot be solved by the same methods as the two previous cases. The best approach to this situation is to consider the system of a finite length, L, and match solutions for $n < n_d$ and $n > n_d + 1$ with a solution for $na < z < na + (b-a)$, which is schematically shown in Fig. 6.3. Eigen frequencies can be derived then considering limit $L \to \infty$. Solutions for the finite system can be constructed using the transfer matrix approach. The state of the system at the m-th well is described by a two dimensional vector v_m with components $E(x_m)$ and $(1/k_0)(dE(x_m)/dx)$:

$$v_m = \prod_{n=1}^{m} \widehat{\tau}_n v_0 = \widehat{T} v_0. \tag{6.11}$$

The 2×2 transfer matrix $\widehat{\tau}_n$ at the n-th well is

$$\widehat{\tau}_n = \begin{pmatrix} \cos(k_0 a_n) + \beta \sin(k_0 a_n) & \sin(k_0 a_n) \\ -\sin(k_0 a_n) + \beta \cos(k_0 a_n) & \cos(k_0 a_n) \end{pmatrix}, \tag{6.12}$$

where $a_n = x_{n+1} - x_n$ and β is defined by Eq. (6.6). The eigen quasi-states for a finite system, $n \in (1, N)$, can be found if one looks for non-trivial solutions when no wave is incident upon the system. This corresponds to the boundary conditions of the form

$$v_0 = \begin{pmatrix} r \\ -ir \end{pmatrix} \text{ and } v_N = \begin{pmatrix} t \\ it \end{pmatrix}.$$

A resulting dispersion equation for the eigenfrequencies can be expressed in terms of the elements of the total transfer matrix $\widehat{T}$:

$$(T_{11} + T_{22}) - i\,(T_{12} - T_{21}) = 0. \tag{6.13}$$

It is clear that for finite samples the solutions of this equation are complex, reflecting the fact that the modes are not stationary; they have lifetimes which tend to infinity only in the limit $N \to \infty$.

Eq. (6.13) for the a-defect in the infinite MQW system, after some cumbersome but straightforward algebra, can be presented in the form

$$\cot(k_0 b) = -\frac{\sin(k_0 a) - \beta\lambda_-/2}{cos(k_0 a) - \lambda_-}, \tag{6.14}$$

where $\lambda_- = \left[\cot(k_0 a) + \beta/2 - \sqrt{D}\right] \sin(k_0 a)$ is one of the eigenvalues of the transfer matrix, Eq. (6.12), and $D = -1 + \beta^2/4 + \beta \cot(k_0 a)$. This equation, as well as in the cases of Γ- and Ω-defects, has two solutions - above and below Ω_0. These solutions can be approximated as

$$\omega_{def}^{(1)} = \Omega_0 - \frac{\omega_u - \omega_l}{2} \frac{(-1)^{\left[\frac{\xi+1}{2}\right]} \sin(\pi\xi/2)}{1 + \frac{\omega_u - \omega_l}{2\Omega_0} \xi (-1)^{\left[\frac{\xi+1}{2}\right]} \cos(\pi\xi/2)}, \tag{6.15}$$

$$\omega_{def}^{(2)} = \Omega_0 + \frac{\omega_u - \omega_l}{2} \frac{(-1)^{\left[\frac{\xi+1}{2}\right]} \cos(\pi\xi/2)}{1 - \frac{\omega_u - \omega_l}{2\Omega_0} \xi (-1)^{\left[\frac{\xi+1}{2}\right]} \sin(\pi\xi/2)}, \tag{6.16}$$

where $\xi = b/a$, and [...] denotes an integer part. Therefore, for $\Gamma_0 \ll \Omega_0$ and not very large ξ, $\xi \ll (\Omega_0/\Gamma_0)^{1/2} \simeq 10^2$, and both solutions are almost periodic functions of b/a with the period of 1, as shown in Fig. 6.2b. These solutions oscillate between respective boundaries of the gap (ω_u or ω_l) and the exciton frequency Ω_0. At the integer values of ξ, one of the frequencies $\omega_{def}^{(1)}$ or $\omega_{def}^{(2)}$ becomes equal to Ω_0, and the other reaches ω_u or ω_l depending upon the parity of ξ. When ξ crosses an integer value, the solution passing through Ω_0 changes continously, while the second one experiences a jump toward the opposite gap boundary. The observable manifestations of the defect modes (for instance, transmission resonances as described in the next section) vanish when the defect frequencies approach the gap boundaries. This jump, therefore, would manifest itself as a disappearance of the transmission peak near one of the gap boundaries, and a gradual reappearance at the opposite edge as ξ changes through an integer value. It is interesting to note again that the exciton resonance frequency Ω_0, which formally lies at the center of the gap, behaves as one of the gap boundaries. This is another manifestation of the fact that the polariton gap in the Bragg structures is formed by two adjacent gaps with a degenerate boundary at Ω_0.

Calculations of the defect frequencies for the b-defect can be done in the framework of both schemes. The transfer-matrix approach, however, turns out to be less cumbersome. The dispersion equation for LPM's in this case takes the form

$$\begin{aligned} &\frac{\beta^2}{2}\sin^2[k_0(b-a)]\left[-1+\frac{\beta}{2\sqrt{D}}+\frac{\cot(k_0a)}{2\sqrt{D}}\right] \\ &+\quad \cos^2(k_0a)+\sin^2(k_0a)\left(\frac{\beta}{2}-\sqrt{D}\right)^2+\sin(2k_0a)\left(\frac{\beta}{2}-\sqrt{D}\right)=0. \end{aligned} \tag{6.17}$$

This equation can be solved approximately assuming that the splitting of the solution from the Bragg frequency, Ω_0, is much smaller than the width of the gap. Expanding different terms of Eq. (6.17) in terms of powers of $(\omega - \Omega_0)$ and keeping the lowest non-zero contribution, one obtains two different solutions for frequencies of LPM's:

$$\omega_{def}^{(1,2)} = \Omega_0\left[1 \pm \left(\frac{2}{\pi}\right)^{1/4}\left(\frac{\Gamma_0}{\Omega_0}\right)^{3/4}\left|\sin\pi(\xi-1)\right|\right]. \tag{6.18}$$

The relative splitting of these modes from Ω_0 is of the order of $(\Gamma_0/\Omega_0)^{3/4}$, and is much smaller than the relative width of the gap, which is proportional to $(\Gamma_0/\Omega_0)^{1/2}$ in accord with our initial assumption. Similar to the case of the a-defect, these frequencies change periodically with ξ, but unlike the previous case, they both split off the center of the gap, Ω_0, and at integer values of ξ merge back to Ω_0. The maximum deviations of the local frequencies from Ω_0 are of the order of $(\Gamma/\Omega_0)^{3/4}$, they take place for half-integer values of ξ.

One can notice that the b-defect involves two adjacent wells, and in the Green's function approach one would have to deal with a system of two coupled equations. Accordingly, it can be expected that there must be four possible local frequencies (two in each half of the gap), while we found only two of them. The reason for this is that the Bragg condition makes a pair of frequencies, which are both above or below Ω_0, nearly degenerate, and the difference between them is much smaller than the terms we kept in our approximate solution. This can be understood if one notices that the transfer matrices in Eq. (6.12) contain factors $\cos(kb)$, $\sin(kb)$ and $\cos[k(2a-b)]$, $\sin[k(2a-b)]$ for the first and the second of the involved wells, respectively. Exactly at the Bragg frequency, $ka = \pi$, these factors

coincide leading to the degeneracy. Since the shift of the actual local frequency from the Bragg frequency is relatively small, the solutions remain nearly degenerate. The fact that obtained solutions are symmetrical with respect to the replacement of b with $2a - b$ is not surprising and reflects the symmetry of the transfer matrices discussed above.

6.3 Defect LPM's and transmittance and reflectance experiments

In this Section we study how the local defect modes obtained above affect the reflection and transmission spectra of the finite size periodic Bragg MQW's in the presence of homogeneous broadening. Transmission and reflection coefficients can be expressed in terms of the elements of the total transfer matrix defined by Eq. (6.11) as

$$T = |t|^2 = \left| \frac{2 \det \widehat{T}}{(T_{11} + T_{22}) - i\,(T_{12} - T_{21})} \right|^2, \tag{6.19}$$

$$R = |r|^2 = \left| -\frac{(T_{11} - T_{22}) + i\,(T_{12} + T_{21})}{(T_{11} + T_{22}) - i\,(T_{12} - T_{21})} \right|^2. \tag{6.20}$$

Without absorption, T and R in the form of Eqs. (6.19) and (6.20) can be shown to add up to unity. In the denominators of T and R one can recognize the dispersion relation Eq. (6.13) that was obtained in the previous section by matching the decaying solutions on both sides of the defect.

Γ- and Ω-defects differ from the original QW's only in the definition of the parameter β, therefore, they both can be dealt with at the same time. The exact expression for T is cumbersome, however, if the length of the system is longer than the penetration length over the frequency region of interest, it can be simplified. In this case the smaller eigenvalue of the total transfer matrix is proportional to $\exp(-Na/l_0(\omega))$, where l_0 is given by Eq. (6.5), and can be neglected. The expression for the transmission coefficient then can be presented as [see also Eq. (2.31)]

$$t = \frac{t_0}{(1+\varepsilon) + i \exp(-ik_0 Na)\, \varepsilon \Phi t_0 \cosh[(N - 2n_0 + 1)\kappa a]}, \tag{6.21}$$

where we introduce the defect parameter $\varepsilon = (\beta_{def} - \beta)/2\sqrt{D}$, which is equal to zero when $\beta_{def} = \beta$; n_0 is the position of the defect QW, $\kappa = 1/l_0(\omega)$, and $\Phi = \beta/(\sin(k_0 a)\sqrt{D})$. For $\varepsilon = 0$, Eq. (6.21) gives the transmission coefficient, t_0, of the pure system,

$$t_0 = \frac{2e^{ikL} \exp(-\kappa L)}{1 + i\,[2 - \beta \cot(ka)]/\sqrt{D}}, \tag{6.22}$$

exhibiting an exponential decay characteristic of the evanescent modes from a band gap.

Eq. (6.21) describes the resonance tunneling of the electromagnetic waves through MQW with the defect. The equation

$$1 + \varepsilon = 0$$

can be shown to coincide with the dispersion equations for local defect modes of the infinite structure in the case of Ω and Γ defects. Given this fact and the structure of Eq. (6.21), it

seems natural to assume that the transmission reaches its maximum value at the frequencies of the local modes. More careful consideration shows, however, that the systems under consideration behave in a less trivial way, and as we mentioned in Chapter 2, that maxima of the transmission occur at frequencies shifted from the frequency of LPM's. This is quite unusual behavior that distinguishes the systems under consideration from other instances of resonance tunneling. Moreover, we shall show that, as well as in Chapter 2, the transmission at the maximum is always equal to unity (in the absence of absorption).

Evaluation of the exact analytical expression for the transmission coefficient, Eq. (6.19), obtained from the total transfer matrix, showed that the distinctive resonance transmission occurs only if local modes lie not too close to the boundaries or the center (which is, strictly speaking, also a degenerate boundary) of the gap. Γ defects, therefore, can be excluded from consideration, as well as one of the solutions for the Ω-defect. For frequencies close to the remaining local mode (the solution for the Ω-defect given by Eq. (6.8) the expression for the transmission coefficient Eq. (6.21) can be simplified. Expansion in the vicinity of the local mode gives

$$T = \frac{\left(\dfrac{\omega-\Omega_1}{\omega_{def}-\Omega_1}\right)^2}{1+A_1\left|\dfrac{\omega-\omega_T\cosh\left[(N-2n_0+1)\kappa a\right](1+iA_2)}{\omega_{def}-\omega_T}\right|^2\left(\dfrac{\omega_T-\Omega_1}{\omega_{def}-\Omega_1}\right)^2}. \tag{6.23}$$

Parameters A_1, A_2 and ω_T are defined by

$$A_1 = \frac{(\omega_+-\omega_{def})^2(\omega_{def}-\omega_-)^2}{4(\omega_{def}-\Omega_0)^2(\omega_{def}-\omega_l)(\omega_u-\omega_{def})}, \tag{6.24}$$

$$A_2 = \frac{(\omega_{def}-\Omega_0)\sqrt{(\omega_{def}-\omega_l)(\omega_u-\omega_{def})}}{(\omega_+-\omega_{def})(\omega_{def}-\omega_-)}\tanh[(N-2n_0+1)\kappa a], \tag{6.25}$$

$$\omega_T = \omega_{def}+\pi\frac{(\omega_+-\omega_{def})(\omega_{def}-\omega_-)}{\Omega_0}\frac{(\omega_{def}-\Omega_0)}{\sqrt{(\omega_{def}-\omega_l)(\omega_u-\omega_{def})}}e^{-\kappa Na}, \tag{6.26}$$

where $\omega_\pm = \Omega_0 \pm (\omega_u-\Omega_0)/\sqrt{2}$. The resonance transmission occurs when the defect layer is located in the center of the system $N-2n_0+1=0$. In this case the coefficient A_2 becomes zero and Eq. (6.23) can be presented in the following form

$$T = \frac{4\gamma_\Omega^2}{Q^2}\frac{(\omega-\omega_T+Q)^2}{(\omega-\omega_T)^2+4\gamma_\Omega^2}, \tag{6.27}$$

where $Q=\omega_T-\Omega_1$, and the parameter γ_Ω is given by

$$\gamma_\Omega = \pi\Omega_0\left(\frac{\omega_{def}-\Omega_0}{\Omega_0}\right)^2 e^{-\kappa Na}. \tag{6.28}$$

The transmission spectrum described by Eq. (6.27) has a shape known as a Fano resonance [117], where ω_T is the resonance frequency, at which the transmission turns to unity, and parameters γ_Ω and Q describe the width and the asymmetry of the resonance respectively. One can see from Eq. (6.26) that in general the transmission resonance frequency is shifted with respect to the frequency of the local mode. The shift, though exponentially small

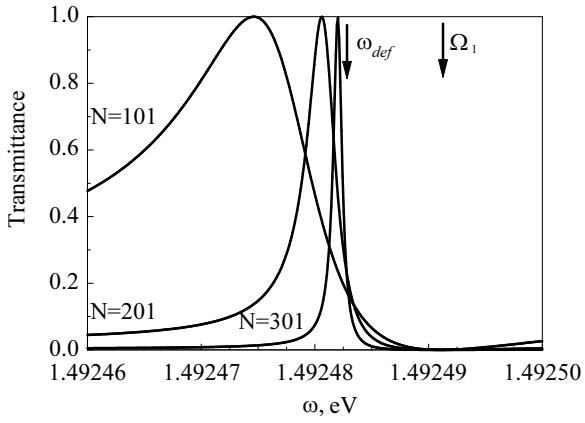

Figure 6.4: The shape of the transmission maximum for 3 lengths $N = 101, 201, 301$. For all lengths, the Ω-defect is in the center of the system. $\Omega_1 = 1.492491$ eV is the exciton frequency of the defect layer. The exciton resonant frequency Ω_0 is 1.491 eV, the exciton-light coupling constant Γ_0 is 27 μeV as in the InGaAs/GaAs structures studied in Ref. [27], however, no homogeneous broadening is assumed.

for long systems considered here, is of the same order of magnitude as the width of the resonance γ_Ω, and is, therefore, significant. These two frequencies, ω_T and ω_{def}, coincide in the special case when $\omega_{def} = \omega_\pm$. The fact that the transmission is equal to one, in this particular case, was obtained in Chapter 2.

At $\omega = \omega_T - Q = \Omega_1$ the transmission equals zero, which is a signature of Fano resonances. Usually the presence of Fano resonances is associated with interaction between a discrete level and a continuum of states. This is not the case in the situation under consideration. Zero of the transmission in our case is caused by the fact that the Ω-defect brings to the dielectric function of the system a new pole at Ω_1, which describes the interaction between electromagnetic waves and excitons of the defect well. The penetration length diverges at Ω_1, and transmission, therefore, vanishes. The interaction with excitons, at the same time, leads to the radiative shift of the frequency of the local mode, and hence, the frequency of the transmission resonance, away from Ω_1. The combination of these two factors is responsible for the Fano-like shape of the transmission resonance. The actual form of the Fano spectrum in an ideal system without absorption is determined by the interplay between the width parameter γ_Ω and the asymmetry parameter Q. The former exponentially decreases with an increase of the length of the system, while the latter is length independent. However, the pre-exponential factor in γ_Ω is of the order of the exciton resonance frequency, Ω_0, while Q is of the order of Γ, i.e. significantly smaller. Therefore, in principle, there are two possible cases: $\gamma_\Omega \gg Q$ for shorter systems $[1 \ll \kappa N a \ll \log(\Omega_0/Q)]$, and $\gamma_\Omega \ll Q$ for longer systems. In the first case, the transmission spectrum has a distinctively Fano-like asymmetrical shape, while in the second limit the spectrum attains the symmetrical Lorentzian shape characteristic for Wigner-Breight [118] resonances. Fig. 6.4 shows the evolution of the shape of the transmission resonance in the absence of absorption from Fano-like to Wigner-Breight-like behavior with increase of the length of the system. One can also see from this figure how the position of the transmission maximum moves with an

increase of the length. An actual possibility to observe the Fano resonance in the considered situation depends strongly upon the strength of absorption in the system, which must be at least smaller than Q. More detailed discussion of absorption related effects is given below in the present section.

Calculation of the transmission coefficient for the a-defect can be carried out in a similar manner. Dropping the exponentially small contribution from the smaller eigenvalue the transmission matrix can be written in the following form:

$$t = \frac{t_0}{(1+\varepsilon_a) + ie^{-i\frac{\omega}{c}Na}\Phi^2 \sin\left[\frac{\omega}{c}(b-a)\right] t_0 \cosh\left[(N-2n_0)\kappa a\right]}, \tag{6.29}$$

where

$$\varepsilon_a = \frac{\sin(\frac{\omega}{c}b) - \sin(\frac{\omega}{c}a) - \lambda_+\left(1 - \frac{\beta}{2\sqrt{D}}\right)\sin(\frac{\omega}{c}(b-a))}{\sin(\frac{\omega}{c}a)}.$$

Similar to the previous defects, $1+\varepsilon_a = 0$ coincides with the dispersion equation for an infinite system, but the transmission resonance is shifted with respect to the local mode. In the vicinity of the resonance, Eq. (6.29) can be presented as:

$$T = \frac{1}{1 + A_1\left|\frac{\omega - \omega_T \cosh\left[(N-2n_0)\kappa a\right](1 + i\cdot A_2)}{\omega_{def} - \omega_T}\right|^2}, \tag{6.30}$$

where parameters A_1 and A_2 are again given by Eqs. (6.24) and (6.25), respectively. One only needs to replace $N - 2n_0 + 1$ in Eq. (6.25) with $N - 2n_0$, which reflects the new symmetry of the system. The frequencies of local modes ω_{def} are now given by Eqs. (6.15) and (6.16), and ω_T is defined by

$$\omega_T = \omega_{def} + 2(\omega_{def} - \Omega_0)\frac{(\omega_+ - \omega_{def})(\omega_{def} - \omega_-)(\omega_{def} - \omega_l)(\omega_u - \omega_{def})}{(\omega_u - \Omega_0)^4}e^{-\kappa Na}. \tag{6.31}$$

The resonance transmission again occurs when $N - 2n_0 = 0$, which requires an even number of wells in the system. Eq. (6.30) in this case takes the standard Wigner-Breight shape

$$T = \frac{4\gamma_a^2}{(\omega - \omega_T)^2 + 4\gamma_a^2}, \tag{6.32}$$

with the half-width, γ_a, given now by

$$\gamma_a = 2\frac{(\omega_{def} - \Omega_0)^2(\omega_{def} - \omega_l)^{3/2}(\omega_u - \omega_{def})^{3/2}}{(\omega_u - \Omega_0)^4}e^{-\kappa Na}, \tag{6.33}$$

The frequency ω_T, where the transmission coefficient takes the maximum value of unity, is again shifted from the frequency of the defect mode. The two frequencies coincide, however, when the defect frequency is made equal to $\omega_\pm$, which are the same frequencies at which transmission resonance and the local mode coincide for the Ω-defect. As one can see from Eq. (6.15), these conditions can be satisfied simultaneously for both defect frequencies of the a-defect when $b \simeq (integer + 1/2)a$ (see Fig. 6.2b). In this case the position of the transmission resonance becomes independent of the length of the system.

Finally, the b-defect gives an expression for the transmission coefficient very similar to Eq. (6.21) with the only distinction that ϵ has to be replaced by a different expression, which

is too cumbersome to be displayed here. The maximum transmission for a given defect is again achieved when the defect is in the center of the system (N is odd). Expanding the transmission coefficient near the frequency of the respective local mode, one obtains

$$T = \frac{1}{1 + \frac{1}{4}\left(\frac{\omega_u - \Omega_0}{\omega_{def} - \Omega_0}\right)^2 \left| \frac{\omega - \omega_T}{\omega_{def} - \omega_T} + i \cdot \sinh\left[(N - 2n_0 + 1)\kappa a\right] \right|^2}, \tag{6.34}$$

with ω_T now given by

$$\omega_T = \omega_{def} - 2(\omega_{def} - \Omega_0)e^{-\kappa N a}. \tag{6.35}$$

Unlike other types of defects, in this case the transmission resonance is always different from ω_{def}. When the defect is at the resonance position $N - 2n_0 + 1 = 0$, the transmission spectrum again takes the Wigner-Breight shape with the resonance width determined by parameter γ_b, where γ_b is given by

$$\gamma_b = 2\frac{(\omega_{def} - \Omega_0)^2}{\omega_u - \Omega_0} e^{-\kappa N a}, \tag{6.36}$$

In real systems, enhancement of the transmission coefficient is usually limited by homogeneous broadening of exciton resonances. Two cases are possible when exciton damping is taken into account. It can suppress the resonance transmission, and the presence of the local states can only be observed in not very long systems as a small enhancement of absorption at the local frequency. This can be called a weak coupling regime for LPM, when incident radiation is resonantly absorbed by local exciton states. The opposite case, when the resonance transmission persists in the presence of damping, can be called a strong coupling regime. In this case, there is a coherent coupling between the exciton and the electromagnetic field, so that the local states can be suitably called local polaritons. Qualitatively we can assess the effect of absorption on resonances caused by different defects by looking at the widths of the respective spectra. For all types of defects the width of respective resonances exponentially decreases with the length of the system, consequently, in sufficiently long systems all resonances dissappear. However, pre-exponential factors make different defects behave differently at intermediate distances. A simple qualitative estimate would require that the width of the resonances be smaller than the exciton relaxation parameter. Therefore, the resonances, where the pre-exponential factor of the width is considerably larger than the relaxation parameter, can be observed in the systems of intermediate length. On the one hand, the length must be greater than the localization length of the respective local mode. On the other hand, it must be small enough for the width of the resonance to remain larger than the exciton relaxation parameter. The Fano resonance arising in the case of the Ω-defect though, requires special consideration since its vitality is determined by the asymmetry parameter Q rather than by the width parameter γ_Ω. Although the latter is determined by the large pre-exponent (of the order of the exciton resonance frequency Ω_0), the former is of the order of the light-exciton coupling constant Γ_0, which is much smaller. The Fano resonance will likely be washed out as soon as the relaxation rate exceeds this asymmetry parameter Q. This circumstance will prevent observation of the Fano resonance due to Ω-defect in $InGaAs/GaAs$ MQW's, experimentally studied in Ref. [27] which is, to the best of our knowledge, the only system, where radiative coupling was observed for systems as long as 100 wells. In this system, the exciton resonance frequency, Ω_0, and the exciton-light coupling parameter, Γ_0, were respectively equal to $\Omega_0 = 1.491\ eV$, and

$\Gamma_0 = 27\ \mu eV$, while the exciton relaxation parameter was estimated as $\gamma_{nr} = 280\ \mu eV$ [27]. This parameter, however, includes both homogeneous and non-homogeneous contributions. Experiments carried out in Ref. [26] with Bragg $GaAs/AlGaAs$ MQW system provide information about the magnitude of pure homogeneous broadening in this system. According to Ref. [26] radiative and non-radiative rates in $GaAs/Al_{0.3}Ga_{0.7}As$ system consisting of 10 wells are equal respectively to $\Gamma_0 = 67\ \mu eV$ and $\gamma_{nr} = 12.6\ \mu ev$. One can see that if the inhomogeneous broadening could be reduced, the conditions for observation of the Fano resonance would be significantly improved.

The pre-exponent of the resonance width in the case of the a-defect is of the order of magnitude of the gap width, which is proportional to $\sqrt{\Gamma_0\Omega_0}$. It is considerably larger than γ_{nr} for the $InGaAs/GaAs$ MQW's and we expect, therefore, that it can be easily observed in readily available samples of this composition. As far as the b-defect is concerned, it gives rise to extremely narrow transmission peaks, which are characterized by a pre-exponential factor of the order of Γ_0. It, therefore, will be washed out in $InGaAs/GaAs$ MQW's, but can be reproduced in $60 - 80$ wells long systems with the parameters similar to $GaAs/AlGaAs$ MQW's studied in Ref. [26] if inhomogeneous broadening could be significantly reduced.

We compliment the qualitative arguments presented above with numerical evaluation of exact expressions for the transmission, and reflection coefficients, Eqs. (6.19) and (6.20), using parameters of the mentioned $InGaAs/GaAs$ systems. In order to illustrate what kind of effects could be observed in samples with reduced inhomogeneous broadening, we also present results obtained with parameters of $GaAs/AlGaAs$ systems with only homogeneous relaxation included. To account for non-radiative decay quantitatively, we add an imaginary part to the denominator of the parameter β:

$$\beta = \frac{4\Gamma_0\omega}{\omega^2 - \Omega_0^2 + 2i\gamma_{nr}\omega}.$$

Fig. 6.5 shows transmission and reflection coefficients of the Bragg MQW lattice made of 201 quantum wells with the Ω-defect in the center with parameters corresponding to the $InGaAs/GaAs$ system. One can see that absorption washes out the strong asymmetric pattern of the Fano resonance, but some remains of the resonance are still quite prominent, and can probably be observed in high quality samples. Fig. 6.6 represents the spectra of 101 well long system with parameters corresponding to $GaAs/AlGaAs$, but without contribution from inhomogeneous broadening. One can see a characteristic assymetric profile of the Fano resonance both in transmission and reflection. There is also a remarkably strong and narrow absorption line at the resonance frequency with more than 8-fold growth of absorption at the resonance. This behavior should be contrasted with the previous figure, where absorption spectrum is rather flat with only insignificant increase at the resonance frequency. In the case of the b-defect, strong exciton absorption characteristic for the $InGaAs/GaAs$ structures washes out any resonance features from the spectrum. The resonances, however, survive if only homogeneous broadening is included. In this case one would have very narrow symmetric transmission, reflection and absorption lines (Fig. 6.7) located rather close to the center of the gap. It is interesting to compare resonance behavior of the b-defect and the Ω-defect in the regime of strong coupling. The latter results in absorption that, though increased sharply at the resonance, is still rather weak, at the same time the transmission reaches in this case almost 80%. In the former case, however, the transmission does not grow that dramatically (up to about 0.4), but absorption increases by two orders of magnitude. The difference is caused by the different shapes of the resonances: the Fano resonance is considerably wider and, therefore, results in less dramatic increase in the maximum absorp-

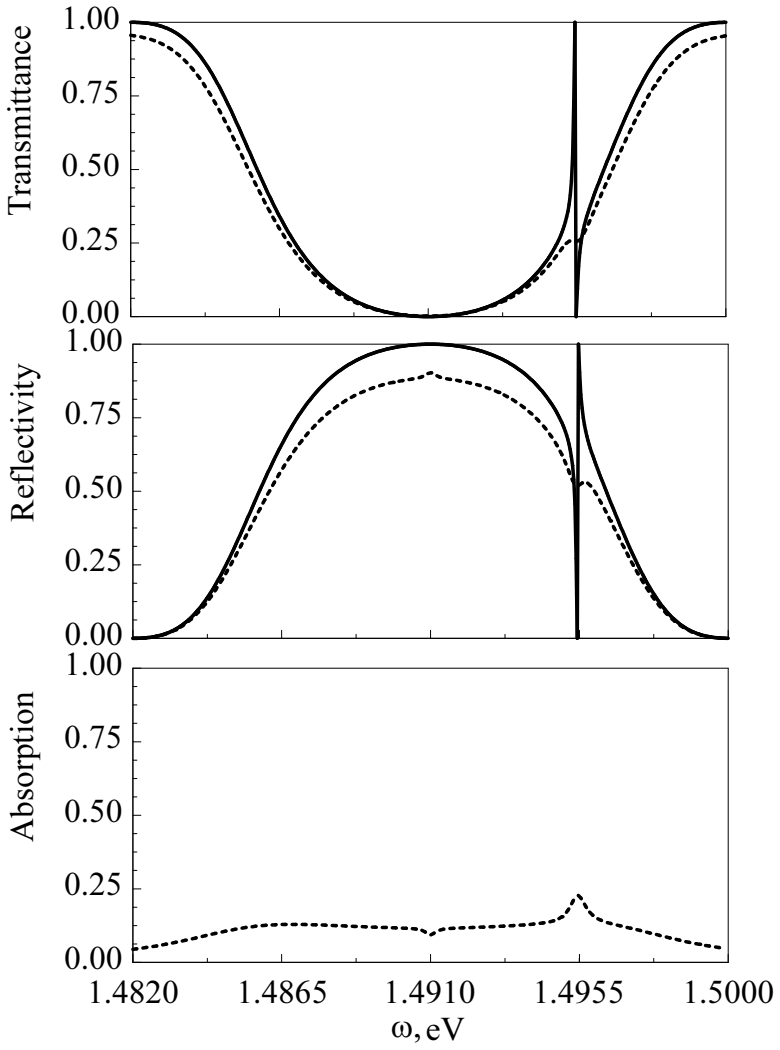

Figure 6.5: Transmission, reflection and absorption coefficients for the Ω-type defect. The defect is placed in the center of the MQW with 201 quantum wells. The exciton frequency of the defect well Ω_1 is chosen such that $(\Omega_1 - \Omega_0)/\Omega_0 = 1.003$. Numerical values of the exciton resonant frequency and the exciton-light coupling constant were taken for $InGaAs/GaAs$ structures studied in Ref. [27]. Solid lines show results obtained in the absence of absorption, and dashed lines were calculated in the presence of experimentally observed [27] homogeneous broadening.

tion.

Fig. 8 shows the transmission and reflection of the Bragg MQW lattice of 200 quantum wells with the a-defect with $\xi = b/a = 1.5$ and parameters of the $InGaAs/GaAs$ system. This is the only defect for which the strong coupling regime can be realized for this material. But since this is the only system, for which the samples with large number of wells were experimentally grown, we shall discuss the related results in more details. For the a-defect with the strength $\xi = 1.5$, one has two symmetric with respect to the center resonances. The peaks are very pronounced in the tranmission, and the contrast in reflection is very large - about 30%, and can be made even larger if one increases the length of the system. The spectra shown in Fig. 6.8 can, however, be affected by the presence of the additional resonance due to $2s$ excitons. In Ref. [27] it was shown that this resonance causes asymmetry of the reflection spectrum. We expect that it could have the similar effect upon spectra presented in Fig. 6.8 causing an assymetry between low- and high- frequency portions of the spectra. Even if $2s$ excitons contribute additional resonances to the spectra, they would be rather weak [27], and could be clearly distinguished from the effects considered in the present work. As an additional identification tool, one can use the dependence of the defect induced features upon the defect parameter b/a, while a contribution from the $2s$ exciton resonance would not be affected by changes in this parameter. Besides, changing the parameters of the defect, one can move the transmission resonances closer to the center of the gap and farther away from the $2s$ exciton resonance. We can conclude, therefore, that the strong coupling between local excitons and local photons can be experimentally realized in readily available samples of $InGaAs/GaAs$ MQW's. If, however, one could reduce disorder in the samples, the optical resonances due to a-defect would be even more pronounced with more dramatic increase in transmission and absorption at the resonance frequencies.

It is interesting to note that the effects of local modes on the resulting absorption of the incident wave is very weak in the case of weak coupling. Even though there is some small enhancement of absorption at the resonance frequencies, it is much weaker than absorption peaks when strong coupling is realized. In other words, local polaritons in the regime of strong coupling demonstrate resonance behavior in both transmission and absorption at the same time, while in the weak coupling regime there is only a small effect of the local states upon all optical spectra of the system. The explanation for this behavior lies in the spatial distribution of the electromagnetic wave intensity throughout the system. In the absence of absorption, the electric field at the resonance frequency decays exponentially away from the defect layer, i.e. there occurs a strong exponential enhancement of the incident field at the defect layer [119] similar to what we found in Chapter 2. We used self-embedding technique, adopted for the discrete systems in Appendix, to calculate numerically the electromagnetic field inside MQW structure. In the absence of absorption we observed the exponential increase of the field compared to the amplitude of the incident electromagnetic wave E_{in}

$$|E_{max}| = |E_{in}| \cdot e^{(N/2)\kappa a}. \tag{6.37}$$

Non-radiative broadening suppresses not only the resonance transmission but also the exponential enhancement of the electric field. If the strong coupling regime is not realized, the intensity of the wave decreases exponentially throughout the sample almost as it would in the absence of the defect, and is just slightly larger at the resonance frequency than off-resonance. Therefore, the peaks in absorption in these cases are also only minute. At the same time, Fig. 6.9 shows that even in the presence of absorption the a-defect in the $InGaAs/GaAs$ MQW's, which remains in the regime of strong coupling, demonstrates more than a three-fold enhancement of $|E|^2$ at the location of the defect for the system

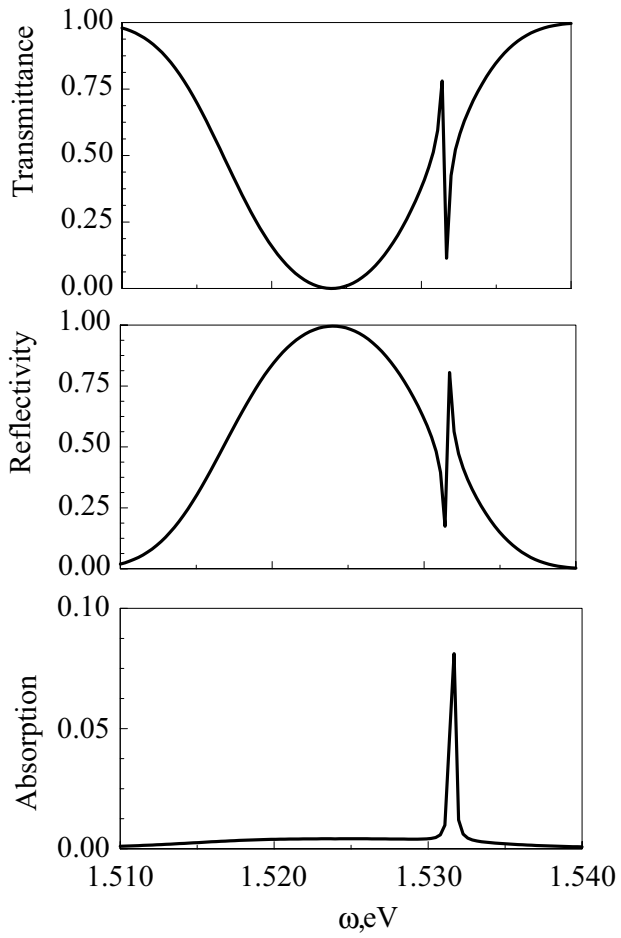

Figure 6.6: Transmission, reflection and absorption coefficients for the Ω-type defect. The defect is placed in the center of the MQW with 101 quantum wells. The exciton frequency of the defect well Ω_1 is chosen such that $(\Omega_1 - \Omega_0)/\Omega_0 = 1.003$. Numerical values of the exciton resonant frequency and the exciton-light coupling constant were taken for $GaAs/AlGaAs$ structures studied in Ref. [26]. All results were obtained in the presence of experimentally observed [26] homogeneous broadening.

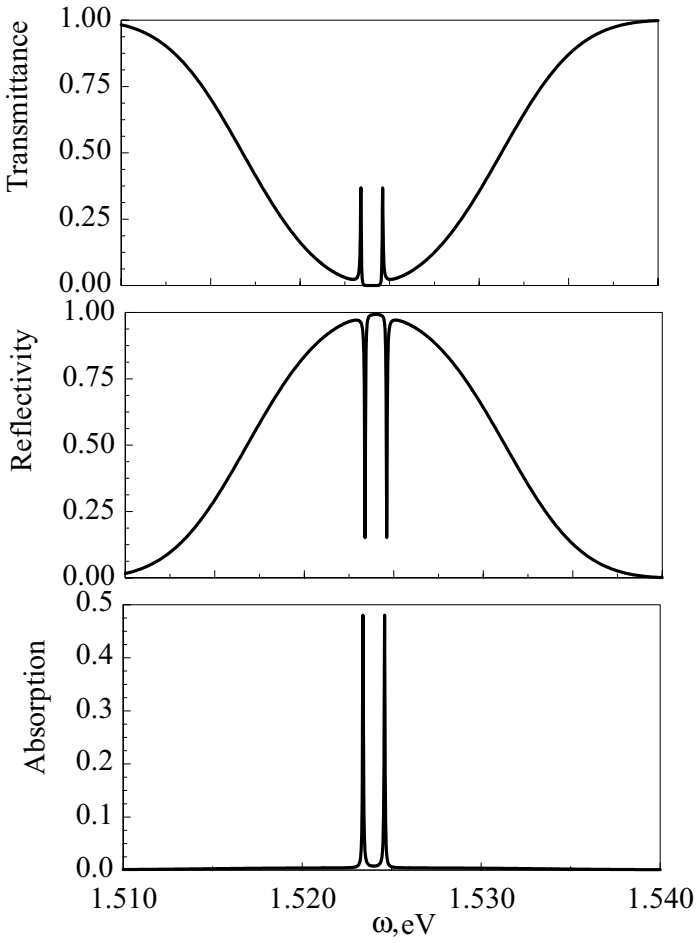

Figure 6.7: Transmission, reflection and absorption coefficients for the b-type defect. The defect is placed in the center of the MQW with 101 quantum wells. The defect strength is $\xi = b/a = 1.5$. Numerical values of the exciton resonant frequency and the exciton-light coupling constant were taken for $GaAs/AlGaAs$ structures studied in Ref. [26]. All results were obtained in the presence of experimentally observed [26] homogeneous broadening.

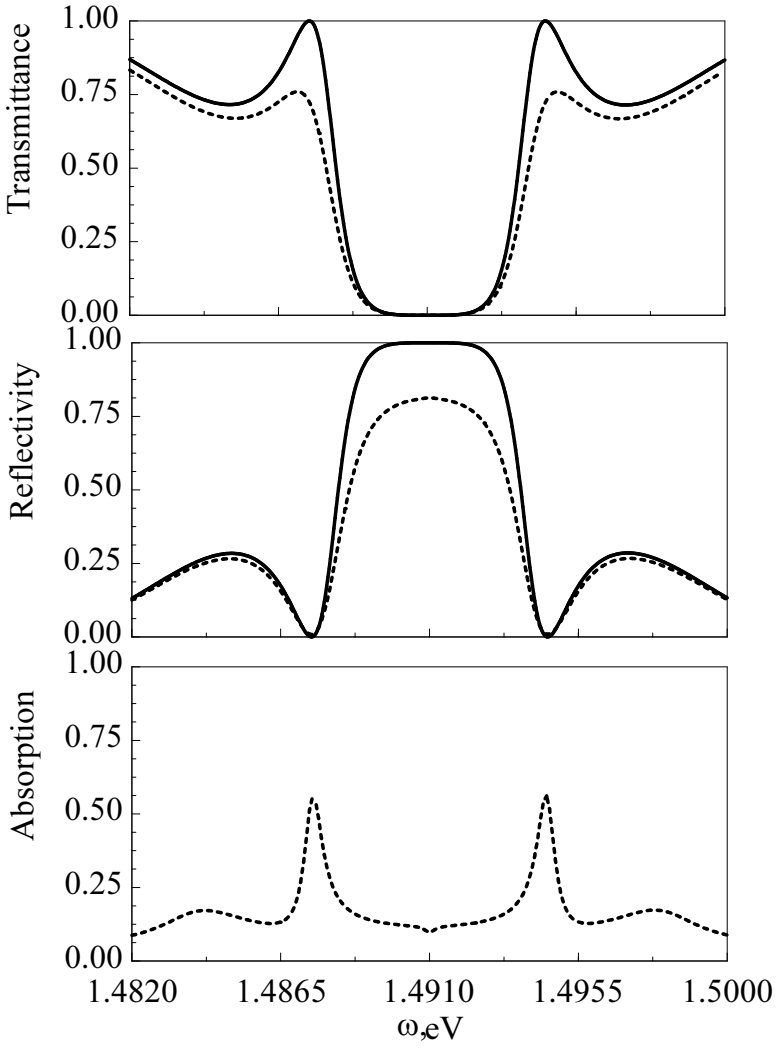

Figure 6.8: Transmission, reflection and absorption coefficients for the a-type defect. The defect is placed in the center of the MQW with 200 quantum wells. The defect strength is $\xi = b/a = 1.5$. Numerical values of the exciton resonant frequency and the exciton-light coupling constant were taken for $InGaAs/GaAs$ structures studied in Ref. [27]. Solid lines show results obtained in the absence of absorption, and dashed lines were calculated in the presence of experimentally observed [27] homogeneous broadening.

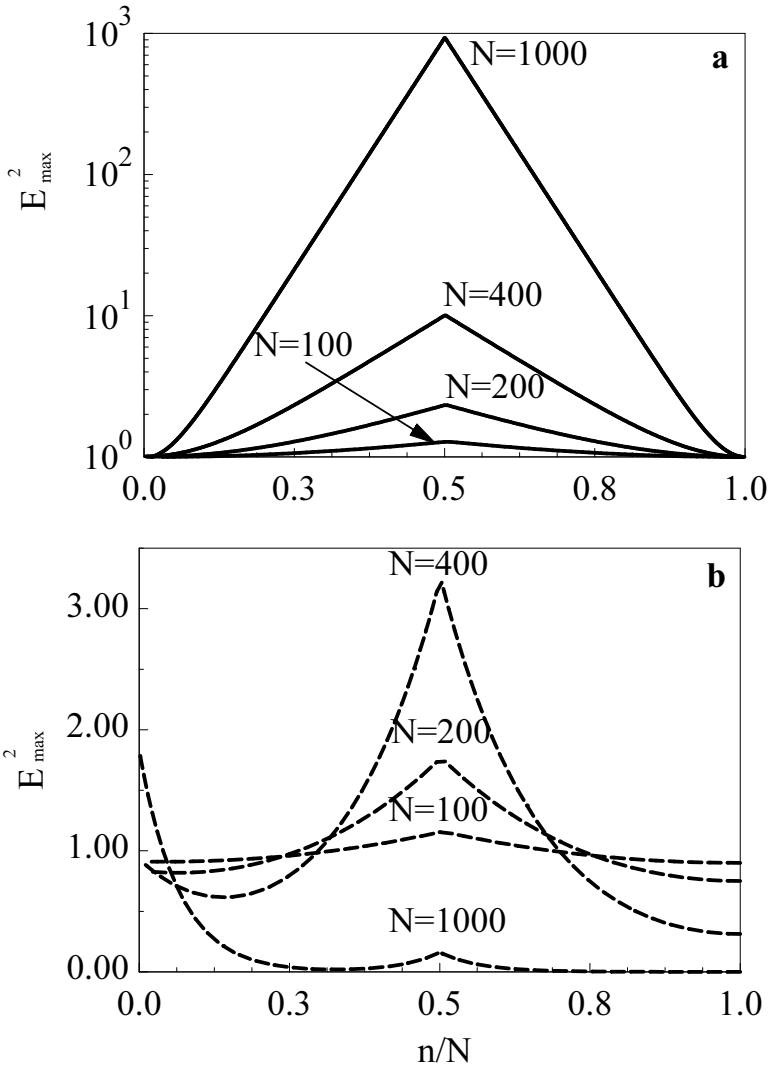

Figure 6.9: The distribution of the electric field at the frequency ω_T in the system with the a-defect placed exactly in the middle without (a) and with (b) experimentally observed [27] homogenous broadening. The defect strength is $\xi = b/a = 1.5$. Numerical values of the exciton resonant frequency and the exciton-light coupling constant were taken for $InGaAs/GaAs$ structures studied in Ref. [27]. Four curves correspond to different sizes of the system: 100, 200, 400 and 1000 QW's.

of an optimal length. Fig. 6.10a shows the evolution of the electric field at frequency ω_T at the location of the defect as the size of the system grows (for systems with different sizes the defect is always located in the center of the structure). One can see that the exponential growth of the field in the absence of absorption (solid curve) changes to a nonmonotonic behavior when absorption is included (dashed line). For the particular system under consideration, the field reaches its maximum at about N_m=450, where we see the crossover from the resonant enhancement regime ($N < N_m$) to the exponential decay ($N > N_m$). Enhancement of the field at the defect explains both transmission and absorption resonances.

In the absence of the inhomogeneous broadening much stronger enhancement of the field at the resonance for three types of defects takes place (Fig. 6.10b). We see that for $N = 100$ the intensity of the electric field at the location of the b-defect is enhanced by the factor of 50. It correlates with the strong increase of absorption in this case. The difference in absorption between b- and Ω-defects also signals about the difference in the field distribution. The fact that the Ω-defect leads to the vanishing transmission at the frequency Ω_1 translates, as computer simulations show, into the vanishing electric field everywhere behind the defect at this frequency – the defect acts as an almost perfect reflector. The growth of the intensity of the field at spectrally close frequency Ω_0 is also limited to only 1.5 of the incident intensity, which is much smaller than in the case of the b-defect. The strong enhancement of the field at the location of the b-defect has simple physical explanation. The frequency of the local states due to the b-defect lies close to the exciton frequency that is tuned such that $\lambda/2 = a$. This means that at the frequency of the local mode all QWs but one (the defect one, see also Fig. 6.1b) lie in the nodes of the electromagnetic wave [22]. Therefore, one could expect stronger then usual growth of the electric field at the defect. From this considerations, one should expect the maximum effect to occur when the defect QW is placed in an antinode, where the electric field is the largest. We already encountered this condition, when we studied the transmittance in the presence of this type of defect – the most favorable value of the defect strength was $b/a = 0.5$ or $b/a = 1.5$. This peculiar spatial distribution of the electric field explains the narrow transmission peak and strong enhancement of the electric field on the defect. This fact has great potential for applications if this type of the defect is realized experimentally.

6.4 Discussion

Among four types of defect considered in here, three are of special interest. First of them, the Ω-defect, arises when one of the QW is replaced by a well with a different exciton resonance frequency Ω_1. In this case two new local modes arise within the band-gap of the original structure, but only one of them, which manifests radiative shift from Ω_1, can significantly effect optical spectra of the system. We found that the resonance transmission of radiation due to the local state results in strongly assymetric Fano-like transmission spectrum. This transmission resonance turned out to be very sensitive to the presence of non-radiative broadening, it can only survive if the total broadening (including both homogeneous and non-homogeneous contributions) does not exceed the strength of radiative coupling between excitons and light. Using available data we concluded that the Fano resonance could not be observed in $InGaAs/GaAs$ systems, but would survive if inhomogeneous broadening could be significantly reduced. Absorption spectrum of such a structure would demonstrate a narrow line with absorption though increased at resonance, but still relatively weak. The

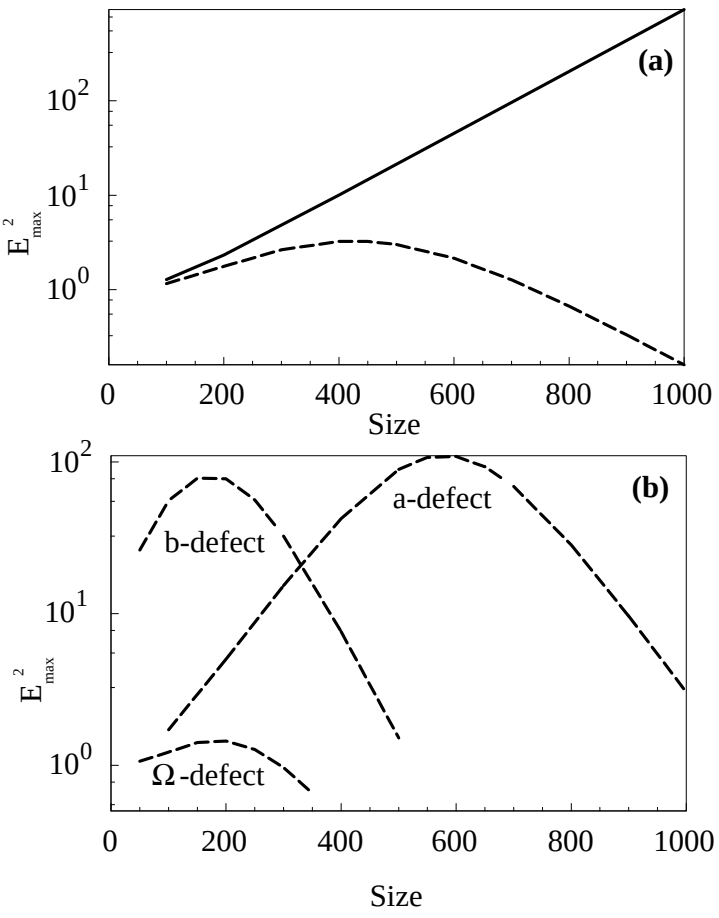

Figure 6.10: (a) The dependence of the strength of the electric field at the position of the a-defect in $InGaAs/GaAs$ structures (from Fig. 6.9) at ω_T on the size of the system with (dashed line) and without (solid line) homogeneous broadening. The other defects did not demonstrate resonance enhancement of the electric field and are not shown here. (b) The dependence of the strength of the electric field at the position of the a-, b-, and Ω-defects in $GaAs/AlGaAs$ structures at ω_T on the size of the system is shown. Numerical values of the exciton resonant frequency and the exciton-light coupling constant were taken from Ref. [26]. All results were obtained in the presence of experimentally observed [26] homogeneous broadening. The defect strengths are $\xi = b/a = 1.5$ for a- and b-defects, and $(\Omega_1 - \Omega_0)/\Omega_0 = 0.9963$ for the Ω-defect. In the presence of the realistic homogeneous broadening, all 3 types of the defects show the resonance enhancement of the electric field.

weakness of the absorption correlates with the fact that the intensity of the field at this defect increases only slightly.

Another defect with interesting properties considered in this Chapter is the b-defect, which arises when one shifts the position of one of the wells keeping coordinates of all others intact. This corresponds to changes in the thicknesses of two adjacent barriers. This defect produces two local modes with frequencies close to the center of the gap. Respective transmission resonances have regular symmetric Lorentzian shapes but with rather narrow widths. The last circumstance makes these defects also very vulnerable to the non-radiative broadening, and they can only survive in systems with the radiative decay rate greater than the non-radiative one. If, however, this resonance is realized, one can obtain a narrow absorption line with almost two orders of magnitude increase in absorption at the resonance, or what is even more important, 50-fold increase in the intensity of the electromagnetic field at the defect QW (for zero inhomogeneous but realistic homogeneous broadenings).

The most robust of the local polariton modes is produced by the a-defect. In this case the width of one of the barriers is increased, while all other barriers remain the same. The defect produced in this way resembles a regular microcavity, but with optically active mirrors. This fact distinguishes the system considered here from regular cavities with, for instance, Bragg distributed mirrors. Local states arising in this case give rise to rather wide resonances in optical spectra, which can survive strong enough non-radiative broadening and can be observed in readily available $InGaAs/GaAs$ samples.

The results obtained demonstrate that one has a great variety of opportunities to tailor optical properties using defect MQW's. These systems can have a range of different applications. For example, the great sensitivity of the defect induced features of optical spectra to characteristics of the system can be used for characterization of both host QW's and defect wells. This sensitivity also leads to possibilities to tune the frequencies of local modes by means of application of stress, electric or magnetic field, or other stimuli. Another important feature with great potential for applications is the increase of the field intensity in the vicinity of the defect well. It can be utilized in order to enhance optical non-linearity of the system. It is also worth noting that the local modes considered here can be useful as tunable sources of narrow luminescent lines at the frequencies of the local modes.

Chapter 7

Summary

The problem of local photon states and EM wave tunneling attracts a great deal of attention. It is necessary, therefore, to distinguish the situation we considered here from other cases considered in the literature. One of this cases is local photons arising due to macroscopically sized defects in photonic crystals. The period of the crystal structure of this artificial materials and the size of the defect are of the order of the electromagnetic wave length. The defects in this case do not have their own optical activity - they just locally modify the original structure. The different kind of local photons arises when an optically active element, such as an atom with dipole active transitions, is considered. In this case, if the transition frequency falls into the gap region caused by the periodicity in the case of photon crystals or the polariton effects in the case of regular polar dielectrics, photons emitted by the atoms cannot propagate, so they form what was called "atom-field bound state." These two kind of local states are physically different, and are supposed to play different role in possible applications.

Local states considered here, LPM's, do not belong to any of these two groups of phenomena. It differs from defect states in photonic crystals because we deal with *microscopic* defect - impurity atom in a regular crystal. But unlike the case of atom-field bound states our defect does not have its own optical activity. Its dipole moment caused solely by its mechanical motion. The common sense would say that such a defect cannot effect optical properties of the host material, and this would be correct if there is no coupling between electromagnetic waves and internal excitations of the material (phonons, excitons, etc.). However, if such coupling exist, or, in other words, if the *polariton effects* are significant, the situation changes. There is no problem with phonons or excitons being localized due to a defect atom. Such local phonon or exciton, if dipole active, would emit light, and if the frequency of the local state belongs to the polariton gap, the emitted light remains localized around the defect. One could say that the entire phonon or exciton local mode plays a role of active atoms in the case of atom-field bounded states, but this mode has macroscopic spatial extension, and hence, macroscopic dipole moment.

By the exact analytical solution of the tunneling of electromagnetic waves through a chain of noninteracting atoms with a single defect we showed that at the frequency of LPM the effect of the resonant tunneling occurs. The transmission coefficient in the resonance is strongly enhanced, and if the defect is placed exactly in the middle of the chain, the transmission coefficient becomes unity. The electromagnetic field at the defect site is strongly enhanced at the resonance. Actually, this field grows exponentially with an increase of the

length of the system. This effect is an electromagnetic analogue of the charge accumulation in the case of electron tunneling, where it is known to cause interesting nonlinear phenomena [120, 121, 122]. In our situation a strong local field will also result in nonlinear effects, which will eventually saturate the exponential growth.

Numerical simulations in 1D chain of dipoles demonstrated also a transition between two transport regimes: the one associated with resonance tunneling and the other one occurring when the resonances spatially overlap and the pass band (IPB) of extended states emerges. The transition occurs when an average distance between the defects becomes equal to the localization length of the single local state. At the same time the collective localization length at the peak transmission frequency, characterizing the transport properties of the entire chain, becomes comparable to the total length of the system.

The method of microcanonical ensemble in conjunction with the expansion in the parameter $l_{def}/l_0 \ll 1$, where l_{def} is the average distance between the impurities and l_0 is the localization radius of a single local polariton state, produces a clear physical description of the excitations, and shows excellent agreement with the results of numerical simulations. In the zeroth order of this expansion, we recover the density of states and the dispersion law of excitations in the system with uniform continuously distributed impurities. Corrections to this solution describe effects due to local fluctuations in the positions of impurities such as a finite localization length of the excitations, a renormalization of the spectral boundaries and the effective mass of the excitations. The parameter l_{def}/l_0, therefore can be considered as a measure of disorder in the system.

In Chapter 5 it was shown that the concept of LPM's can be used to describe optical properties of mixed crystals in the frequency region of their *restrahlen* band. We showed that this concept allows for a physically transparent explanation of the presence of weak features in the spectra of so called one-mode crystals, and for one-two mode behavior. The previous models were able to explain these features only with the use of many fitting parameters. We demonstrated that under certain conditions new impurity induced LPM's may arise within the *restrahlen* of the host crystals, and studied their dispersion laws and density of states. Particularly, we found that the group velocity of these excitations is proportional to the concentration of the impurities and can be thousands of times smaller then the speed of light in vacuum.

We also studied LPM's that arise due to deep defect centers with strong electron-phonon coupling. Electron transitions involving deep levels may result in alteration of local elastic constants. In this case, substantial reversible transformations of IPB density of states occur, which include the appearance/disappearance of the polariton impurity band, its shift and/or the modification of its shape. Such changes can be induced by thermo- and photo-excitation of the localized electron states or by trapping of injected charge carriers. We showed a possibility to effectively control the optical properties, in particular, light transmission, of polar crystals in the far IR region in the vicinity of the polariton bandgap, by modifying the charge state of the deep center by means of light from the visible or near IR region. We also developed a simple model, which is applied to the O_P center in GaP and discussed further possible experimental realizations of the effect.

In the last Chapter we studied analytically defect polariton states in Bragg multiple-quantum-well structures, that are mathematically similar to LPM's in 1D polar crystals, and defect induced changes in transmission and reflection spectra.

Defect layers can differ from the host layers in three ways: exciton-light coupling strength, exciton resonance frequency, and inter-well spacing. We showed that a single defect leads to two LPM's in the photonic bandgap. These modes cause peculiarities in reflection and

transmission spectra. Each type of defect can be reproduced experimentally, and we show that each of these plays a distinct role in the optical properties of the system. For some defects, we predict a narrow transmission window in the forbidden gap at the frequency set by parameters of the defect. We obtained analytical expressions for corresponding local frequencies as well as for reflection and transmission coefficients. We showed that the presence of the defects leads to resonant tunneling of the electromagnetic waves via LPM's accompanied by resonant enhancement of the field inside the sample, even when a realistic absorption is taken into account. On the basis of the obtained results, we made recommendations regarding the experimental observation of the effects studied in readily available samples.

Besides opportunities for applications, the considered effects are interesting from the academic point of view. The tunneling resonances associated with the local polaritons have a number of peculiarities compared to other examples of resonance tunneling phenomena. For instance, the Fano-like transmission produced by the Ω-defect appears here under new circumstances, specific for this particular system. Another interesting feature of LPM's is that the frequencies of transmission resonances are always shifted with respect to the eigen frequencies of the modes and depends upon the length of the system. Concluding, the structures considered in the last Chapter demonstrate a number of interesting optical effects and have a potential for a variety of applications. We hope that this study will stimulate experimental observation and utilization of the predicted here effects.

Appendix A

Invariant embedding algorithm for the transfer-matrix equation

In this Appendix we develop invariant embedding approach to transfer-matrix equations (2.20,2.21,2.22) of a general form and deduce the recurrent equations on the total transfer matrix. Consider a typical difference equation of the transfer-matrix method,

$$u_{n+1} = T_n u_n, \tag{A.1}$$

with boundary conditions of a general form:

$$Gu_0 + Hu_N = v. \tag{A.2}$$

Here u_n is a vector of an appropriate dimension that characterizes the state of the system at the nth site, T_n is a respective transfer-matrix; G and H are matrices of the same dimension as the transfer-matrix, together a with the vector v they specify boundary conditions at the left and right boundaries of the system (cites 0 and N respectively). The regular Maxwell boundary conditions and the fixed ends boundary condition for polarization can be presented in the form Eq. (A.2) with the following matrices G,H, and vector v

$$G = \begin{pmatrix} 1 & -i & 0 & 0 \\ 1 & -i & 0 & 0 \\ 0 & 0 & 1 & 0 \\ 0 & 0 & 1 & 0 \end{pmatrix}, \qquad H = \begin{pmatrix} 1 & i & 0 & 0 \\ -1 & -i & 0 & 0 \\ 0 & 0 & 0 & 1 \\ 0 & 0 & 0 & -1 \end{pmatrix}, \qquad v = \begin{pmatrix} 2 \\ 2 \\ 0 \\ 0 \end{pmatrix}. \tag{A.3}$$

These matrices are singular, but one should not worry about this, because we will only need to invert their sum, which has a non-zero determinant. In accord with the ideas of the invariant embedding method [40], we consider the dynamic vector, u_n, as a function of the current site n, the length of the system N, and the boundary vector v:

$$u_n \equiv u(n, N, v) \equiv S(n, N)v \tag{A.4}$$

In the last equation we use the linear nature of Eq. (A.1) in order to separate out the dependence upon the vector v. Substituting Eq. (A.4) into Eqs. (A.1) and (A.2) we have the dynamical equation and boundary conditions for the matrix S :

$$S(n+1, N) = T_n \times S(n, N), \tag{A.5}$$

$$G \times S(0,N) + H \times S(N,N) = I, \tag{A.6}$$

where I is a unit matrix. The matrix $S(n,N+1)$, which describes the system with one additional scatterer, obviously satisfies the same equation (A.5) as $S(n,N)$. Relying again upon the linearity of Eq. (A.5) we conclude that $S(n,N)$ and $S(n,N+1)$ can only differ by a constant (independent of n) matrix factor $\Lambda(N)$.

$$S(n,N+1) = S(n,N) \times \Lambda(N). \tag{A.7}$$

In order to find $\Lambda(N)$ we first substitute Eq. (A.7) into boundary conditions Eq. (A.6) which yield

$$\Lambda(N) = G \times S(0,N+1) + H \times S(N,N+1). \tag{A.8}$$

Boundary conditions Eq. (A.6) do not change if N is replaced by $N+1$, therefore we can write down that

$$G \times S(0,N+1) = I - H \times S(N+1,N+1). \tag{A.9}$$

Substituting this expression into Eq. (A.8) we have for the matrix $\Lambda(N)$:

$$\Lambda(N) = I + H \times [S(N,N+1) - S(N+1,N+1)]. \tag{A.10}$$

The quantity $S(N+1,N+1)$ can be eliminated from this equation by means of Eq. (A.1): $S(N+1,N+1) = T_N\ S(N,N+1)$, and we have for $\Lambda(N)$

$$\Lambda(N) = I + H \times [I - T(N)] \times S(N,N+1). \tag{A.11}$$

Substituting this formula into Eq. (A.7) we obtain the equation that governs the evolution of the matrix $S(n,N)$ with the change of the parameter N:

$$S(n,N+1) = S(n,N) + S(n,N) \times H \times [I - T(N)] \times S(N,N+1). \tag{A.12}$$

This equation, however, is not closed because of an unknown matrix $S(N,N+1)$. This matrix can be found by setting $n = N$ in Eq. (A.12):

$$S(N,N+1) = \{I - S(N,N) \times H \times [I - T(N)]\}^{-1} S(N,N). \tag{A.13}$$

Introducing notation

$$\Xi(N) = \{I - S(N,N) \times H \times [I - T(N)]\}^{-1} \tag{A.14}$$

the previous expression can be rewritten in the following compact form:

$$S(N,N+1) = \Xi(N) \times S(N,N). \tag{A.15}$$

Inserting Eq. (A.15) into Eq. (A.12) we finally obtain:

$$S(n,N+1) = S(n,N) + S(n,N) \times H \times [I - T(N)] \times \Xi(N) \times S(N,N). \tag{A.16}$$

This equation still has an unknown quantity $S(N,N)$ which must be determined separately. We achieve this combining the original transfer matrix equation (A.1) and Eq. (A.15) to obtain the following:

$$S(N+1,N+1) = T_N \times \Xi(N) \times S(N,N). \tag{A.17}$$

Eq. (A.17) is a nonlinear matrix equation with an initial condition given by

$$(G + H) \times S(0, 0) = I. \tag{A.18}$$

Eqs.(A.16)-(A.18) constitute the complete set of embedding equations for the transfer matrix problem. In order to find the transmission coefficient one has to multiply the matrix $S(N, N)$ by the boundary vector v; the first component of the resulting vector is equal to $t \exp(ikL)$, where t is the complex transmission coefficient. If one is interested in the distribution of the state vector $u(n, N)$ throughout the entire system, one has to find $S(N, N)$ and then to solve Eq. (A.16).

The presented algorithm was proved to be extremely stable, it produced reliable results for transmission as small as 10^{-17}. This stability is due to the operation of inversion involved in the calculations [see Eq. (A.14)]. This operation prevents elements of the matrix S to grow uncontrollably in the course of calculations.

Bibliography

[1] E. Yablonovitch, Phys. Rev. Lett. **58**, 2059 (1987).

[2] S. John and T. Quang, Phys. Rev. A **50**, 1764 (1994)

[3] S. John and J. Wang, Phys. Rev. Lett. **64**, 2418 (1990); Phys. Rev. B **43**, 12772 (1991).

[4] S. John and T. Quang, Phys. Rev. A **52**, 4083 (1995).

[5] J. D. Joannopoulos, R. D. Meade, and J. N. Winn, *Photonic Crystals: Molding the Flow of Light* (Princeton Univ. Press, 1995).

[6] B. I. Shklovskii and A. L. Efros. *Electron properties of doped semiconductors* (Springer, New York, 1984).

[7] I. M. Lifshitz, Nuovo Cim. (Suppl. A1) **3**, 591 (1956).

[8] A. A. Maradudin, E. W. Montroll, G. H. Weiss, and I. P. Ipatova, *Theory of Lattice Dynamics in the Harmonic Approximation*, 2nd edition (Academic Press, New York, 1971).

[9] I. M. Lifshitz and A. M. Kosevich, in: *Lattice Dynamics* (Benjamin, New York, 1969), p. 53.

[10] A. A. Maradudin, in: *Lattice Dynamics* (Benjamin, New York, 1969), p. 1.

[11] G. F. Koster and J. C. Slater. Phys. Rev. **95**, 1167 (1954).

[12] E. I. Rashba, Optika i Spectroskopia **2**, 586 (1957); R. E. Merrifield, J. Chem. Phys. **38,** 920 (1963).

[13] V. M. Agranovich, *Crystal optics with spatial dispersion, and excitons* (Springer, New York, 1984).

[14] E. Yablonovitch, T. J. Gmitter, R. D. Meade, A. M. Rappe, K. D. Brommer, and J.D. Joannopoulos. Phys. Rev. Lett. **67** 3380 (1991).

[15] R. D. Meade, K. D. Brommer, A. M. Rappe, and J. D. Joannopoulos, Phys. Rev. B **44** 13772 (1991).

[16] A. Figotin and A. Klein, J. Stat. Phys. **86**, 165 (1997).

[17] L. I. Deych and A. A. Lisyansky, Phys. Lett. A **240**, 329 (1998).

[18] V. I. Rupasov and M. Singh, Phys. Rev. A **54**, 3614 (1996); Phys. Rev. A **56**, 898 (1997).

[19] L. I. Deych and A. A. Lisyansky, Phys. Lett. A **243**, 156 (1998).

[20] J. M. Deutsch and G. Paladin, Phys. Rev. Lett. **62**, 695(1989).

[21] D. S. Citrin, Solid State Commun. **89**, 139 (1994).

[22] E. L. Ivchenko, A. I. Nesvizhskii, and S. Jorda, Phys. Solid Sate **36**, 1156 (1994).

[23] L. C. Andreani, Phys. Status Solidi B **188**, 29 (1995).

[24] T. Stroucken, A. Knorr, P. Thomas, and S. W. Koch, Phys. Rev. B **53**, 2026 (1996).

[25] Y. Merle D' Aubigné, A. Waseila, H. Mariette, and T. Dietl, Phys. Rev. B **54**, 14003 (1996).

[26] M. Hübner, J. Kuhl, T. Stroucken, A. Knorr, S. W. Koch, R. Hey, K. Ploog, Phys. Rev. Lett. **76**, 4199 (1996).

[27] M. Hübner, J. P. Prineas, C. Ell, P. Brick, E. S. Lee, G. Khitrova, H. M. Gibbs, S. W. Koch, Phys. Rev. Lett. **83**, 2841 (1999); J. P. Prineas, C. Ell, E. S. Lee, G. Khitrova, H. M. Gibbs, S. W. Koch, Phys. Rev. B **61**, 13863 (2000).

[28] A. Dereux, J.-P. Vigneron, P. Lambin, and A. Lucas, Phys. Rev. B **38**, 5438 (1988).

[29] M. L. H. Lahlaouti, A. Akjouj, B. Djafari-Rouhani, and L. Dobrzynski, Phys. Rev. B **61**, 2059 (2000-I).

[30] L. Deych, A. Yamilov, and A. A. Lisyansky, Phys. Rev. B **59**, 11339 (1999).

[31] L. Deych, A. Yamilov, and A. A. Lisyansky, Europhys. Lett. **46**, 534 (1999).

[32] A. Yamilov, L. I. Deych, and A. A. Lisyansky, J. Opt. Soc. Amer. B **17**, 1498 (2000).

[33] L. I. Deych, A. Yamilov, and A. A. Lisyansky, Phys. Rev. B **62**, 6301 (2000).

[34] A. Yamilov, L. I. Deych, and A. A. Lisyansky, Ann. Phys. **8**, 293 (1999).

[35] L. I. Deych, A. Yamilov, and A. A. Lisyansky, Opt. Lett. **25**, 1705 (2000).

[36] L. I. Deych, A. Yamilov, and A. A. Lisyansky, *Resonance transmission of the electromagnetic waves through long periodic Bragg Multiple Quantum Well structures via localized polariton defect states*, submitted to Phys. Rev. B.

[37] M. Foygel, A. Yamilov, L. I. Deych, and A. A. Lisyansky, "*Tunable local polariton modes in semiconductors,*" submitted to Phys. Rev. B.

[38] V. S. Podolsky, L. I. Deych, and A. A. Lisyansky, Phys. Rev. B **57**, 5168 (1998).

[39] S. I. Pekar, Zh. Eksp. Teor. Fiz. **33**, 1022 (1957) [Soviet Phys. JETP **6**, 785 (1958)].

[40] R. Bellman and G. Wing, *An introduction to invariant embedding* (Wiley, New York, 1976).

[41] A. V. Chaplik and M. V. Entin, Zh. Eksp. & Teor. Fiz. **67**, 208 (1974) [Sov. Phys.-JETP **40**].

[42] M. Weidemüller, A. Hemmerich, A. Görlitz, T. Esslinger, and T. W. Hänsch, Phys. Rev. Lett. **75**, 4583 (1995).

[43] G. Birkl, M. Gatzke, I. H. Deutsch, S. L. Rolston, and W. D. Phillips, Phys. Rev. Lett. **75**, 2823 (1995).

[44] J. N. Tan, J. J. Bollinger, B. Jelenkovic, and D. J. Wineland, Phys. Rev. Lett. **75**, 4198 (1995).

[45] I. M. Lifshitz, S. A. Gredeskul, and L. A. Pastur, "Introduction to the theory of disordered systems," (Wiley, New York, 1988).

[46] D. J. Thouless, J. Phys. C **5**, 77 (1972).

[47] M. R. Singh and W. Lau, Physica Status Solidi B **203**, 401 (1997).

[48] I. M. Lifshitz and V. Ya. Kirpichnikov, Zh. Eksp. & Teor. Fiz. **77**, 989 (1979) [Sov. Phys.- JETP **50**].

[49] D. W.Taylor, in: "Optical Properties of Mixed Crystals," edited by R. J. Elliott, I. P. Ipatova, North-Holland, Amsterdam, 1988, pp. 35-132.

[50] A. S. Barker, Jr., A. J. Sievers, Rev. Mod. Phys. **47**, Suppl. 2 (1975).

[51] D. W.Taylor, *Photon Response Theory and the Infrared and Raman experiments* pp.35-132 in *Optical Properties of Mixed Crystals* edited by R. J. Elliott and I. P. Ipatova, North-Holland, Amsterdam, 1988.

[52] I. F. Chang and S. S. Mitra, Adv. Phys. **20**, 359 (1971).

[53] T. S. Moss *Optical Properties of Semiconductors* (Betterworth, London, 1959).

[54] G. Lucovsky, M. Brodsky, and E. Burstein, in *Localized Excitations in Solids* edited by R. F. Wallis, p. 592, Plenum Press, New York, 1968.

[55] H. Harada and S. Narita, J. Phys. Soc. Japan **30**, 1628 (1971).

[56] H. W. Verleur and A. S. Barker, Jr., Phys. Rev. **164**, 1169 (1967).

[57] R. K. Chang, B. Lacina, and P. S. Pershan, Phys. Rev. Lett. **17**, 755 (1966).

[58] P. Kleinert and E. Jahne, Phys. Status Solidi B **107**, 177 (1981).

[59] H. Finkenrath, G. Franz, and N. Uhle, Phys. Status Solidi B **95**, 179 (1979).

[60] J. H. Fertel and C. H. Perry, Phys. Rev. **184**, 874 (1969).

[61] B. Renker, N. M. Butt, and N. E. Massa, Phys. Rev. B **27**, 1450 (1983).

[62] Y. S. Chen, W. Shockley, and G. L. Pearson, Phys. Rev. **151**, 648 (1966).

[63] H. W. Verleur and A. S. Barker, Jr., Phys. Rev. **149**, 715 (1966).

[64] R. J. Elliott, J. A. Krumhansl, and P. L. Leath, Rev. Mod. Phys. **46**, 465 (1974).

[65] R. Bonneville, Phys. Rev. B **24**, 1987 (1981).

[66] P. J. Dean, D. D. Manchon, Jr. and J. J. Hopfield, Phys. Rev. Lett. **25**, 1027 (1970).

[67] T. B. Norris, *Strong Coupling in Semiconductor Cavities*, in: *Confined Electrons and Photons*, ed. by E. Burnstein and C. Weisbuch (Plenum Press, New York, 1995)

[68] G. Livescu, Z. Vardeny, and O. Brafman, Phys. Rev. B **24**, 1952 (1981).

[69] G. Livescu and O. Brafman, Phys. Rev. B **34**, 4255 (1986); S.H. Wei, S.B. Zhang, and A. Zunger, Phys. Rev. Lett. **70**, 1639 (1993).

[70] J.N. Plendl, A. Handi, J. Claudel, Y. Henninger, G. Morlot, P. Strimer, and L. C. Mansur, Applied Optics **5**, 397 (1966).

[71] M. Born and K. Huang, *Dynamical Theory of Crystal Lattices*, Oxford, Clarendon Press, 1954.

[72] H. Bilz and W. Kress, *Phonon Dispersion Relations in Insulators,* Springer-Verlag, New York, 1979.

[73] J. Groenen, R. Carles, G. Landa, C. Guerret-Piecourt, C. Fontaine, and M. Gendry, Phys. Rev. B **58**, 10452 (1998).

[74] A. Ishimaru, *Wave Propagation and Scattering in Random Media,* Academic Press, New York, 1978.

[75] F. Bechstedt, U. Grossner, and J. Furthmuller, Phys. Rev. B **62**, 8003 (2000).

[76] M. Krauzman, R. M. Pick, H.Poulet, G. Hamel, and B. Prevot, Phys. Rev. Lett. **33**, 528 (1974); M. L. Shand, H. D. Hochheimer, M. Krauzman, J. E. Potts, R. C. Hanson, and C. T. Walker, Phys. Rev. B **14**, 4637 (1976); G. Kanellis, W. Kress, and H. Bilz, Phys. Rev. Lett. **56**, 938 (1986); Phys. Rev. B **33**, 8724 (1986); **33**, 8733 (1986); A. Gobel, T. Ruf, M. Cardona, C. T. Lin, and J. C. Merle, Phys. Rev. Lett. **77**, 2591 (1996); A. Gobel, T. Ruf, M. Cardona, and C. T. Lin, Physica B **219&220**, 511 (1996); A. Gobel, T. Ruf, C. T. Lin, and M. Cardona Phys. Rev. B **56**, 210 (1997); C. Ulrich, K. Syassen, and M. Cardona, Phys. Rev. B **60**, 9410 (1999).

[77] S. T. Pantelides, in *Deep Centers in Semiconductors*, edited by S. T. Pantelides, 2nd edition (Gordon and Breach, New York, 1992), p.1.

[78] G. F. J. Garlick, Reports on Progress in Physics, London, 1967, v. 30, part 2, p. 491.

[79] P. T. Landsberg, Physica Status Solidi **41**, 457 (1970).

[80] M. Lax, Phys. Rev. **119**, 1502 (1960).

[81] K. Huang and A. Rhys, Proc. Royal Soc. A **204**, 406 (1950).

[82] C. H. Henry and D. V. Lang, Phys. Rev. B **15**, 989 (1977).

[83] V. N. Abakumov, I. A. Merkulov, V. I. Perel', and I. N. Yassievich, Zh. Eksp. Teor. Fiz. **89**, 1472 (1985) [Sov. Phys. JETP **62**, 853 (1985)].

[84] P. J. Dean, in *Deep Centers in Semiconductors,* ed. by S. T. Pantelides, 2nd edition (Gordon and Breach, New York, 1992), p.215.

[85] H. Ch. Alt, Phys. Rev. Lett. **65**, 3421 (1990).

[86] M. Skowronski, in *Deep Centers in Semiconductors,* ed. by S. T. Pantelides, 2nd edition (Gordon and Breach, New York, 1992), p.379.

[87] E. V. Lavrov, B. B. Nielsen, J. R. Byberg, B. Hourahine, R. Jones, S. Öberg, and P. R. Briddon, Phys. Rev. B **62**, 158 (2000).

[88] E. V. Lavrov, L. Hoffmann, and B. B. Nielsen, Phys. Rev. B **60**, 8081 (1999).

[89] C. Wetzel, H. Amano, I. Akasaki, J. W. Ager III, I. Gregory, M. Topf, and B. K. Meyer, Phys. Rev. B **61**, 8202 (2000).

[90] W. K. Ge, C. Y. Song, and D. S. Jiang, Phys. Rev. B **53**, 9809 (1996).

[91] Zh.-G. Wang, L.-A. Ledebo, and H. G. Grimmeiss, J. Phys. C **17**, 259 (1984).

[92] J. A. Wolk, M. B. Kruger, J. N. Heyman, W. Walukiewicz, R. Jeanloz, and E. E. Haller, Phys. Rev. Lett. **66**, 774 (1991).

[93] V. P. Markevich, M. Suezawa, and L. I. Murin, J. Appl. Phys. **84**, 1246 (1996).

[94] H. Ono, and T. Baba, Phys. Rev. B **47**, 16628 (1993).

[95] A. I. Baz', Ya. B. Zeldovich, and A. M. Perelomov, *Scattering, Reactions and Decay in Nonrelativistic Quantum Mechanics*, IPST, Jerusalem, 1969.

[96] S. V. Meshkov, Zh. Eksp. Teor. Fiz. **89**, 1734 (1985) [Sov. Phys. JETP **62**, 1000 (1985)]

[97] P. W. Anderson, Phys. Rev. Lett. **34**, 953 (1975).

[98] N. F. Mott and E. A. Davis, *Electronic Processes in Non-Crystalline Materials*, 2nd ed., Clarendon Press, Oxford (1979).

[99] A. G. Petukhov, A. V. Radchik, and M. G. Foygel, Pis'ma Zh. Eksp. Teor. Fiz. **41**, 502 (1985) [JETP Lett. **41**, 612 (1985)].

[100] A. G. Petukhov and M. G. Foygel, Fiz. Tekh. Poluprovodn. **21**, 118 (1987) [Sov. Phys. Semicond. **21**, 71 (1987)].

[101] M. Foygel, A. G. Petukhov, and A. S. Andreyev, Phys. Rev. B **48**, 17018 (1993).

[102] U. S. Qurashi, M. Z. Iqbal, C. Delerue, and M. Lannoo, Phys. Rev. B **23**, 13331 (1992).

[103] H. Bilz, W. Kress, *Phonon Dispersion Relations in Insulators,* Springer-Verlag, New York, 1979.

[104] *Semiconductors. Group IV elements and III-V Compounds,* ed. by O. Madelung, Springer-Verlag, New York, 1991.

[105] *Imperfections in III/V materials*, ed. by E. R. Weber, *Semiconductor and Semimetal* series, vol. 38, Academic Press, San Diego, 1993.

[106] R. C. Newman *Infra-red Studies of Crystal Defects*, Taylor and Francis, London, 1973.

[107] I. H. Deutsch, R. J. C. Spreeuw, S. L. Rolston, and W. D. Phillips, Phys. Rev. A **52**, 1394 (1995).

[108] G. Björk, S. Pau, J.M. Jakobson, H. Cao, and Y. Yamamoto, Phys. Rev. B **52**, 17310 (1995).

[109] M. P. Vladimirova, E. L. Ivchenko, and A. V. Kavokin, Semiconductors **32**, 90 (1998).

[110] L. I. Deych, and A. A. Lisyansky, Phys. Rev. B **60**, 4242 (2000).

[111] D. S. Citrin, Appl. Phys. Lett. **66**, 994(1995).

[112] L.C. Andreani, "Optical Transitions, Excitons, and Polaritons in Bulk and Low-Dimensional Semiconductor Structures," in: *Confined Electrons and Photons* (edited by E. Burstein and C. Weisbuch, Plenum, New York, 1995).

[113] A. Yu. Sivachenko, M. E. Raikh, and Z. V. Vardenu, cond-mat/0005396.

[114] C. Ell, J. Prineas, T. R. Nelson, Jr., S. Park, H. M. Gibbs, G. Khitrova, and S. W. Koch , Phys. Rev. Lett. **80**, 4795 (1998).

[115] L. V. Keldysh, Superlattices and Microstructure **4**, 637 (1988).

[116] E. L. Ivchenko, Phys. Solid State **33**, 1344 (1991).

[117] U. Fano, Phys. Rev. **124**, 1866 (1961).

[118] G. Breit and E. Wigner, Phys. Rev. **49**, 519 (1936).

[119] M. Ya. Azbel, Solid State Comm. **45**, 527 (1983).

[120] V.J. Goldman, D.C. Tsui, and J.E. Cunningham, Phys. Rev. Lett. **58**, 1256 (1987).

[121] V.J. Goldman, D.C. Tsui, and J.E. Cunningham, Phys. Rev. B. **35**, 9387 (1987).

[122] A. Zaslavsky, V.J. Goldman, D.C. Tsui, and J.E. Cunningham, Appl. Phys. Lett. **53**, 1408 (1988).